UNIVERSIDADE ESTADUAL DE CAMPINAS
FACULDADE DE CIÊNCIAS FARMACÊUTICAS

VIVIANE LUCIA BERALDO DE ARAÚJO

NANOSTRUCTURED CARRIERS TO LOAD LEVOFLOXACIN AS A POTENTIAL TREATMENT OF PULMONARY INFECTIONS

CARREADORES NANOESTRUTURADOS PARA VEICULAÇÃO DE LEVOFLOXACINO COMO POTENCIAL TRATAMENTO DE INFECÇÕES PULMONARES

CAMPINAS
2023

VIVIANE LUCIA BERALDO DE ARAÚJO

NANOSTRUCTURED CARRIERS TO LOAD LEVOFLOXACIN AS A POTENTIAL TREATMENT OF PULMONARY INFECTIONS

CARREADORES NANOESTRUTURADOS PARA VEICULAÇÃO DE LEVOFLOXACINO COMO POTENCIAL TRATAMENTO DE INFECÇÕES PULMONARES

Tese apresentada à Faculdade de Ciências Farmacêuticas da Universidade Estadual de Campinas como parte dos requisitos exigidos para a obtenção do título de Doutora em Ciências, na área de Ciências Farmacêuticas — Insumos Farmacêuticos Naturais, Biotecnológicos e Sintéticos.

Thesis presented to the Faculty of Pharmaceutical Sciences of the State University of Campinas in partial fulfilment of the requirements for the degree of Doctor in Sciences, in the area of Pharmaceutical Sciences — Pharmaceutical products of natural, biotechnological or synthetical origin.

Orientadora: Profª Drª Laura de Oliveira Nascimento

ESTE TRABALHO CORRESPONDE À VERSÃO FINAL DA TESE DEFENDIDA PELA ALUNA VIVIANE LUCIA BERALDO DE ARAÚJO, ORIENTADA PELA PROFª DRª LAURA DE OLIVEIRA NASCIMENTO.

CAMPINAS
2023

Ficha catalográfica
Universidade Estadual de Campinas
Biblioteca da Faculdade de Ciências Médicas
Maristella Soares dos Santos - CRB 8/8402

B45n

Beraldo de Araujo, Viviane Lucia, 1983-
Nanostructured carriers to load levofloxacin as a potential treatment of pulmonary infections / Viviane Lucia Beraldo de Araujo. – Campinas, SP : [s.n.], 2023.

Orientador: Laura de Oliveira Nascimento.
Tese (doutorado) – Universidade Estadual de Campinas, Faculdade de Ciências Farmacêuticas.

1. Delineamento experimental. 2. Levofloxacino. 3. Carreadores lipídicos nanoestruturados. 4. Degradação de fármaco. 5. Tensoativos. 6. Calu-3. I. Nascimento, Laura de Oliveira, 1980-. II. Universidade Estadual de Campinas. Faculdade de Ciências Farmacêuticas. III. Título.

Informações Complementares

Título em outro idioma: Carreadores nanoestruturados para veiculação de levofloxacino como potencial tratamento de infecções pulmonares
Palavras-chave em inglês:
Design of experiments
Levofloxacin
Nanostructured lipid carriers
Drug degradation
Surface-active agents
Calu-3
Área de concentração: Ciências Farmacêuticas: insumos farmacêuticos naturais, biotecnológicos e sintéticos
Titulação: Doutora em Ciências
Banca examinadora:
Laura de Oliveira Nascimento [Orientador]
Taís Gratieri
Marlus Chorilli
Ana Lucia Tasca Gois Ruiz
Newton Andreo Filho
Data de defesa: 23-05-2023
Programa de Pós-Graduação: Ciências Farmacêuticas

Identificação e informações acadêmicas do(a) aluno(a)
- ORCID do autor: https://orcid.org/0000-0002-6868-5208
- Currículo Lattes do autor: http://lattes.cnpq.br/2436607926407132

UNIVERSIDADE ESTADUAL DE CAMPINAS
FACULDADE DE CIÊNCIAS FARMACÊUTICAS

Autora: Viviane Lucia Beraldo de Araújo
Orientadora: Profª Drª Laura de Oliveira Nascimento

Tese aprovada em 23 de maio de 2023

Comissão Examinadora:

Profª Drª Laura de Oliveira Nascimento
Profª Drª Taís Gratieri
Prof. Dr. Marlus Chorilli
Profª Drª Ana Lucia Tasca Gois Ruiz
Prof. Dr. Newton Andréo Filho

A ata de defesa com as respectivas assinaturas dos membros encontra-se no SIGA/Sistema de Fluxo de Dissertação/Tese e na Secretaria de Pós-Graduação da Faculdade de Ciências Farmacêuticas.

Campinas, 23 de maio de 2023.

Dedico esta tese à minha família:
Obrigada por acolher, compreender,
incentivar e fazer parte dessa jornada.

AGRADECIMENTOS

Agradeço a Deus pela vida, pelo privilégio de ter capacidade cognitiva, pela saúde e resiliência para percorrer os caminhos da ciência.

Agradeço à minha família, cada um com seu papel fundamental na manutenção dos meus pilares emocionais.

Aos meus pais, Lúcia e Vadiney, por me ensinarem, à sua maneira, o quão valioso é o conhecimento. Agradeço por me educarem a ser uma pessoa boa e justa e me permitirem ter uma vida dedicada aos estudos e à ciência, mesmo sem compreenderem ao certo o que isso significa.

Aos meus irmãos, Erick e Patrícia, pela companhia, doação e por me ensinarem como podemos amar e respeitar pessoas tão diferentes [e tão semelhantes] a nós mesmos. Aos meus cunhados, Vanessa e Renan, pelo companheirismo, compartilhando nossos medos, anseios e *spoilers*. Aos queridos sobrinhos, Enzo, Enrico, Lorenzo e Paçoca: a vida é mais colorida [e agitada] com vocês!

Ao Anderson, meu marido, companheiro, amigo e parceiro científico (que sempre quer saber o que estou fazendo, deixando-me às vezes impaciente): seu apoio, carinho e confiança me incentivam a desenvolver o meu melhor sempre! Obrigada por isso, por embarcar nas aventuras científicas mundo afora e por nossa maior conquista, nosso filho Antoni. É lindo ver como podemos crescer juntos!

Ao Antoni, o leonino que me ensina diariamente a ser mãe e a ser um ser humano cada dia melhor, que me surpreende com seu carinho, cuidado e criatividade. Obrigada, Totinho, por me escolher como mãe e por compreender os horários malucos de seus pais cientistas! Vocês são o meu porto seguro!

Agradeço ao privilégio de ter familiares generosos, que mesmo distantes emanam carinho, sentimento de união e incentivo. Em especial ao vô Henrique (*in memoriam*), que junto à vó Laura (*in memoriam*) espalhou a alegria nessa família!

Aos meus sogros, Marlene e Vilmar, meus cunhados Matheus, Mariel, Rafael, meu sobrinho Martiel, e os tios e primas que me acolheram desde sempre como família. Obrigada por compreenderem o trabalho árduo e as raras visitas. A distância não diminui o carinho por vocês.

À família que não é de sangue, mas é um membro importante. Gratidão pelo cuidado, suporte e amizade que a gestação me deu: Noemi, Juliano, Daniel e vovó Valéria.

Ao querido cuidador da minha sanidade física e mental, o professor de yoga que a pandemia me trouxe: William Gásparo. Seus cuidados e generosidade não são desse mundo!

Agradeço ao prof. Pessine e aos seus alunos que me receberam como aluna de IC em seu laboratório. Aprendi muito com todos vocês! Obrigada por ter acompanhado não apenas minha jornada acadêmica, mas também minhas vivências pessoais e por ter interesse em acompanhar, mesmo que remotamente, a etapa final do meu doutorado antes de sua aposentadoria. Sua curiosidade e interesse pelo conhecimento são fascinantes!

Agradeço por minha base científica ter sido sediada no LATEF, coordenado pela professora Laura, que me acolheu desde o mestrado e acompanhou meus desenvolvimentos acadêmicos e pessoais, além das trocas de experiências da maternidade. Obrigada pelas oportunidades e por me mostrar do que eu sou capaz. Fico feliz em ver o quanto crescemos juntas!

Agradeço a todos os amigos que o LATEF me proporcionou, desde os da “velha guarda” (Juliana e Danilo, que estavam junto comigo desde quando “tudo era mato”. Agradeço pela companhia e amizade até hoje!). À Renata e Marcelo, que me mostraram como ser perseverante. À Victória, dona de um coração generoso, acolhedor e que compartilha as melhores técnicas milenares para solução de problemas. A todas as ICs que passaram pelo laboratório (todos representados pelas atuais Camila, Laura, Rafaela e pelo Matheus). Em especial, às minhas queridas ICs, Samira e Ana Flávia, que abraçaram nossos projetos com comprometimento e permitiram com que eles avançassem até aqui. Sou grata a vocês por minha valiosa experiência como coorientadora.

Aos amigos novos, aos antigos que a pós-graduação me permitiu resgatar e aos de outras vidas. Ana Thereza, Gabriela, Arthur, Gleisy. Obrigada por podermos compartilhar de forma leve e divertida a rotina na pós-graduação e fora dela.

Agradeço a oportunidade de ter tido duas experiências internacionais no doutorado. Em Portugal, pelo acolhimento fraterno do prof. Miguel Gama na Universidade do Minho e orientações, junto ao prof. Bruno Sarmento e à profa. Eliana Souto. A todos do LTEB que me receberam com curiosidade contida, mas de coração

aberto. Em especial à Cecília, que partilhou técnicas e parte do seu tempo em me auxiliar; à técnica Paula pelos treinamentos; e à Magda, que mesmo estando de passagem por lá, me rendeu uma amizade divertida e valiosa.

Na Irlanda, agradeço imensamente a todos os esforços da profa. Lidia em me receber no ápice da pandemia e lidar com todas as burocracias na Trinity College Dublin para que eu tivesse a experiência mais proveitosa possível. Isso foi realizado com o auxílio da Anita, que também me acolheu e ensinou diversas técnicas analíticas, além de outras colegas do departamento. À Verônica, por organizar nossos encontros na fria e chuvosa Dublin, deixando o coração mais aquecido, e à Angélica, por compartilharmos as mesmas experiências em Dublin. Nós conseguimos!

Agradeço à Universidade Estadual de Campinas (UNICAMP) e à Faculdade de Ciências Farmacêuticas (FCF- UNICAMP), pela infraestrutura, apoio e dedicação do dos secretários do Programa de Pós-Graduação (Karen, Gustavo e Renata). Obrigada pelos esclarecimentos e pronta disposição em todas as situações.

Aos laboratórios da FCF, sem os quais esta pesquisa teria rumos mais tortuosos: Ao Laboratório de Ensino e todo o suporte dado pelos técnicos: Débora, Arthur, Matheus e Fernanda. Laboratório de Mecanismo de Sinalização (prof. Jorg), onde desenvolvi os ensaios celulares e tive muitas trocas valiosas com a Fernanda, Ivan e Pedro. Ao LABFAM (profa. Karina), onde pude realizar os ensaios microbiológicos, e à sua aluna Rafaela, com quem aprendi muito mais sobre a vida e amadurecemos juntas. Ao Labiotec (prof. Marcelo e João) pela realização de ensaios microbiológicos. Ao Lafatecs (profa. Priscila), pela amizade, troca de experiências, conhecimentos e equipamentos, em especial à Janaína, Érica, Júlia, Ana Cláudia e Luíza. À colaboração nos ensaios biológicos com a profa. Catarina, Natália e Gabriel.

Ao Laboratório de Biomembranas (Instituto de Biologia, Unicamp), da profa. Eneida, pelo livre acesso à caracterização físico-química das nanopartículas. Agradeço aos seus alunos, pelas trocas de experiências e aos técnicos Érika e Márcio (*in memoriam*).

Ao laboratório do prof. Erich Vinicius de Paula, da Faculdade de Ciências Médicas, Unicamp, pela colaboração facilitada pela Carla, emprestando materiais e equipamento essenciais para a continuidade dos ensaios biológicos.

Agradeço à dedicação dos técnicos dos laboratórios prestadores de serviços: Flávia, do Centro de Microscopia e Imagens (FOP – Unicamp); Paula e Breno, do Laboratório de Microscopia Eletrônica (IB – Unicamp), com o suporte da

Denise e prof. Alexandre; Celso e Eliana, do Laboratório de Recursos Analíticos e de Calibração (LRAC – FEQ - Unicamp); Hugo, do Laboratório de Microscopia Eletrônica (IQ – Unicamp); Mariana, do Laboratório Nacional de Nanotecnologia (LNNano, CNPEM).

Além do suporte emocional e de infraestrutura, esta pesquisa foi realizada com auxílio financeiro concedido pela Fundação de Amparo à Pesquisa do Estado de São Paulo (FAPESP): Bolsa de doutorado (processo 2018/03666-3), Projeto Regular FAPESP (processo 2020/08059-8), bolsas de Iniciação Científica (processos 2019/09719-4 e 2022/05047-4); pela Coordenação de Aperfeiçoamento de Pessoal de Nível Superior - Brasil (CAPES): bolsa de doutorado e Programa Institucional de Internacionalização CAPES (CAPES-PrInt); Conselho Nacional de Desenvolvimento Científico e Tecnológico (CNPq) e Programa de Mobilidade Internacional Santander (edital 31/2018).

Aos membros da banca examinadora, agradeço por aceitarem participar desse momento tão importante em minha vida, contribuindo para o meu desenvolvimento e progresso na qualidade do meu trabalho.

A todos que, direta ou indiretamente, contribuíram para a realização e otimização do meu trabalho: à faxina animada da Jane na FCF; ao restaurante universitário e às feirinhas da Unicamp; aos vendedores e representantes de empresas, pelo meu desenvolvimento em administração de estoques, compras, frustrações e busca de alternativas para solução de problemas. Essas vivências agregaram muito na minha formação.

O presente trabalho foi realizado com apoio da Coordenação de Aperfeiçoamento de Pessoal de Nível Superior - Brasil (CAPES) - Código de Financiamento 001.

RESUMO

As infecções pulmonares, como a pneumonia adquirida na comunidade (PAC), são a maior causa de mortalidade e morbidade no mundo, podendo ser causadas por vírus, bactérias ou fungos. A PAC de origem bacteriana geralmente é tratada por antibióticos β-lactâmicos, macrolídeos, tetraciclina e/ou fluorquinolonas, como levofloxacino (LV). LV possui amplo espectro e é eficaz contra PAC, mas alguns eventos adversos raros, como tendinite e risco de ruptura de tendão tornam seu uso cauteloso. Idealmente, o tratamento da PAC deve combater não apenas o agente etiológico, mas a inflamação alveolar exacerbada decorrente da doença. Nesse contexto, o objetivo desta tese foi desenvolver carreadores lipídicos nanoestruturados (NLCs) para carrear LV por via pulmonar, no intuito futuro de tratar infecções pulmonares localmente, com potencial de reduzir a concentração sistêmica de LV e seus eventos adversos. Para tal, foi realizado estudo de pré-formulação incluindo a solubilidade do fármaco nos excipientes e compatibilidade LV-excipiente, caracterizados por análise termogravimétrica, calorimetria de varredura diferencial, difração de raios-X e espectroscopia no infravermelho. Para otimização da formulação foram avaliados seus parâmetros críticos e de seu processo por análise multivariada, buscando um sistema estável e com alta eficiência de encapsulação (EE) do fármaco. NPLLV_033 foi a formulação otimizada que atingiu as características desejadas (tamanho < 200 nm, polidispersão ≤ 0,3, potencial zeta cerca de −20 mV, EE > 71% e um nível aceitável de produtos de degradação de LV (0,37-1,13%). Porém, a presença das impurezas de LV após a produção do NLC levou ao estudo de outros tensoativos (NPLLV_034, com poloxamer 407 e NPLLV_035, com poloxamer 188). Os três NLCs apresentaram características físicas adequadas, sendo NPLLV_034 e NPLLV_035 com menor degradação de LV. Nos testes biológicos, valores de concentração inibitória mínima (MIC) dos três NLCs foram similares a LV livre, indicando a manutenção da potência do fármaco nas nanoestruturas contra as bactérias testadas (*K. pneumoniae* and *S. aureus*). A viabilidade celular da Calu-3 (linhagem pulmonar) mostrou que LV e NPLLV_034 não reduziram viabilidade em 50 ug/mL. No sistema de *transwell*, com Calu-3 diferenciada, NPLLV_034 foi capaz de reduzir a produção de IL-8 após estímulo de lipopolissacarídeo comparada com LV livre, indicando uma potencial atividade anti-inflamatória da formulação. A determinação da atividade hemolítica das NLCs indicou diferentes concentrações seguras, em ordem de segurança NPLLV_034 > NPLLV_033 > NPLLV_035, podendo ser consideradas seguras para a via de administração pulmonar. A NPLLV_034 destacou-se nos ensaios físico-químicos (maior estabilidade do fármaco) e biológicos, apresentando-se a mais segura e menos citotóxica para Calu-3, com potencial redução da inflamação exacerbada, sendo vantajoso no tratamento de infecções pulmonares.

PALAVRAS-CHAVE: Delineamento experimental; Levofloxacino; Carreadores lipídicos nanoestruturados; Degradação de fármaco; Tensoativos; Calu-3.

ABSTRACT

Lung infections, such as community-acquired pneumonia (CAP), are the leading cause of mortality and morbidity worldwide and can be caused by viruses, bacteria, or fungi. Bacterial CAP is usually treated with β-lactam, macrolides, tetracycline, and/or fluoroquinolones antibiotics such as levofloxacin (LV). LV has a broad spectrum and is effective against CAP, but some rare adverse events such as tendinitis and risk of tendon rupture make its use cautious. Ideally, the treatment of CAP should not only target the etiological agent but also the exacerbated alveolar inflammation resulting from the disease. Therefore, the aim of this thesis was to develop nanostructured lipid carriers (NLCs) to deliver LV via pulmonary route, with the future intention of locally treating lung infections, potentially reducing the systemic concentration of LV and its adverse events. A pre-formulation study was conducted, including drug solubility in excipients and LV-excipient compatibility, characterized by thermogravimetric analysis, differential scanning calorimetry, X-ray diffraction, and infrared spectroscopy. The formulation step involved determining and evaluating critical formulation and process parameters using multivariate analysis for formulation optimization, aiming for a stable system with high drug entrapment efficiency (EE). NPLLV_033 was the optimized formulation that achieved the desired characteristics (size < 200 nm, polydispersity ≤ 0.3, zeta potential around -20 mV, EE > 71%, and an acceptable level of LV degradation products (0.37-1.13%). However, the presence of LV impurities after NLC production led to the search for alternatives to reduce them, resulting in NLCs produced with other surfactants (NPLLV_034, with poloxamer 407, and NPLLV_035, with poloxamer 188), as surfactants play a crucial role as coating agents for nanoparticles, affecting their physicochemical and biological characteristics. The three NLCs exhibited similar physicochemical characteristics as described above, with NPLLV_034 and NPLLV_035 showing lower LV degradation. In the biological assays, the minimum inhibitory concentration (MIC) values of the three NLCs were similar and did not differ from free LV, indicating that the NLC-incorporated drug remained effective against the tested bacteria (*Klebsiella pneumoniae* and *Staphylococcus aureus*). The cell viability of Calu-3 (lung model) showed that NPLLV_034 did not reduced viability at 50 µg/mL.In the transwell system, with differentiated Calu-3 cells, NPLLV_034 was able to reduce the production of IL-8 after lipopolysaccharide stimulation compared to free LV, indicating a potential anti-inflammatory activity of the formulation. Haemolytic activity determination of the NLCs indicated different safe concentrations, in order of safety: NPLLV_034 > NPLLV_033 > NPLLV_035, making them considered safe for pulmonary administration. NPLLV_034 stood out in the physicochemical (greater drug stability) and biological assays, being the safest and least cytotoxic to Calu-3 cells, with the potential to reduce exacerbated inflammation, making it advantageous in the treatment of lung infections.

KEYWORDS: Design of experiments; Levofloxacin; Nanostructured lipid carriers; Drug degradation; Surface-active agents; Calu-3

SUMMARY

1. INTRODUCTION

1.1. Community-acquired Pneumonia (CAP)

Pneumonia is a type of infection that affects the lung alveoli, leading to inflammation that hinders regular pulmonary function and causing difficulty with the exchange of gases (Metlay e Waterer 2020). It can be acquired during hospitalization or in the community. The CAP is the pneumonia developed in the community, and not in the hospital environment. It is the major cause of mortality from infectious diseases worldwide ("Country Profiles" 2016), caused by viruses, bacteria, and fungi, with *Streptococcus pneumoniae* as the main bacterial etiological agent in adulthood and *Mycoplasma pneumoniae* in children ("Causes of Pneumonia | CDC" 2023).

The proportion of viral causes, including respiratory syncytial virus (RSV) and influenza, has been increasing in recent years. Approximately one-third of CAP cases worldwide were viral in 2016, equivalent to around 100 million cases (Cilloniz et al. 2016). The COVID-19 pandemic increased this proportion, with approximately 10% of infections leading to severe pneumonia and prolonged hospitalization, raising the risk of bacterial coinfection or aspiration of oral microbiota ("Community-Acquired Pneumonia in the Era of COVID-19" s.d.). Studies have reported cases of COVID-19 and bacterial coinfection, with most patients receiving antimicrobial therapy upon hospital admission, considering that the bacteria responsible for CAP are similar to those that commonly colonize the upper respiratory tract and therefore may infect the lungs during a respiratory illness (e.g., *S. pneumoniae*, *Haemophilus influenzae*, *Staphylococcus aureus* and *Chlamydia pneumonia)* (Metlay e Waterer 2020).

Although the relationship between the severity and mortality of this disease and coinfections, as well as the sensitivity of the pathogens to antimicrobials used, has not yet been fully explored, there is a guideline treatment for low and high-risk inpatients. For the low risk, it is recommended a β-lactam (e.g., ampicillin-sulbactam, ceftriaxone or cefotaxime) and a macrolide (azithromycin or the clarithromycin) or doxycycline as combination therapy or a monotherapy with a respiratory fluoroquinolone (levofloxacin or moxifloxacin). For the high risk, the recommendation is the treatment with a β-lactam plus macrolide or β-lactam with a fluoroquinolone. (Cox et al. 2020; Torrego et al. 2020; Metlay e Waterer 2020).

As the pneumonia conducts to an inflammatory response, it would be interesting that the treatment eradicates the pathogen and also regulates the exacerbated lung inflammation.

1.2. Levofloxacin

Levofloxacin (LV, Figure 1) is a broad-spectrum fluoroquinolone antibiotic used to treat a variety of bacterial infections (Liu 2010), and is effective in treating pneumonia. It is commonly included in guidelines for severely illness or intensive care unit's patients. It is available for oral, intravenous, and eye drop administration, and the most common side effects of LV are nausea, diarrhoea, and difficulty sleeping (Noel et al. 2007). Some major side effects may include tendon rupture and inflammation, seizures, psychosis, and potentially causing permanent damage to the peripheral nerve (Hall, Finnoff, and Smith 2011). LV is active against both gram-positive and gram-negative bacteria, and like other quinolones, its mechanism of action occurs by inhibiting prokaryotic topoisomerase II (DNA gyrase) and topoisomerase IV , which are fundamental for DNA replication and transcription (Yacouba, Olowo-okere, e Yunusa 2021; Nightingale, Grant, e Quintiliani 2000). Fluoroquinolones also have been studied by virtue of their potential antiviral activity against DNA and RNA viruses (Richter et al. 2004; Yacouba, Olowo-okere, e Yunusa 2021).

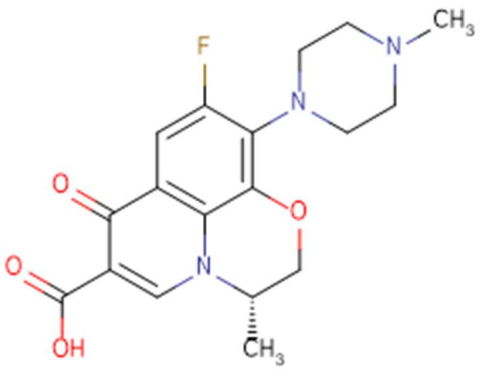

LV: light yellow powder

Molecular weight: 361.4 g/mol

Melting point: 225 – 225 °C

Solubility: freely soluble in glacial acetic acid and chloroform; sparingly soluble in water

LogP: 2.1

pKa: 8.1 (basic) and 6.1 (acidic)

Figure 1. Representation of chemical structure and main physicochemical characteristics of levofloxacin (From Pubchem).

While there is no conclusive evidence of its effectiveness against Covid-19, the Chinese therapeutic regimen recommends the use of fluoroquinolones in cases of

confirmed viral pneumonia, as severe cases are believed to be highly susceptible to bacterial coinfection. LV's high efficacy against pneumococci and its anti-inflammatory action, which inhibits the dimerization of TLR4, a receptor responsible for triggering relevant inflammatory signalling in bacterial and viral infections, makes it a potential treatment option. Additionally, in vitro studies have shown that LV can reduce the production of IL-6 and IL-8 in lung cells (Tsivkovskii et al. 2011). Besides, this immune-modulatory activity of the fluoroquinolones reducing the cytokine response is essential to prevent the development of the cytokine storm syndrome (Yacouba, Olowo-okere, e Yunusa 2021). However, due to the side effects of fluoroquinolones, such as arthralgia, tendon rupture, or neuropathies, they are not recommended for mild cases of pneumonia. It is also contraindicated to use LV with substances that increase the cardiac QT interval, such as azithromycin, according to the medication's label.

The use of LV nanoparticles for drug delivery has yielded positive outcomes in various studies. Anionic liposomes loaded with LV demonstrated prolonged drug release, retained antibacterial activity against *Pseudomonas aeruginosa*, remained stable in nebulization, and were able to effectively deposit in the deep lung area where the infection resides (Derbali et al. 2019). LV-loaded PLGA nanoparticles also displayed sustained release for up to 120 hours in simulated lung fluid (Nightingale, Grant, e Quintiliani 2000). Additionally, NLCs containing LV exhibited good encapsulation efficiency (56 ± 2%), controlled release profiles, antimicrobial activity against *Pseudomonas aeruginosa* and *Staphylococcus aureus*, and reduced bacterial biofilm formation, being a valuable strategy to cystic fibrosis treatment (Islan et al. 2016). Nevertheless, this study did not run a quantitative antimicrobial analysis to compare with the literature outcomes, e.g., the minimum inhibitory concentration. The lack ok cell viability analysis did not guarantee that their formulation is safe or stimulate an inflammatory process when delivered to the lungs. Therefore, our approach brought along new perspectives to cover the gaps regarding a deep nanoparticle evaluation, Calu-3 cell viability and haemolytic activity, together with the anti-inflammatory activity evaluation of the formulation.

1.3. Drug delivery systems

The increasing prevalence of antibiotic-resistant bacteria has created a significant need for improving drug delivery to the site of action, which could improve

the treatment by increasing drug efficacy. One promising strategy is the development of micro/nanostructured carriers, which can improve drug delivery, protect the antibiotic from degradation, and potentially prevent side effects that are concentration-dependent (Abed e Couvreur 2014). Liposomes have increased the therapeutic index of antibiotics via systemic administration by reaching infected intracellular compartments and allowing combination therapy. However, these formulations have some disadvantages, such as the instability of the vesicles, as they are dynamic and can disintegrate or release content rapidly when compared to other nanocarriers (Abed e Couvreur 2014; Sharma e Sharma 1997).

Nanoformulations have shown promise in improving the delivery of antibiotics and overcoming issues of instability seen with liposomes (Fattal, Rojas, Roblot-Treupel, et al. 1991; Fattal, Rojas, Youssef, et al. 1991). Polymeric nanoparticles have been successful in carrying antibiotics such as β-lactams and ciprofloxacin, resulting in better antimicrobial activity compared to free drugs (Page-Clisson et al. 1998). However, complete eradication of infections has not been achieved, likely due to the presence of bacteria that are less sensitive to treatment (Garcia et al. 2013). The use of biodegradable polymers such as poly (lactic-co-glycolic acid) (PLGA) is a thriving strategy, as they offer desirable properties such as safety, biodegradability, sustained drug release, and targeting of specific organs. These biomaterials can degrade within the body through enzymatic or non-enzymatic processes, producing safe and compatible by-products, which are eliminated from the organism through its natural physiological pathways (Mir, Ahmed, e Rehman 2017).

The lipid nanocarriers are low-toxicity colloidal systems with the ability to carry mostly lipophilic molecules, sustain drug release, and scalability (Müller, Radtke, e Wissing 2002) . Solid lipid nanoparticles (SLNs) have been developed to deliver drugs for tuberculosis treatment with high efficacy *in vivo*. SLNs have also been used to encapsulate other antibiotics such as tilmicosin, gatifloxacin, and norfloxacin (Abed e Couvreur 2014). Furthermore, multiple emulsions (w/o/w) prepared SLNs allow encapsulating both hydrophobic and hydrophilic drugs, minimizing stress on drug molecules (Fangueiro et al. 2012).

The Nanostructured Lipid Carriers (NLCs) differ from Solid Lipid Nanoparticles (SLNs) in that they contain at least one oil in their lipid matrix, in addition to the solid lipid and surfactant dispersed in an aqueous medium. This results in

reduced lipid matrix crystallinity, which increases encapsulation efficiency and reduces drug expulsion during storage (Saupe et al. 2005).

To achieve positive results such as eliminating pathogens and promoting quick patient recovery, it is crucial for antimicrobials to reach the infection site effectively. Some classes of antibiotics, such as β-lactams and aminoglycosides, have restricted cellular penetration due to their high hydrophilicity. On the other hand, although fluoroquinolones and macrolides diffuse well into cells, they have low intracellular retention. In addition, the subcellular distribution of antibiotics is not uniform, and therefore there are significant differences depending on the specific antibiotic considered (Tulkens 1991; Kuti e Nicolau 2015).

Lipid nanocarriers are effective systems for delivering drugs to the lower respiratory tract due to their small particle sizes, which result in high drug accumulation and diffusion (Jaques e Kim 2000). Lipophilic constituents of NLCs contribute to their enhanced bioadhesive properties and sustained release behavior (Patlolla et al. 2010). Several studies have shown that nebulized NLCs can effectively deliver drugs to the deep respiratory tract and treat pulmonary diseases such as aspergillosis, tuberculosis, and pulmonary hypertension (Pardeike et al. 2016). Controlled release behavior, suitable aerodynamic diameter, and constant plasma levels have been reported in pharmacokinetics studies of NLCs. NLCs have also been found to avoid macrophagic clearance when their particle sizes are less than 260 nm (Elmowafy e Al-Sanea 2021; Lauweryns e Baert 1977).

All the presented nanocarriers are prepared in a liquid suspension, stabilized by surfactants. These excipients generally have no biological activity, but their broad range of types and structures may implicate not only in different stability capacity but also in different presentation of a nanomaterial to the body, leading to protein interactions or increased toxicity, for example, and therefore need to be carefully studied when formulating a nanocarrier.

1.4. Surfactants

Surfactants are amphiphilic compounds containing hydrophilic and hydrophobic groups. There are four types of surfactants based on the characteristic of their hydrophilic charge group: cationic, anionic, zwitterionic, and nonionic surfactants. Each type has specific properties and applications. Nonionic surfactants have the

advantage of low toxicity and are frequently used in nanomedicine and food nanotechnology. The toxicity of surfactants generally correlates with their ability to migrate to cell membranes, with longer chain lengths and higher hydrophobicity being more toxic. (Miyazawa et al. 2021).

In a single-phase system, surfactants are dispersed and equilibrated in the bulk, while in a multi-phase system, they stabilize the interface between different phases due to their amphipathic chemical structure. The surfactants initiate their interactions and self-assemble into various supramolecular structures like bilayer membrane vesicles, lamellar phases, spherical or cylindrical micelles, etc., depending on the modification of various conditions such as pH, temperature, pressure, electrolyte concentration, and type of solvent. The hydrophilic-lipophilic balance (HLB), indicating the affinity of the surfactant for water and oil, and the critical packing parameter (CPP), predicting the surfactant's self-assembly, are used to predict the properties of the surfactant (Miyazawa et al. 2021).

Surfactants are primarily used in pulmonary drug delivery to enhance absorption, although the exact mechanisms involved are not fully understood yet. In addition, surfactants are also utilized in various other approaches to improve the delivery of inhaled drugs (Morales, Peters, e Williams 2011).

The main non-ionic surfactants are polysorbate 80 (P80), poloxamer 407 (P407) and poloxamer 188 (P188). Their main characteristics are described on Table 1.

Table 1. Chemical structure and main characteristics of the non-ionic surfactants polysorbate 80, poloxamer 407 and poloxamer 188.

	Polysorbate 80	**Poloxamer 407**	**Poloxamer 188**
Chemical structure	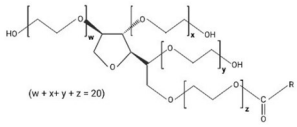 *	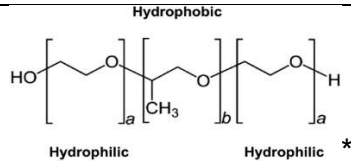 **	
	w + x + y + z = 20	a = 101; b = 56	a = 76; b = 30
Molecular weight (g/mol)	604.8	~12,600	~8400
HLB	15	22	29

* (Cortés et al. 2021)

** (Foligno et al. 2020)

In pulmonary drug delivery, the lungs offer advantages such as avoiding the gastrointestinal environment and reducing first-pass metabolism of drugs, allowing for local and systemic effects. However, there are barriers to drug absorption such as the epithelial and capillary cell barrier and surfactant layer. To overcome these barriers, decreasing particle size and using surfactants at the interface is a useful tool in drug delivery (Morales, Peters, e Williams 2011). Nonionic surfactants, like P80 and P407, have been used to modify drug absorption in the lungs. This combination has increased the lung area under the curve of itraconazole particles up to nine times without pro-inflammatory components. Similarly, PEG and PVA have been used to stabilize sebacic acid particles obtained by an emulsion method. P188 also can be used to stabilize inhalable particles and prevent the absorption of proteins and peptides, which can lead to surface erosion at the air-liquid interface of droplets (Cortés et al. 2021). It is also related that, after nebulization in mice, there were no signs of inflammation or pulmonary histology changes, and there was no association with the production of proinflammatory cytokines when using P407 and P80. (Cortés et al. 2021; Tang e Alavi 2011).

1.5. Calu-3 as a model for *in vitro* pulmonary assays

The assessment of potential treatments and comprehension of a pathogenesis begin with *in vitro* models. These models have been useful in the development of new drugs, with cell line assays playing an important role. The choice of a cell line depends on the administration route and the main organ that will be affected by the treatment. It is crucial that the *in vitro* models represent and express certain characteristics that will be evaluated (for example, proteins expression or cytokines secretion) (Woodall et al. 2021).

Calu-3 is a human lung adenocarcinoma cell line that, together with A549, is very useful to recreate an *in vitro* alveolar model to test formulations candidates to treat lung infections. But, unlike Calu-3 cells, A549 cells cannot establish functional tight junctions, which makes them unsuitable for conducting in vitro permeability studies (Bol et al. 2014).

Although these immortalised cell cultures are simple to acquire and yield reproducible results, the conventional submerged culture techniques do not have the necessary cell polarization or other characteristics unique to the lung, such as mucus,

transport proteins, and motile cilia. However, the use of air-liquid interface (ALI) culture techniques have allowed to develop a superior model for *in vitro* epithelial models using immortalized or primary airway epithelial cells (Woodall et al. 2021) (Figure 2).

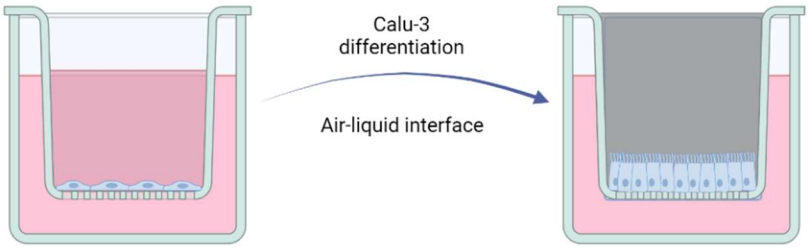

Figure 2. Representation of transwell insert with Calu-3 and cell culture medium in the basolateral and apical compartments (left side) and differentiated Calu-3 in the transwell with the air-liquid interface, with culture medium only in the basolateral compartment (right side). (Created in **BioRender.com**).

The ALI cell culture platform provides a practical and physiological *in vitro* model, considered the gold standard for preclinical airway epithelial model systems (Karp et al. 2002). In this method, cells are grown on semipermeable membranes and exposed to air from the apical side while receiving a basolateral medium supply in a humidified environment (~ 90 %). When exposed to air, the epithelial progenitor cells undergo differentiation into various specialized cell types, including pseudostratified ciliated, goblet and basal. It is related a strong correlation between differentiated epithelium (after 28 days in the ALI condition) and epithelial cells obtained from the original nasal brushing, with a transcriptional profile similarity higher than 96 % (Ghosh et al. 2020).

The ALI system provides two main advantages: it enables accurate and functional outcomes of airway physiology, including measurements of ciliary movement, mucociliary clearance, membrane current or voltage, protein secretion, airway surface liquid height, ion transport, and wound healing; and it can generate airway epithelial cell culture models from any donor, allowing for the representation of various human phenotypes (Woodall et al. 2021).

The dosage of cytokines secretion is a useful tool to predict physiological outcomes after stimulating the cells with different treatments. The IL-8 is a proinflammatory cytokine that acts as a chemoattractant and is produced and secreted by different cells in blood and tissues. Differently from other cytokines, IL-8 targets with

a certain specificity the neutrophils, attracting and activating them in areas of inflammation (Bickel 1993).

Since the secretion of inflammatory cytokines can potentially be altered after introducing a nanomaterial into the bloodstream (Guo et al. 2021), it is important to evaluate this profile changes *in vitro*. Calu-3, as a good pulmonary cell model that is able to secrete IL-8, is an advantageous choice to assay new drug delivery systems designed for pulmonary delivery, evaluating its response to the exposition of a pulmonary infection or injury (Darweesh e Sakagami 2018).

The nanoparticles surface exerts a great influence on the inflammatory response of the organism. Since it is usually coated by surfactants, it is interesting to study how they affect the inflammatory profile: The presence of P407 was found to be associated with a decrease in the inflammatory properties of microspheres, whereas the chitosan formulation coated with P80 resulted in a reduction in the secretion of IL-6 and TNF-α. Additionally, the impact of various surfactants on the cytotoxicity and cytokine production of solid lipid nanoparticles was investigated (Jackson et al. 2000; Elmowafy et al. 2020; Schöler et al. 2002).

1.6. Thesis proposal

Considering the broad spectrum of LV and effectiveness against PAC, the purpose of this thesis was to develop NLCs to deliver LV topically to treat pulmonary infections, avoiding its high systemic concentration and major side effects, and pursuing the enhancement of the drug mucopenetration.

The thesis is structured in three chapters, followed by a discussion and conclusion. In the Chapter 1, we described the predominant physicochemical techniques applied to characterize a nanomaterial. The chapter integrates a Book Chapter written by our lab group, intituled “Physicochemical Characterization of Drug Delivery Systems based on nanomaterials” and accepted for publication in Molecular Pharmaceutics and Nano Drug Delivery: Fundamentals and Challenges, edited by Umesh Gupta and Amit K. Goyal (Academic Press, 2023, ISBN 9780323919241).

In the Chapter 2, we presented our published research paper (Beraldo-Araújo et al. 2022), which is comprised by the main research done to obtain an appropriate nanocarrier to deliver LV. In this chapter, we described the step-by-step to select the best excipients to produce LV-loaded NLCs. Then, we run two designs of

experiments (DoEs): one to determine the amounts and proportions of excipients to compose NLCs; and a second one, where we changed process parameters to improve the outcomes reached in the first DoE, avoiding high LV degradation product production (levofloxacin N-oxide). Then, solid state analyses were run. Two drug release studies were performed to compare LV released in different systems (Franz diffusion cells and directly in PBS buffer). Some alternatives were proposed to avoid levofloxacin N-oxide production, e.g., freeze-drying of formulation and/or including an antioxidant agent to the formulation.

Finally, in the Chapter 3, we showed the application of the chosen formulation, to study its behaviour faced by the antimicrobial activity, haemolytic activity, Calu-3 cell viability and ability to inhibit the secretion of IL-8. In this chapter, we did not run only the best NLC reached in Chapter 2, but also compared the same carrier changing the surfactant: using not only P80, but also P407 and P188, totalling 3 NLCs with one surfactant each (named NPLLV_033, NPLLV_034 and NPLLV_035, respectively). This approach led to interesting results, and a new worthwhile NLC according to their biological outcomes: P407 appeared to be the most promising surfactant. All the further experiments were conducted with NPLLV_034, which exhibited antimicrobial activity similar to the free LV, less toxic to Calu-3 and a potential ability to reduce the secretion of the investigated proinflammatory cytokine, IL-8.

In this thesis, we successfully achieved a nanostructure that exhibited remarkable physicochemical characteristics. NPLLV_034 improved drug stability, with minimal degradation of LV, and showed excellent safety with low cytotoxicity towards Calu-3 cells. Furthermore, it displayed potential in reducing exacerbated inflammation stimulated by lipopolysaccharide, making it a promising candidate for future studies focusing on the treatment of lung infections.

2. CHAPTER 1 - PHYSICOCHEMICAL CHARACTERIZATION OF DRUG DELIVERY SYSTEMS BASED ON NANOMATERIALS

2.1. Authors

Viviane Lucia Beraldo de Araújo, Victória Soares Soeiro, Marcelo Van Vliet Lima, Juliana Souza Ribeiro Costa, Laura de Oliveira-Nascimento.

Faculty of Pharmaceutical Sciences, State University of Campinas, SP, Brazil.

This chapter is part of the submitted book chapter for the entitled book “Molecular Pharmaceutics and Nano Drug Delivery: Fundamentals and Challenges”, from Elsevier.

2.2. Abstract

Drug delivery systems gain better or new performance attributes upon nanostructuration of Active pharmaceutical ingredients (API). Nanomaterials (NM) and related fabrication processes may change API physical and chemical properties. NM dimensions and composition may also change API release rate and region. Therefore, a throughout physicochemical evaluation must be undertaken to assess API stability and release mode, nanomaterial safety regarding impurities, NM related quality attributes and manufacturing reproducibility. This chapter focus on thermal, spectroscopic, x-ray and microscopy-based techniques, relating standards and general applications for nanomedicines to evaluate morphology, composition, surface and dimensional properties.

2.3. Keywords

nanoparticle, drug delivery system, API, physicochemical characterization, drug release, nanomaterial.

2.4. Introduction

Active pharmaceutical ingredients (APIs) can be formulated in a variety of dosage forms and administered by many routes. This flexibility happens if excipients in the formulation fulfill physical, chemical, and biological requirements to allow the pharmacological effect to take place. Among powders, pastes, gels, liquids and patches, the formulation must sustain API stability and promote its local or systemic delivery. In turn, organoleptic and manufacturing aspects also depend on the set of ingredients. The simple content list is not enough to vehicle an active molecule: excipients must go through extensive characterization concerning chemical and physical aspects of the molecule, bulk material, and API compatibility (Dave 2019).

Nanostructuration may enhance API properties or enable a new one. A broad range of nanosized dosage forms have been developed and some of them already became drug products. The commercial types include nanocrystals, nanoemulsions, dendrimers, polymeric nanoparticles, lipid-based nanoparticles, dendrimer and iron-based ones (Figure 1). Besides material diversity, there are also a variety of processes, from bottom up to top down nanostructuration, which employ high or low energy mixing methods, precipitation, centrifugation, comminution and sculpturing steps, among others (Halwani 2022).

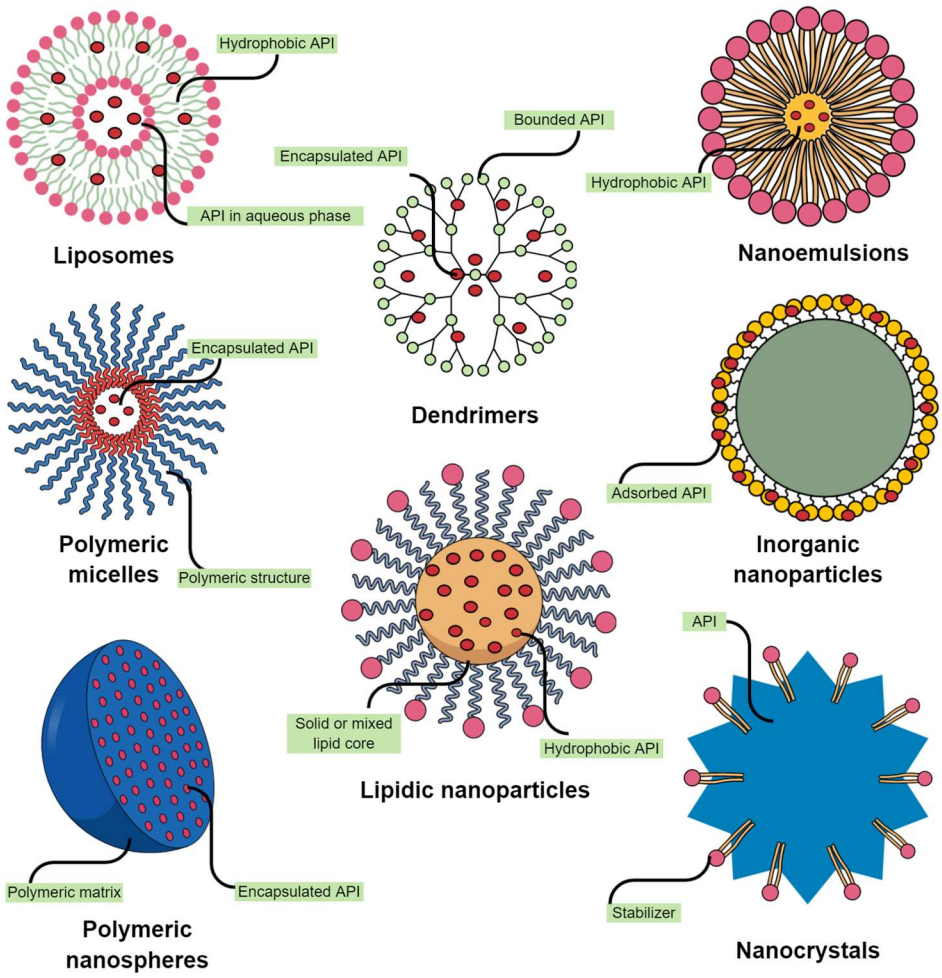

Figure 1. Examples of particulate nanostructures for API delivery. **Liposomes:** vesicles formed by a hydrophobic lipid bilayer and a hydrophilic aqueous core with a nanometric size. **Polymeric micelles:** an aqueous core surrounded by an amphiphilic copolymer shell. **Polymeric nanospheres:** a solid hydrophobic and polymeric nucleus or a hydrated nucleus of crosslinked hydrophilic polymers, possibly with an excipient to stabilize the colloid (stabilizer). **Dendrimers:** branched polymeric molecules that can carry API by loading or crosslinking. **Lipid nanoparticles:** a solid or mixed lipid core surrounded by stabilizers (nanostructured lipid carrier - NLC, solid lipid nanoparticles - SLN), but also structures with a lipid monolayer shell, surfactants and internal lipid vesicles. **Nanoemulsions:** metastable dispersions of immiscible phases joined by surfactant molecules. **Inorganic nanoparticles:** solid inorganic cores surrounded by stabilizers. **Nanocrystals:** API crystal cores separated by stabilizers.

Even nanomaterials with the same chemical composition but with a different shape or internal structure bring the possibility of a different physicochemical stability, pharmacological performance, or toxicity/environmental impact. Thus,

physicochemical characterization remains an essential milestone that drives risk assessment and precede efficacy studies of nanomedicines. To harmonize concepts and techniques, several institutions around the world publish standard documents and guidelines for nanostructures. The International Organization for Standardization (ISO), the Organization for Economic Cooperation and Development (OECD), the American Society for Testing and Materials (ASTM), and others have specific projects concerning nanomaterials, regardless of their use. The European Medicines Agency (EMA), the Food and Drug administration Agency from USA (FDA) and other health governmental agencies have committees focused on nanomaterials related with health products, including API delivery (which includes drug delivery).

As with any other pharmaceutical product, characterization of nanomedicines evaluates the critical quality attributes defined for the intended route of administration, dosage form and specific properties of each composition. In 2022, the United States Pharmacopeia (USP) released a general chapter of “drug products containing nanomaterials” (USP 2022) that defines structures and list quality attributes. Figure 2 relates general quality attributes of nanomaterials, as described by the USP and FDA (FDA/CDER/"Yeaton 2017). Obviously, size is an essential parameter since it defines if the material has nanosized dimensions. However, some measurement techniques rely on mathematical models that assume a certain shape, which requires the previous assessment of NM morphology. Size has been related with NM cell uptake, interaction, biodistribution, plasma half-life and clearance outcomes (Hoshyar et al. 2016), apart from drug solubility and colloidal stability.

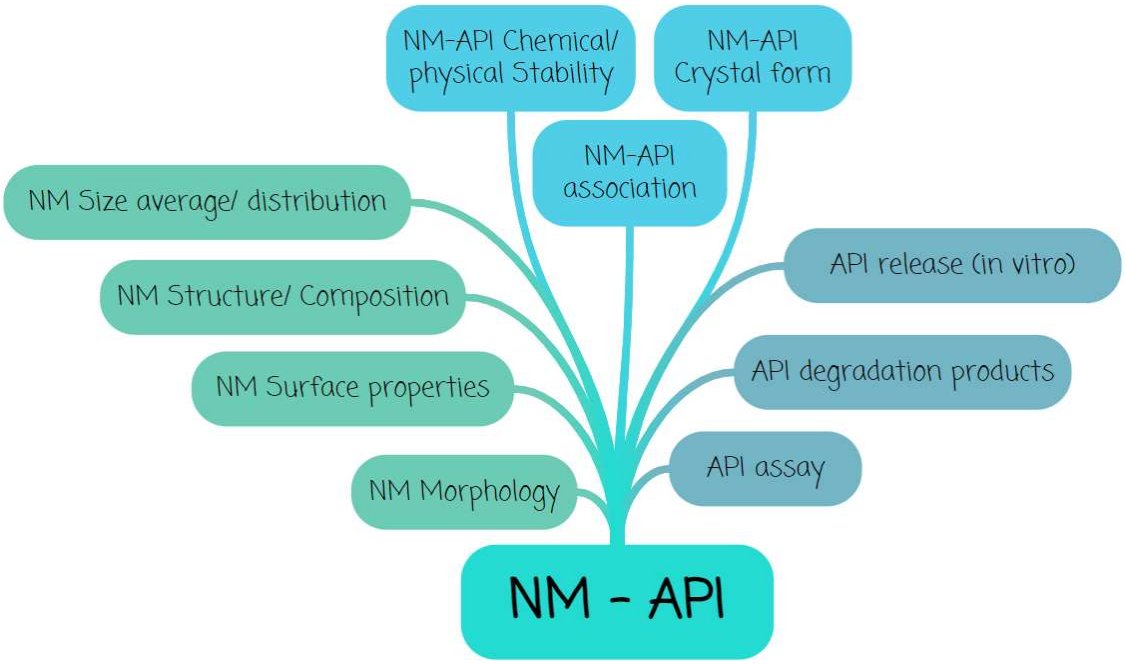

Figure 2. General attributes of Nanomaterials (NM) associated with Active Pharmaceutical Ingredients (API) in medicines.

The NM organization and chemical features can dictate its physiological role, as pointed before, but also determine the type of physicochemical analysis and stability concerns. Nanomaterial composition should be described by its individual ingredients, such as polymer identity/molecular weight, but also by its structure, such as multilamellar vesicles, coated material, or crystalline content. In turn, the material surface contains valuable information for delivery systems. Surface topography, charge and coating type, when present, influence carrier properties: the charge and coating modify NM interaction with cell membranes and physiological media, what may change targeting, toxicity and clearance properties. Coating can provide cargo protection and retention in the way to the desired release site. Regarding formulation stability, charge do influence colloidal stability of dispersions and flow properties of solid bulk material.

Once in the body, another key point is how the active molecules will be related to the carrier though time and different body compartments. Dissolution/release *in vitro* assays can screen batch to batch inconsistencies that may bring changes in pharmacokinetics; furthermore, they can even predict the resultant API in vivo release and stablish an in vitro/in vivo correlation.

Although there are more properties that can be evaluated, this chapter will focus on the USP listed general attributes, so the reader can have a broader understanding. Each property can be assessed by more than one method; however, only a few are described in the guidelines. Standardization is paramount to reproducibility and interlaboratory/company robustness, in addition to offer proper product comparisons. Another important aspect of using standard methods comes from the need of accurate data to support manufacturing, toxicological, clinical, and environmental studies. So, this chapter will concentrate on techniques that are standardized by at least one of the previously cited institutions. Due to the stated relevance of physicochemical analysis, techniques will be briefly discussed in the next topics. They were organized by attribute and specific literature is related on the reference section. For an overall glance, table 1 relates the techniques to evaluate nanostructured API attributes that has a standard protocol published by ISO or ASTM. Both are rich and tested sources of protocols and specific information for test application, comparison and good practices.

Table 1. Techniques standardized by ASTM and ISO that address directly NM attributes applicable to API nanostructuration.

Technique	Atribute	ASTM guidelines	ISO guidelines
AFM (Atomic force microscopy)	Structure-morphology	**E2859-11(2017)** Standard Guide for Size Measurement of Nanoparticles Using Atomic Force Microscopy	**ISO 13095:2014** Surface Chemical Analysis — Atomic force microscopy — Procedure for in situ characterization of AFM probe shank profile used for nanostructure measurement
Asymmetrical -flow (AF4) and centrifugal (CF3) field-Flow Field Fractionation	Size/ NM concentration/ chemical composition (various detectors)	X	**ISO/TS 21362:2018** - Nanotechnologies — Analysis of nano-objects using asymmetrical-flow and centrifugal field-flow fractionation
Brunauer–Emmett–Teller method (BET)	Surface – area, porosity	X	**ISO/TS 17200:2020** Nanotechnology — Nanoparticles in powder form — Characteristics and measurements

Technique	Atribute	ASTM guidelines	ISO guidelines
Cryo-Transmission Electron Microscopy (Cryo-TEM)	Structure-morphology	**E3143-18b** Standard Practice for Performing Cryo-Transmission Electron Microscopy of Liposomes	X
DC (Circular Dichroism)	Structure (protein-based)	X	**ISO/TS 23459:2021** Nanotechnologies — Assessment of protein secondary structure during an interaction with nanomaterials using ultraviolet circular dichroism
Dynamic Light Scattering (DLS)	Size	**E2490-09(2021)** Standard Guide for Measurement of Particle Size Distribution of Nanomaterials in Suspension by Photon Correlation Spectroscopy (PCS**); E3247-20** Standard Test Method for Measuring the Size of Nanoparticles in Aqueous Media Using Dynamic Light Scattering	**ISO 22412:2017**- Particle size analysis — Dynamic light scattering (DLS); **ISO/TR 22814:2020** - Good practice for dynamic light scattering (DLS) measurements
Electroacoustic spectroscopy	Surface – charge	X	**ISO 13099-3:2014** Colloidal systems — Methods for zeta potential determination — Part 3: Acoustic methods
Inductively Coupled Plasma mass Spectrometry (ICP-MS)	Size, NM concentration, chemical composition (inorganic NM)	X	**ISO/TS 19590:2017** Nanotechnologies — Size distribution and concentration of inorganic nanoparticles in aqueous media via single particle inductively coupled plasma mass spectrometry
Nanoparticle Tracking Analysis (NTA)	Size/ NM concentration	**E2834-12(2018)** Standard Guide for Measurement of Particle Size Distribution of Nanomaterials in Suspension by Nanoparticle Tracking Analysis (NTA)	X
Scanning Electron	Size/ shape /morpholo	X	**ISO 19749:2021** Nanotechnologies — Measurements of particle size

Technique	Atribute	ASTM guidelines	ISO guidelines
Microscopy (SEM)	gy/ chemical composition		and shape distributions by scanning electron microscopy
Static Multiple Light Scattering (SMLS)	Size/ NM concentration	X	**ISO/TS 21357:2022** Nanotechnologies — Evaluation of the mean size of nano-objects in liquid dispersions by static multiple light scattering (SMLS)
Transmission Electron Microscopy (TEM)	Size/ shape/ morphology	X	**ISO 21363:2020** - Nanotechnologies — Measurements of particle size and shape distributions by transmission electron microscopy
X-ray diffraction (XRD)	Crystal properties	X	**ISO/TS 17200:2020** Nanotechnology — Nanoparticles in powder form — Characteristics and measurements
Zeta potential (Electrophoretic Light Scattering)	Surface-Charge	**E2865-12(2018)** Standard Guide for Measurement of Electrophoretic Mobility and Zeta Potential of Nanosized Biological Materials	**ISO 13099-2:2012** Colloidal systems — Methods for zeta-potential determination — Part 2: Optical methods

Source: ASTM and ISO websites. **OBS:** “ISO/TR 18196:2016 Nanotechnologies — Measurement technique matrix for the characterization of nano-objects” describes several other methods, such as thermal and spectroscopy characterization, relating applicable standards that were not made for NM but are applicable to them. This table did not include specific Carbon nanotube protocols because of its scarce use as drug delivery tool. In vitro assessments with cells were not included. Standards have a life-cycle, so always check if there is a newer version on the institution sites.

2.5. NM shape / morphology

NMs assume various shapes, with different assemblies like multivesicular units or solid cores with a fluid corona. It is essential to characterize their morphology to predict and comprehend API dynamics and biological interactions, which include

cellular uptake, API release, surface-binding capability, “asbestos-like” behaviour, etc. From the analytical point of view, several techniques rely on mathematical models based on spherical particles, so shape will influence the choice of method for NM size distribution (Pettitt e Lead 2013; Faria et al. 2018).

The assessment of NM morphology depends on the sample state (dry or wet), conductibility and particle sensitiveness to the technique. Shape characterization is mainly obtained from high-resolution microscopy techniques, providing meticulous and direct information on the NM morphology. They are settled in the interaction between the NM atomic structure with the scanning probe (AFM), or the impinging electron beam. The electrons provide a relatively superficial scanning (SEM) or a more in-depth analysis in the transmission mode through ultrathin samples (TEM), providing information towards the physical dimension of a NM particle size, shape and structure. AFM provides the same type of information, in addition to surface texture (USP 2022).

The classical electronic microscopy (TEM/SEM) is widely used, with the requirement of fixed, dehydrated and conductive samples. Drying liquid samples can lead to NM agglomeration or aggregation, which alters shape information. For beam-sensitive or non-conducting NMs, they generally need a coating (platinum, gold or graphite) or staining (especially TEM) before imaging. Coatings enhance brightness and contrast at the expense of changes in shape, size and surface-texture. One more limitation of these techniques relates to the single-particle evaluation in a very small sample quantity, which turns questionable the representativeness of the data and its statistical relevance in the evaluation of batch homogeneity. Besides coating and staining downsides, images must be carefully interpreted since artefacts could modify the imaging of the NPs, such as crystals related to buffer drying (Caputo et al. 2019).

Nevertheless, electron microscopy evolved considerably. As an example, SEM can be configured with an ultra-high resolution field emission setup (FE-SEM) that can drastically reduce the accelerating voltages and increase spatial resolution. This feature reduces charge accumulation in the sample, but may still need coating and dehydration. As most nanosized medicines are vehicled as suspensions, vitrification of samples in amorphous ice by cryogenic techniques became a great choice: samples freeze very quickly and resembles the liquid spatial distribution. The coating over the frozen sample gives a more accurate shape description. Several drug products are evaluated by Cryo-EM, specially liposomes (“Standard Practice for

Performing Cryo-Transmission Electron Microscopy of Liposomes" s.d.). Of note, the cryogenic setup is more expensive and still scarce in analytical laboratories.

The AFM gives 3D analysis of NMs with a nanometric topographic resolution and also some mechanical properties. It is a good tool to directly image NMs and works also on samples rich in water (USP 2022). On the other hand, AFM has a few contrast materials and lack other options offered by SEM. It can also be difficult to perform AFM for samples that are not well attached to a surface and can be displaced by the AFM tip (Modena et al. 2019).

2.6. Size average, distribution, and NM concentration

Size can be measured in the nano range through equipment and methods based mainly on laser-light scattering/diffraction, EM and physical separation followed by detection of a NM property. Microscopy methods allow particle visualization and consequent shape assessment with absolute number description, whereas laser-based methods depend on mathematical models related with the particle shape for size determination. Physical separation happens mainly through analytical ultracentrifugation (AUC), field flow fractionation and gel permeation (GP), with the former also relying on shape models (¨perfect sphere¨) and the latter on comparison with model particles.

The analytical choice comes from equipment availability, capability to detect and characterize the NM in the specific size range; sample characteristics (amount, composition, and physical state) and intended use of data (formulation characterization, production in-line, at-line, offline control). It should also be accounted that a method may impose drying, dilution and other sample modifications that might alter the NP original attributes (USP 2022). For example, organic NM may be subjected to substantial changes in size in the wet and dry states, leading to minor dimensions measured by EM in dry matter than the ones measured in liquid state by Dynamic Light Scattering (DLS) (Faria et al. 2018). For this reason, it is important to report the "type" of size measured (e.g., hydrodynamic versus projected particle radius, ensemble versus single particle analysis) and the NP state (dry or wet). The USP chapter also recommends the use of complementary methods when the measured attribute is critical (for example, performing DLS and EM analyses) (USP 2022).

The same microscopy methods used for shape determination apply to size evaluation, but they require higher training/ cost/ time requirements than scattering techniques and may take several samples to determine a reliable size distribution. In particular, AFM precisely gives the particle size and shape, even in a polydisperse sample. The disadvantage of AFM is that the number of NMs analysed is smaller than that from DLS, and it is important to critically evaluate the results to avoid under/overestimation of the total sample size distribution (Bhattacharjee 2016).

Light scattering techniques (DLS and Nano Tracking Analysis - NTA) are low/medium cost techniques, easy to manipulate, require little sample preparation and provide screening analysis with a fast check of the sample, but with low-resolution results. DLS helps especially when biological interactions are pursued (e.g., protein corona) and it is the first choice for quality control for most nanostructured drug products (Maguire et al. 2018; Caputo et al. 2019). DLS can measure the hydrodynamic size and distribution of NM based on intensity, determining the fluctuations in the intensity of light scattering from NMs in Brownian motion. For that, the software assumes that NM has a spherical shape, and the sample viscosity and refractive index is known. Since scattering intensity is much higher for bigger particles, polydisperse samples can present higher size averages. One more concern is with particle aggregation state: the method does not distinguish between larger particles and small aggregates. However, in purified samples with known particle individual, such as protein solutions, DLS does provide aggregation kinetic profiles (Caputo et al. 2019; USP 2022).

NTA has a number-based measurements of size, which allows to distinguish different populations in a polydisperse sample and gives a more reliable size distribution than DLS. It also complements DLS measuring by giving the NM concentration in the sample (number of particles per mL) (Maguire et al. 2018). Since NTA requires lower NM density (10^8 to 10^{12} particles/mL and 10^7 to 10^9 particles/mL, respectively), it has better resolution than DLS, being less susceptible to the influences of high intensity scattering from bigger NMs. But, it is more expensive than DLS equipment and may require extensive sample dilution, together with a more complicated sample insertion in the equipment (Bhattacharjee 2016).

Part of the uncertainty brought in DLS measurements of polydispersed samples comes from the high sensitivity to bigger nanoparticles. Data acquisition in multiple angles of DLS (MADLS) counterbalance this phenomena, bringing a better

correlation of size and scattering, and consequent better size determination of distinct particle populations (Austin et al. 2020). So far, due to the novelty, this methodology is not standardized and fewer publications use it for drug product analysis.

Laser diffraction (LD) differs from dynamic measurements because it looks at diffraction or scattered laser intensity vs diffraction angle pattern to determine particle size, therefore movement of particles are not considered as a size parameter. DLS is more suitable for NMs ≤ 50nm, while LD provides better results for bigger particles (starting from 50-100 nm, depending on the equipment) (Bhattacharjee 2016). Due to the low limit of detection of size, this technique is not standardized for NM material characterization.

Another multi angle option refers to the Static light Scattering (MALS), a standardized technique that can determine size of undiluted samples and follow aggregation /agglomeration kinetics (Modena et al. 2019; USP 2022).Small Angle x-ray Scattering (SAXS) can also be used to obtain NM morphological and heterogeneity/aggregation information, despite of providing less detail than EM/AFM and requiring dilution of monodisperse populations.

All these techniques perform measurements under a liquid or powder condition, in a static or flow mode. But to monitor nanoaerosols produced in manufacturing, or NM distribution after aerolization (inhalation products), it is required an impactor equipment to separate particles between its stages according to their aerodynamic particle size distribution ("United States Pharmacopeia. General Chapter, 〈1603〉 Good Cascade Impactor Practices. USP-NF. Rockville, MD: United States Pharmacopeia." 2022; "ISO/TR 27628:2007(en), Workplace atmospheres — Ultrafine, nanoparticle and nano-structured aerosols — Inhalation exposure characterization and assessment" s.d.). Some of these techniques give a concentration data (e.g., NTA, MADLS) based on direct nanoparticle properties; fluorescence also relates to NM concentration, allowing direct determination or indirect quantification by fluorescent probes. Fluorescence principles are better explored in API content section.

2.7. NM surface properties

NMs have a high surface area to volume ratio, which renders them a huge reactive interface with the local environment. This means that the same material can

change its properties depending on how it is used - as bulk or nanomaterial, together with the chemical composition, charge and reactivity (USP 2022). The charge of a NM suspension interferes with the toxicity, environmental impact and physiological fate. Hence, the knowledge of NM surface properties enable us to predict, stablish and optimize formulations (Bantz et al. 2014).

Surface charge assessment rely on acoustic, electric and optical properties, with emphasis on zeta potential determination by electrokinetic potential of colloidal suspensions. A non-standardized method that worth mention is the sensitive Tunable Resistive Pulse Sensing (TRPS), which is capable of solving charge and size of individual particles. However, polydisperse populations require change of the conical pore to accommodate different size ranges and make absolute measurements more difficult (Faria et al. 2018; Modena et al. 2019).

ZP measurement is helpful to predict whether NP will be favoured to aggregate or agglomerate or will remain in suspension as discrete particles. High ZP values ($|\zeta| \geq 15$ mV) indicate high repulsion among NMs, and low ZP values indicate that NMs are prone to aggregate, from an electrostatic point of view (USP 2022). However, NMs that have steric stabilization could have low ZP values and maintain discrete particles (Pettitt e Lead 2013). It is important to consider several details of ZP measurement because it depends on the local environment, solvents, pH and background electrolyte concentration (Bhattacharjee 2016; Faria et al. 2018; Modena et al. 2019).

NM surface reactivity and loading may depend on porosity and surface area. Pores interfere drastically in NM surface-to-volume ratio, which can increase API loading, decrease NM sealing, interfere in targeting and cell uptake, etc. Porosity needs to be characterized according to the size, dimensions and volume of the pore cavity. Along with direct pore visualization by EM, dry samples of nanomaterials absorb Nitrogen or expand Helium according to its surface area and porosity, reason why analytical techniques based on these phenomena are frequent and standardized. Of note, samples need to be frozen at very low temperatures, step that may change surface area or pore density (Kéri et al. 2020).

Dynamic Vapour Sorption (DVS) also evaluate pore distribution and surface area in dried particles, with the advantage of working at room temperature. As a downside, DVS analysis follows water sorption and desorption profiles on a NM surface, which could lead to hydrolysis degradation or solid-state transformations

(verifiable by powder X-ray diffraction after DVS). Nevertheless, the transformations upon water uptake are useful to determine sample stability under humidity, crystal changes and other properties which are relevant for formulation design and optimization. Some experiments show octanol as an alternative vapour to sorption experiments (Mesallati, Umerska, e Tajber 2019; Kondor et al. 2021).

Both gravimetric and gas adsorption analysis rely on the application of mathematical equations to model the NM behaviour, with the Brunauer-Emmet-Teller (BET) theory for surface area calculation (Kondor et al. 2021) other models can be fit to isotherms to represent different aspects of the NM, such as hydrophilic layers and hydrophobic cores (Beraldo-Araújo et al. 2022).

2.8. NM-API structure, composition and crystal form

Structure, composition and crystal form compose a set of features one should know for practically all medicines. Therefore, most techniques are not built up for nanomaterials, so that data should be carefully interpreted to take this into account. The most common properties measured are thermal behaviour, crystal profile and chemical composition.

Differential Scanning Calorimetry (DSC) and Thermal Gravimetric Analysis (TGA) are usual techniques to understand the thermal behaviour of NMs, APIs and their interactions. Besides the final product, thermal analysis aid in process development, since one can mimic thermal conditions of real unit operations and follow their consequences in physical and chemical states. TGA detect mass variation derived from a change in physical state and / or chemical composition of samples upon controlled heating. So, a TG curve may contain different weight loss processes such as dehydration, decomposition, oxidation and loss of volatiles (Nasrollahzadeh et al. 2019). Dehydration mass loss correlates with residual moisture, a property directly related with dry product stability and drying process efficiency. There are five main factors to consider to obtain good and reproducible TGA results: sample purity and particle size; heating rate; atmosphere (static or dynamic and type of gas); crucible and sample weight (higher weight increases sensitivity and decreases resolution) (Heal 2002). It is interesting to consider this fast and user-friendly technique when analysing API-NM interactions, since NM could protect the API from degradation but could also accelerate this process. It is also possible to analyze gas products from TGA (TGA-

FTIR, TGA-MS and TGA-GC/MS) (Mansfield e Banash 2021). In particular cases, such as inorganic nanoparticles coated with organic substances, it is possible to determine coating mass proportion due to mass loss of the organic material. For the same reason, API encapsulation rate can be determined by TGA if the NM is inorganic and the loading relates to organic material. Both assay types need more samples and a highly sensible TGA (Dongargaonkar e Clogston 2018).

If TGA associates the weight loss to the temperature increments (up to 1500 °C), then DSC gives information of thermal events (crystallization, melting and glass transition). Phase changes are recorded according to the heat flow of the sample compared to the reference crucible at a certain temperature treatment (Gabbott 2008a). These characterizations bring information upon compatibility between NM-API and further formulation stability. A DSC analyzer submits the sample to controlled cooling, heating, temperature holding and combination of thermal steps. These treatments provoke endothermic and exothermic events including melting of crystals, glass transitions and thermal degradation. Therefore, thermal shifts can be related with API or NM crystal form and the purity of that physical species.

DSC allows to identify whether an API-NM incorporation changed the original API crystalline state to an amorphous compound or to a different polymorph (if it has a different melting point). It also predicts original crystalline API internalization into the nanocarrier due to the lack of its crystalline melting peak. The dislocation of melting peaks of NM and API indicates their interaction, which can be further investigated by complementary techniques (Gabbott 2008a). As for TGA, temperature and the velocity it changes in DSC direct influence property measurement. For example, at slow heating rates, resolution of melting peaks can be greater, whereas faster rates increase sensitivity but it can slow down crystallization events or dislocate peaks (Gabbott 2008a), (Gabbott 2008b). Generally, it is not necessary to prepare a sample for analysis and the measurements are straightforward, but in the characterization phase several temperatures and rates must be tested to evaluate time-related transitions (Gabbott 2008a).

X-ray diffraction (XRD) also detects the presence of polymorphs, solvates or co-crystals that can be created due to formulation manufacturing or excipient interaction. XRD is more precise than DSC in this matter because different crystals diffract the laser in a different way, but not necessarily have different melting points. In addition, it verifies the degree of crystallinity of the API and API-NM formulation (Holder

e Schaak 2019). Powder XRD (PXRD) is a non-destructive and most common technique applied to pharmaceutical NMs, but higher sensitivity comes with the use of small angle X-ray scattering (SAXS). SAXS can elucidate particle size, polydispersity and NM morphology (Mourdikoudis, Pallares, e Thanh 2018). Since crystalline material has a diffraction signature, NM composition can be elucidated when comparing diffractograms of samples with databases. However, most drug related compounds have amorphous content that does not diffract light significantly, so excipients may be disregarded in this analysis.

One of the spectroscopic techniques most applied to study API-NMs interactions and surface composition is the Fourier-Transform Infrared Spectroscopy (FTIR). It evaluates the absorption of infrared electromagnetic radiation by the molecules in the sample and gives spectra that comprises the fingerprint of pure molecules and their binding modifications and changes in the functional groups binding due to the presence of other compounds. The interpretation of the spectra brings information upon molecule structures and interactions, and its recommended by health agencies and pharmacopeias as substance identification (Mourdikoudis, Pallares, e Thanh 2018). UV, fluorescence and mass spectrometry also give NM information, but will be discussed in the API section.

Nuclear magnetic resonance (NMR) also applies for quantitation and structure determination of NMs, besides morphology *in situ* in solid phase or solution. It is often applied to analyze interactions or coordination between the surface of a certain NM and the ligand. Ligand density, atomic composition and its influence on NM shape and size are also characterizations provided by NMR technique (Mourdikoudis, Pallares, e Thanh 2018).

It is pertinent to consider the NM-API characterization by different analytical techniques, since they are often complementary. For example, despite DSC is a rapid, user-friendly technique that does not require sample preparations, it does not provide structural information and its information would be enriched if combined to a spectroscopic technique. Evidently, it is of major importance to verify the particularities and limitations of both the sample and the technique. The overview of techniques presented here is not exhaustive due to the large number of alternatives in chemical analysis.

2.9. API content

The NM-based delivery system can be associated with the total or partial API content from the formulation. Therefore, characterization must include the API-NM associated amount, assurance of API content integrity post-production and detection of impurities and degradation products (Beraldo-Araújo et al. 2022).

The API-NM association can be measured related with the percentage of API incorporated in the carrier, generally called encapsulation efficiency, regardless of where the carried substance is located within the carrier. Drug loading, in turn, is concerned with the carrying weight capacity of the carrier system. For both determinations, there is a need to separate the free from the carrier-associated API, for example using centrifugal filter devices, size exclusion spin columns or solid phase extraction (SPE) columns (USP 2022).

Quantification of API relies mainly on UV-vis spectrophotometry. UV-vis determines API content by its discrete wavelength absorption, which is directly proportional to API concentration over a range that varies among the analytes in solution (Beer-Lambert law) (Siddiqui, AlOthman, e Rahman 2017). The absorption of a specific wavelength of UV/Vis radiation occurs by one or more chromophores that are molecular groups with π bond and atoms with non-bonding orbitals. The spectrum of emission and detection goes from 185 nm up to 1000 nm, detected by an UV/Vis spectrophotometer ("What Causes Molecules to Absorb UV and Visible Light" 2013). Although this works well for pure substances, excipients for the formulation or API degradation products may also absorb on the same wavelength, bind to the API or alter pH, which can also cause change intensity and the maximum absorbance wavelength (λ) (Beraldo-Araújo et al. 2022).

The intensity of fluorescence emitted by a sample upon light stimulation also relates with molecule concentration. Emission measurements implicate that the excited electrons from the API returns to the relaxed state with photon emission ("15.1: Theory of Fluorescence and Phosphorescence" 2022). Measuring the emission spectra with the fluorimeter brings high sensitivity and selectivity, especially useful when the API has low absorption of light in the UV region. A second useful situation concerns measurement of highly diluted drug in biological fluids, a common need for pharmacokinetic studies (Siddiqui, AlOthman, e Rahman 2017).

Fluorescence or UV/vis detection gained a higher specificity when preceded by a column chromatographic step to separate samples into their constituents. In special, High Performance Liquid Chromatography (HPLC) dominated API content protocols, since it separates excipients, degradation products and deliver it with high sensitivity, repeatability, and specificity (Weich et al. 2007; Rahman e Manirul Haque 2021). Although at the cost of sensitivity, UV/Vis detector can be replaced by multiple photodiode arrays that give information over several wavelengths at the same time (Singh 2012).

HPLC separations rely mainly on differences of molecule partition between the mobile liquid phase and the column stationary phase, which makes analytes reaching detectors in different times (Raghavan e Joseph 2015). The normal phase (NP) HPLC has stationary phases more polar than the mobile phase, and reversed phase (RP) has the opposite polarity mode. RP-HPLC is the method of choice for most APIs due to the stability and reproducibility of the stationary phases, together with the wide range of components for the mobile phase Concerning mobile phase formulation, it is usually composed of water and buffered solutions, with methanol or acetonitrile to reduce the polarity; adjustments in these components provide adequate retentive characteristics for the compounds of interest. Other factors that affect the retention time of analyzes include temperature, pH of the buffer and/or mobile phase, stationary phase properties, flow rate and mobile phase composition (Martin et al. 2003; de Villiers et al. 2006).

The columns most used in RP-HPLC are silica-based, with C3, C4, C8 or C18 alkyl chains attached. They are compatible with aqueous and some organic mobile phases, since it does not react, dissolve or swell in them. (Vervoort et al. 2000). High molecular weight substances, such as protein drugs, can benefit of a size exclusion column that separates species by size, by HPLC or LC systems with lower pressure. Classical silica-based columns also do not perform well with highly polar drugs, and alternative ion-exchange chromatography is a compendial alternative. They can be based on modified silica to became anionic or cationic, besides other polymers and resins (Derayea e Ahmed 2019; “United States Pharmacopeia Vol 31, National Formulary 26, General Chapter: <621> Chromatography” s.d.).

When the compounds are volatile, gas chromatography stands out. Substances separate between an inert gas flow and a liquid or solid stationary phase inside the column. Like HPLC, drug polarity influence interactions and consequent

retention times in the column. Then, separated compounds pass generally through a Flame ionization detector (FID) or a more expensive mass spectrometry (the last one especially useful for degradation products). The sample undergoes pyrolysis under the air-hydrogen flame in the FID, decomposing in ions and electrons that are detect by a high-impedance picometer.

Regardless of the method choice, they must be developed and validated during formulation development in order to assess the loading of the API as well as the possible interaction between the formulation components (ICH 2005). For that, it is necessary to comply with the criteria of specificity, linearity, precision, repeatability, determination of the analytical curve range, detection limit and quantification limit (ICH 2005).

2.10. References

"15.1: Theory of Fluorescence and Phosphorescence". 2022. Chemistry LibreTexts. 30 de janeiro de 2022. https://chem.libretexts.org/Bookshelves/Analytical_Chemistry/Instrumental_Analysis_(LibreTexts)/15%3A_Molecular_Luminescence/15.01%3A_Theory_of_Fluorescence_and_Phosphorescence.

Austin, Jake, Caterina Minelli, Douglas Hamilton, Magdalena Wywijas, e Hanna Jankevics Jones. 2020. "Nanoparticle Number Concentration Measurements by Multi-Angle Dynamic Light Scattering". *Journal of Nanoparticle Research* 22 (5): 108. https://doi.org/10.1007/s11051-020-04840-8.

Bantz, Christoph, Olga Koshkina, Thomas Lang, Hans-Joachim Galla, C James Kirkpatrick, Roland H Stauber, e Michael Maskos. 2014. "The surface properties of nanoparticles determine the agglomeration state and the size of the particles under physiological conditions". *Beilstein Journal of Nanotechnology* 5 (outubro): 1774–86. https://doi.org/10.3762/bjnano.5.188.

Beraldo-Araújo, Viviane Lucia, Ana Flávia Siqueira Vicente, Marcelo van Vliet Lima, Anita Umerska, Eliana B. Souto, Lidia Tajber, e Laura Oliveira-Nascimento. 2022. "Levofloxacin in Nanostructured Lipid Carriers: Preformulation and Critical Process Parameters for a Highly Incorporated Formulation". *International Journal of Pharmaceutics* 626 (outubro): 122193. https://doi.org/10.1016/j.ijpharm.2022.122193.

Bhattacharjee, Sourav. 2016. "DLS and zeta potential – What they are and what they are not?" *Journal of Controlled Release* 235 (agosto): 337–51. https://doi.org/10.1016/j.jconrel.2016.06.017.

Caputo, F., J. Clogston, L. Calzolai, M. Rösslein, e A. Prina-Mello. 2019. "Measuring Particle Size Distribution of Nanoparticle Enabled Medicinal Products, the Joint View of EUNCL and NCI-NCL. A Step by Step Approach Combining Orthogonal Measurements with Increasing Complexity". *Journal of Controlled Release: Official Journal of the Controlled Release Society* 299 (abril): 31–43. https://doi.org/10.1016/j.jconrel.2019.02.030.

Dave, Vivek S. 2019. "Chapter 4 - QbD Considerations for Excipient Manufacturing". Em *Pharmaceutical Quality by Design*, editado por Sarwar Beg e Md Saquib Hasnain, 65–76. Academic Press. https://doi.org/10.1016/B978-0-12-815799-2.00004-6.

Derayea, Sayed M., e Hytham M. Ahmed. 2019. "Applications of Ion-Exchange Chromatography in Pharmaceutical Analysis". Em *Applications of Ion Exchange Materials in Biomedical Industries*, editado por Inamuddin, 119–38. Cham: Springer International Publishing. https://doi.org/10.1007/978-3-030-06082-4_5.

Dongargaonkar, Alpana A., e Jeffrey D. Clogston. 2018. "Quantitation of Surface Coating on Nanoparticles Using Thermogravimetric Analysis". Em *Characterization of Nanoparticles Intended for Drug Delivery*, editado por Scott E. McNeil, 57–63. Methods in Molecular Biology. New York, NY: Springer. https://doi.org/10.1007/978-1-4939-7352-1_6.

Faria, Matthew, Mattias Björnmalm, Kristofer J. Thurecht, Stephen J. Kent, Robert G. Parton, Maria Kavallaris, Angus P. R. Johnston, et al. 2018. "Minimum Information Reporting in Bio–Nano Experimental Literature". *Nature Nanotechnology* 13 (9): 777–85. https://doi.org/10.1038/s41565-018-0246-4.

FDA/CDER/"Yeaton, Ayse". 2017. “Drug Products, Including Biological Products, That Contain Nanomaterials - Guidance for Industry”, 29.

Gabbott, Paul. 2008a. “A Practical Introduction to Differential Scanning Calorimetry”. Em *Principles and Applications of Thermal Analysis*, 1–50. John Wiley & Sons, Ltd. https://doi.org/10.1002/9780470697702.ch1.

———. 2008b. “Fast Scanning DSC”. Em *Principles and Applications of Thermal Analysis*, 51–86. John Wiley & Sons, Ltd. https://doi.org/10.1002/9780470697702.ch2.

Halwani, Abdulrahman A. 2022. “Development of Pharmaceutical Nanomedicines: From the Bench to the Market”. *Pharmaceutics* 14 (1): 106. https://doi.org/10.3390/pharmaceutics14010106.

Heal, G. R. 2002. “Thermogravimetry and Derivative Thermogravimetry”. Em *Principles of Thermal Analysis and Calorimetry*, 10–54. https://doi.org/10.1039/9781847551764-00010.

Holder, Cameron F., e Raymond E. Schaak. 2019. “Tutorial on Powder X-ray Diffraction for Characterizing Nanoscale Materials”. *ACS Nano* 13 (7): 7359–65. https://doi.org/10.1021/acsnano.9b05157.

Hoshyar, Nazanin, Samantha Gray, Hongbin Han, e Gang Bao. 2016. “The effect of nanoparticle size on in vivo pharmacokinetics and cellular interaction”. *Nanomedicine* 11 (6): 673–92. https://doi.org/10.2217/nnm.16.5.

ICH. 2005. “Validation of analytical procedures: text and methodology Q2 (R1)”.

“ISO/TR 27628:2007(en), Workplace atmospheres — Ultrafine, nanoparticle and nano-structured aerosols — Inhalation exposure characterization and assessment”. s.d. Acedido a 30 de dezembro de 2022. https://www.iso.org/obp/ui/#iso:std:iso:tr:27628:ed-1:v1:en.

Kéri, Albert, András Sápi, Ditta Ungor, Dániel Sebők, Edit Csapó, Zoltán Kónya, e Gábor Galbács. 2020. “Porosity Determination of Nano- and Sub-Micron Particles by Single Particle Inductively Coupled Plasma Mass Spectrometry”. *Journal of Analytical Atomic Spectrometry* 35 (6): 1139–47. https://doi.org/10.1039/D0JA00020E.

Kondor, Anett, Alba Santmarti, Andreas Mautner, Daryl Williams, Alexander Bismarck, e Koon-Yang Lee. 2021. “On the BET Surface Area of Nanocellulose Determined Using Volumetric, Gravimetric and Chromatographic Adsorption Methods”. *Frontiers in Chemical Engineering* 3. https://www.frontiersin.org/articles/10.3389/fceng.2021.738995.

Maguire, Ciarán Manus, Matthias Rösslein, Peter Wick, e Adriele Prina-Mello. 2018. “Characterisation of particles in solution – a perspective on light scattering and comparative technologies”. *Science and Technology of Advanced Materials* 19 (1): 732–45. https://doi.org/10.1080/14686996.2018.1517587.

Mansfield, Elisabeth, e Mark Banash. 2021. “Thermal Analysis of Nanoparticles: Methods, Kinetics, and Recent Advances”. *NIST*, outubro. https://www.nist.gov/publications/thermal-analysis-nanoparticles-methods-kinetics-and-recent-advances-0.

Martin, Paul D., Graeme R. Jones, Frances Stringer, e Ian D. Wilson. 2003. “Comparison of Normal and Reversed-Phase Solid Phase Extraction Methods for Extraction of β-Blockers from Plasma Using Molecularly Imprinted Polymers”. *Analyst* 128 (4): 345–50. https://doi.org/10.1039/B211787H.

Mesallati, Hanah, Anita Umerska, e Lidia Tajber. 2019. “Fluoroquinolone Amorphous Polymeric Salts and Dispersions for Veterinary Uses”. *Pharmaceutics* 11 (6). https://doi.org/10.3390/pharmaceutics11060268.

Modena, Mario M., Bastian Rühle, Thomas P. Burg, e Stefan Wuttke. 2019. “Nanoparticle Characterization: What to Measure?” *Advanced Materials* 31 (32): 1901556. https://doi.org/10.1002/adma.201901556.

Mourdikoudis, Stefanos, Roger M. Pallares, e Nguyen T. K. Thanh. 2018. “Characterization Techniques for Nanoparticles: Comparison and Complementarity upon Studying Nanoparticle Properties”. *Nanoscale* 10 (27): 12871–934. https://doi.org/10.1039/C8NR02278J.

Nasrollahzadeh, Mahmoud, Monireh Atarod, Mohaddeseh Sajjadi, S. Mohammad Sajadi, e Zahra Issaabadi. 2019. “Chapter 6 - Plant-Mediated Green Synthesis of Nanostructures: Mechanisms, Characterization, and Applications”. Em *Interface Science and Technology*, editado por Mahmoud Nasrollahzadeh, S. Mohammad Sajadi, Mohaddeseh Sajjadi, Zahra Issaabadi, e Monireh Atarod, 28:199–322. An Introduction to Green Nanotechnology. Elsevier. https://doi.org/10.1016/B978-0-12-813586-0.00006-7.

Pettitt, Michala E., e Jamie R. Lead. 2013. “Minimum Physicochemical Characterisation Requirements for Nanomaterial Regulation”. *Environment International* 52: 41–50. https://doi.org/10.1016/j.envint.2012.11.009.

Raghavan, R., e Jose C. Joseph. 2015. “Chromatographic Methods of Analysis: High-Performance Liquid Chromatography”. Em *Encyclopedia of Pharmaceutical Science and Technology, Fourth Edition*, 4º ed. CRC Press.

Rahman, Habibur, e Sk Manirul Haque. 2021. “Development and Validation of Chromatographic and Spectrophotometric Methods for the Quantitation of Rufinamide in Pharmaceutical Preparations”. *Turkish Journal of Pharmaceutical Sciences* 0 (0): 0–0. https://doi.org/10.4274/tjps.galenos.2021.37043.

Siddiqui, Masoom Raza, Zeid A. AlOthman, e Nafisur Rahman. 2017. “Analytical Techniques in Pharmaceutical Analysis: A Review”. *Arabian Journal of Chemistry* 10: S1409–21. https://doi.org/10.1016/j.arabjc.2013.04.016.

Singh, Ranjit. 2012. “Current trends in forced degradation study for pharmaceutical product development”. Em . https://www.semanticscholar.org/paper/Current-trends-in-forced-degradation-study-for-Singh/b08c5fb7f6501cd9423567f1a0b7bc00422cf475.

“Standard Practice for Performing Cryo-Transmission Electron Microscopy of Liposomes”. s.d. Acedido a 13 de dezembro de 2022. https://www.astm.org/e3143-18b.html.

“United States Pharmacopeia. General Chapter, 〈1603〉 Good Cascade Impactor Practices. USP-NF. Rockville, MD: United States Pharmacopeia.” 2022. https://doi.org/10.31003/USPNF_M13055_03_01.

“United States Pharmacopeia Vol 31, National Formulary 26, General Chapter: <621> Chromatography”. s.d. Acedido a 29 de dezembro de 2022. http://www.uspbpep.com/usp31/v31261/usp31nf26s1_c621.asp.

USP. 2022. “〈1153〉 Drug Products Containing Nanomaterials”. https://doi.org/10.31003/USPNF_M13775_02_01.

Vervoort, R. J. M, A. J. J Debets, H. A Claessens, C. A Cramers, e G. J de Jong. 2000. “Optimisation and Characterisation of Silica-Based Reversed-Phase Liquid Chromatographic Systems for the Analysis of Basic Pharmaceuticals”. *Journal of Chromatography A* 897 (1): 1–22. https://doi.org/10.1016/S0021-9673(00)00811-6.

Villiers, André de, François Lestremau, Roman Szucs, Sylvie Gélébart, Frank David, e Pat Sandra. 2006. “Evaluation of Ultra Performance Liquid Chromatography:

Part I. Possibilities and Limitations". *Journal of Chromatography A* 1127 (1): 60–69. https://doi.org/10.1016/j.chroma.2006.05.071.

Weich, Anelise, Daniele Carvalho de OLIVEIRA, Janine de MELO, Karin Goebel, e Clarice Madalena Bueno Rolim. 2007. "Validation of UV Spectrophotometric and HPLC Methods for Quantitative Determination of Atenolol in Pharmaceutical Preparations". *Latin American Journal of Pharmacy*, 6.

"What Causes Molecules to Absorb UV and Visible Light". 2013. Chemistry LibreTexts. 3 de outubro de 2013. https://chem.libretexts.org/Bookshelves/Physical_and_Theoretical_Chemistry_Textbook_Maps/Supplemental_Modules_(Physical_and_Theoretical_Chemistry)/Spectroscopy/Electronic_Spectroscopy/Electronic_Spectroscopy_Basics/What_Causes_Molecules_to_Absorb_UV_and_Visible_Light.

3. CHAPTER 2 - LEVOFLOXACIN IN NANOSTRUCTURED LIPID CARRIERS: PREFORMULATION AND CRITICAL PROCESS PARAMETERS FOR A HIGHLY INCORPORATED FORMULATION

This chapter was published as a research paper in the International Journal of Pharmaceutics (Beraldo-Araújo et al. 2022).

3.1. Authors

Viviane Lucia Beraldo-Araújo [a b c], Ana Flávia Siqueira Vicente [a], Marcelo van Vliet Lima [a d], Anita Umerska [b], Eliana B. Souto [e f], Lidia Tajber [b], Laura Oliveira-Nascimento [a]

[a] Faculty of Pharmaceutical Sciences, State University of Campinas, Campinas, Brazil
[b] School of Pharmacy and Pharmaceutical Sciences, Trinity College Dublin, College Green, Dublin 2, Ireland
[c] Centre of Biological Engineering (CEB), University of Minho, Campus de Gualtar, 4700 Braga, Portugal
[d] Sanofi Medley Farmacêutica Ltda, Campinas, Brazil
[e] Department of Pharmaceutical Technology, Faculty of Pharmacy, University of Porto, Rua de Jorge Viterbo Ferreira, 228, 4050-313 Porto, Portugal
[f] REQUIMTE/UCIBIO, Faculty of Pharmacy, University of Porto, Rua de Jorge Viterbo Ferreira, 228, 4050-313 Porto, Portugal

Received 16 February 2022, Revised 5 August 2022, Accepted 7 September 2022, Available online 13 September 2022, Version of Record 19 September 2022.

Available on https://doi.org/10.1016/j.ijpharm.2022.122193. This is an open access article distributed under the terms of the Creative Commons CC-BY license, which permits unrestricted use, distribution, and reproduction in any medium, provided the original work is properly cited.

3.2. Abstract

The first step of a successful nanoformulation development is preformulation studies, in which the best excipients, drug-excipient compatibility and interactions can be identified. During the formulation, the critical process parameters and their impact must be studied to establish the stable system with a high drug entrapment efficiency (EE). This work followed these steps to develop nanostructured lipid carriers (NLCs) to deliver the antibiotic levofloxacin (LV). The preformulation studies covered drug solubility in excipients and thorough characterization using thermal analysis, X-ray diffraction and spectroscopy. A design of experiment based on the process parameters identified nanoparticles with < 200 nm in size, polydispersity <= 0.3, zeta potential −21 to −24 mV, high EE formulations (>71 %) and an acceptable level of LV degradation products (0.37–1.13 %). To the best of our knowledge, this is the first time that a drug degradation is reported and studied in work on nanostructured lipids. LV impurities following the NLC production were detected, mainly levofloxacin N-oxide, a degradation product that has no antimicrobial activity and could interfere with LV quantification in spectrophotometric experiments. Also, the achievement of the highest EE in lipid nanoparticles than those described in the literature to date and the apparent protective action of NLC of entrapped-LV against degradation are important findings.

3.3. Keywords

Preformulation; Design of experiments; Levofloxacin; Nanostructured lipid carrier; Solid state; Degradation.

3.4. Graphical Abstract

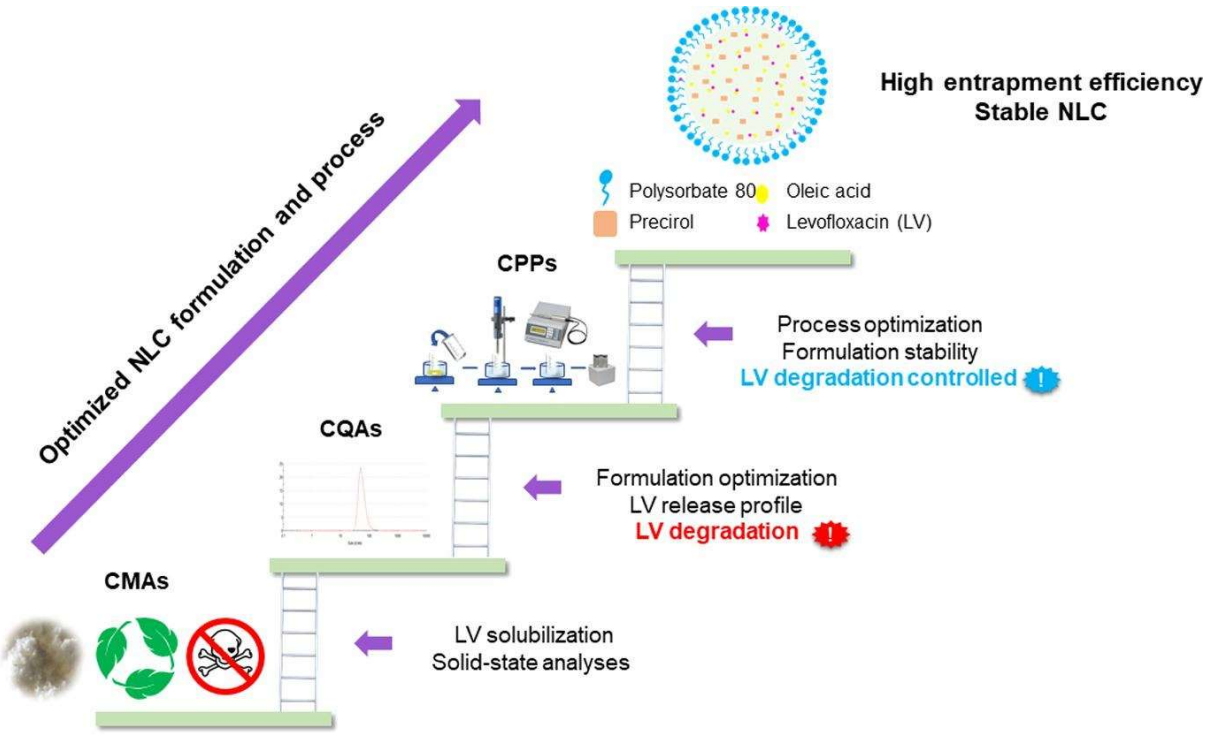

CMAs: Critical Material Attributes; **CQAs**: Critical Quality Attributes; **CPPs**: Critical Process Parameters

3.5. Introduction

Over the last decades, nanostructuring of pharmaceuticals maintains a prominent status as an effective drug delivery strategy. As a result, a range of different types of nanostructures have been developed and studied for this purpose. Examples include liposomes, nanoemulsions, nanomicelles, lipid and polymeric nanoparticles, nanotubes, etc. (Li et al., 2017). Comparing the various types of pharmaceutical nanostructures, lipid nanoparticles (NPs) play a key role due to their particular advantages. They comprise ingredients that are usually biocompatible, biodegradable and have low potential toxicity; the technology might be translated into a large-scale production; can modify and control drug release; enhance drug solubility and are able to incorporate both hydrophilic and lipophilic molecules. Furthermore, the dispersion stabilization is afforded by a mixture of surfactants and cosurfactants (Müller et al., 2000).

Levofloxacin (LV) is a fluoroquinolone drug first introduced in 1993. It shows a broad spectrum of action and is commonly used to treat respiratory, urinary tract, skin and soft tissue bacterial infections. The most common LV side-effects are nausea, diarrhea, headache, but also rare severe effects, such as tendinitis and tendon rupture (Liu, 2010). These pitfalls of LV have encouraged, especially in the past ten years, several studies aiming at incorporating LV into nanoparticles of several types, including polymeric and lipidic systems. Abdel Hady et al. were able to co-incorporate LV and docycycline into solid lipid nanoparticles (SLNs) and to improve the brain targeting via the nose-to-brain route in comparison to the intravenous administration (Abdel Hady et al., 2020). In the study of Ameeduzzafar et al., LV-loaded chitosan NPs showed better results regarding the corneal clearance, drug retention and naso-lachrymal drainage in ocular delivery compared to the LV solution (Ameeduzzafar et al., 2018). Islan et al. produced SLN and nanostructured lipid carriers (NLC)-loaded LV with DNase type I, which reduced the lung viscoelasticity, exacerbated in cystic fibrosis patients, and the formation of bacterial biofilm (Islan et al., 2016). Kumar et al. studied lyophilized NPs of PLGA to deliver LV by the oral route (Kumar et al., 2012). Moreover, lipid nanoparticles were able to prevent the crystallization of LV free drug at the high administered concentrations, reducing the risks of LV-induced crystal nephropathy (Liu et al., 2015).

Unfortunately, the published accounts on LV nanostructures also suffer from drawbacks. From the total of 30 studies on LV NPs analyzed in past 10 years, only 19 determined the entrapment efficiency (EE) of the drug, 15 presented the drug loading and only one presented the drug content in the final formulation to determine EE (Zhang et al., 2019). These data are important to explain the achieved outcomes, to be reliable and reproducible for other researchers. Another concern, when comes to formulating NPs, is the scarceness of studies on the drug degradation during the formulation step. Drug degradation and total drug content also allow us to evaluate the compatibility of drug with excipients and the process parameters that affect the stability of such mixtures. There are few studies reporting that the high temperature during NLC process may promote drug degradation of labile molecules such as astaxanthin (Dhiman et al., 2021, Tamjidi et al., 2014), but no similar studies have been done for LV NPs. For LV, the most common degradation product is levofloxacin N-oxide (LNO). This substance has no antibiotic activity and absorbs UV light at the same wavelength as LV, the reason why spectrophotometric methods with no separation of molecules can hinder degradation (Czyrski et al., 2019).

Although the importance of nanosystems in commercial formulations has not been fully realized yet, a few products have been marketed, for instance Doxil, liposomal doxorubicin and Abraxane, paclitaxel nanoparticles, both approved for the clinical use (Li et al., 2017). Also, the state of art in analytics has improved over time. The improvements and rising rigor from the controlling agencies led to the adoption of Quality by Design (QbD) approach (Q3B/8/9/10/11) and the mandatory drug stability indicating assay, among others, to enable a production of a safe and good quality product (Cunha et al., 2020). However, it is regrettable that academic studies do not have to follow these rules and the published accounts vary in degree of analytical data and often prioritize biological outcomes. Thus, the factors that influence the physicochemical characteristics of nanoformulations and their consequences are not completely clear, hindering the possibility of a clinical translation and industrial production, which must follow the guidelines for quality standards and reproducibility (Li et al., 2017). Nevertheless, a considerable number of articles have recently been published describing the QbD approach in the development of lipid nanoparticles, measuring the impact of formulation composition, such as the lipids and surfactant content, on the parameters intrinsic to the biological performance of NPs (nanoparticle size, polydispersity index (PdI), zeta potential and entrapment efficiency (EE)). The

process variables are also key to be considered during optimization processes, including the number of cycles, the rate and duration of emulsification and, if sonication is used, the amplitude and time of the sonication process (Cunha et al., 2020). The QbD begins to be valued in the field of pharmaceutical NPs as an important tool to help the understand the products and processes, building the quality into the production and following the standards (Li et al., 2017).

For these reasons, this paper focused on the preformulation studies (excipient selection) and process production parameters of nanostructured lipid carriers loaded with LV, evaluating, for the first time, the presence degradation products induced by the formulation process. Critical material attributes (CMA) were studied by selecting biodegradable and non-toxic excipients, screened by the criteria of drug solubility and solid-state analyses. Afterwards, based on the drug-lipid solubility, we determined the formulation critical quality attributes (CQA) according to the NP size, polydispersity, zeta potential and entrapment efficiency. The formulation composition and the process of production were further evaluated considering the selected CMAs and critical process parameters (CPPs) (the sonication time, amplitude and temperature), analyzing the CQAs based on literature and previous studies of the group. We also evaluated formulation stability, sorption kinetics, in vitro drug release and the production of total impurities depending on the CPPs.

3.6. Material and methods

3.6.1. Materials

Levofloxacin hemihydrate (LV, (2S)-7-fluoro-2-methyl-6-(4-methylpiperazin-1-yl)-10-oxo-4-oxa-1-azatricyclo [7.3.1.05,13] trideca-5(13),6,8,11-tetraene-11-carboxylic acid hemihydrate) was purchased from FluoroChem (UK) and also generously donated by Sanofi-Medley Farmacêutica Ltda from Brazil. Levofloxacin N-oxide standard was purchased from Eurobram (Germany). Oleic acid was purchased from Dinâmica Química Contemporânea Ltda (Brazil). Super Refined™ polysorbate-80, Super Refined™ oleic acid, beeswax and Crodamol™ CP (cetyl palmitate) were donated by Croda (UK). Precirol® ATO 5, Compritol® 888 ATO, Geleol™ mono and diglycerides, Gelucire® 50/13 (stearoyl polyoxylglycerides) and Biogapress Vegetal BM 297 ATO (glyceryl dipalmitostearate) were donated by Gattefossé (France), while Tego® care 450 (polyglyceryl-3 methylglucose distearate) was donated by Evonik. Dynasan® 116 (glyceryl tripalmitate) and Dynasan® 118 (glyceryl tristearate) were provided by IOI Oleochemical (Germany). Stearic acid and phosphate buffered saline (PBS) sachets were purchased from Sigma-Aldrich (Germany) (one sachet dissolved in 1000 mL of deionized water yields 0.01 M phosphate buffer, KCl 0.0027 M and NaCl 0.137 M sodium chloride, pH 7.4, at 25 °C). Potassium bromide (KBr) of infrared grade was obtained from Sigma-Aldrich (Ireland). All other chemicals and solvents were of analytical grade.

3.6.2. Methods

3.6.2.1. Pre-selection of excipients

The determination of LV solubility in lipids was made by mixing 1 or 5 mg (1 or 5 % w/w, respectively) of drug with each of the excipients to make a total of 100 mg mixture in a 10 mL glass test tube. The mixtures were kept in a heated water bath (J.P. Selecta Precisterm series, Spain) at 80 °C for 60 min. The pre-selection of excipients was made after visually checking LV solubilization in the mixtures every 15 min. The formation of a clear, pale-yellow mixture was deemed as indication of LV solubility in that excipient. A cloudy mixture or a system containing visible LV particles indicated a partially soluble or insoluble system, respectively.

3.6.2.2. Thermal analysis

Differential scanning calorimetry (DSC) of the bulk materials, physical, binary mixtures of 5 % LV-excipient systems and NLCs were performed using Mettler Toledo DSC 821e model with a refrigerated cooling system LabPlant RP-100 (Mettler-Toledo GmbH, Switzerland) with samples of 3–5 mg weighted in 40 mL pierced lid aluminum pans. The analyses were carried out under nitrogen flow. Physical mixtures of 5 % LV-excipient were prepared using an agate mortar with a pestle. The heating program started from −35 or 25 °C, depending on the sample, up to 300 °C, and a heating rate of 10 °C/min was used for all systems. The samples were weighted on microanalytical balance Mettler Toledo, XP6 model (Mettler-Toledo, Switzerland). Thermograms were evaluated as onset temperatures for melting events and heat of transitions was also determined.

Thermogravimetry (TGA) of the bulk materials, physical mixtures and the NLC samples was performed to evaluate their thermal stability. The starting decomposition temperature was that up to which a maximum of 5 % w/w mass loss was measured (Umerska et al., 2020a). Analyses were carried out in a Mettler Toledo TG50 measuring module coupled to a Mettler Toledo MT5 balance. Samples weighing 8–10 mg were placed in 40 µL open aluminum pans and heated from 25 to 300 °C at a rate of 10 °C/min under nitrogen flow as the purge gas with a flow rate of 40 mL/min. Mettler Toledo STARe software (version 6.10) was used to identify the weight loss based on the slope of TGA trace. TGA was also used to pre-heat the physical mixtures at NLC preparation conditions (58 °C, 30 min) before analyzing them by powder X-ray diffraction as well as infrared analysis and compared to the non-heated mixtures.

3.6.2.3. X-ray diffraction (XRD)

Powder XRD measurements were performed using a Rigaku Miniflex II, desktop X-ray diffractometer (Japan), equipped with an X-ray source using CuKα radiation at 30 kV and 15 mA, with a Haskris cooling unit. Diffractograms were acquired over the 2 θ range between 2° − 40° at a step size of 0.05° per second. This method was adapted from Umerska et al., 2020b.

3.6.2.4. Infrared analysis (FTIR)

FTIR analyses allowed to identify the functional groups of the samples (bulk or mixtures excipient-LV 5 % w/w). The bands in the absorption spectra were obtained

from KBr discs with approximately 10 % w/w of sample loading, prepared by compression using a hydraulic IR press (40 bar for 1–2 min). The spectral range recorded was 4000–650 cm−1, accumulation of 10 scans and resolution of 16 cm−1 was applied. Spectra were recorded on a Spectrum One spectrometer (Perkin Elmer, USA). Following collection, background correction and intensity normalization were applied to the data using Spectrum v. 5.0.1 software.

3.6.2.5. Design of experiments (DoE) approach

A full factorial 2^3 design was performed to optimize the properties of the NLC formulation and determine the CMAs. The inputs (variables) were: the amount of total lipids in the formulations (the lipid to aqueous phase ratio: 0.5, 0.75 and 1.0 g of lipids to 10 g of aqueous phase), proportion of solid and liquid lipids (70:30, 80:20 and 90:10 w/w), and the amount of surfactant (2, 3 and 4 % w/v). They were evaluated at 2 levels of concentrations and a triplicate on the center point (intermediate concentration) was also tested. The order of preparation was randomized. The outputs evaluated to determine the best formulation were z-average size, polydispersity index (PdI), zeta potential and entrapment efficiency (EE). The desirable outputs to choose the best formulation were z-average < 250 nm, PdI < 0.3 and the highest EE value. The results were analyzed by software Minitab® 17.1.0.

A second full factorial 2^3 design was run to optimize the process parameters of NLCs, thus determine CPPs. The best formulation parameters determined in the first DoE were employed in this factorial design. The independent variables were: the temperature, sonication time and sonication amplitude. For the temperature parameter, the values chosen were such to represent conditions in which the solid lipid would be solid (38 °C) or melted (58 and 78 °C). The usual sonication time applied by our group is 30 min (Beraldo-de-Araújo et al., 2019), however, 20 min was also considered. Finally, the sonication amplitude varied to verify its influence on the physicochemical parameters (outputs). The outcomes examined were z-average size, PdI, zeta potential, EE and total impurities, analyzed by software Minitab® 17.1.0.

3.6.2.6. NLC production

NLCs were prepared by the hot emulsification-ultrasonication method (Beraldo-de-Araújo et al., 2019, Schwarz et al., 1994). Shortly, the lipid phase components (the solid and the liquid lipids) were melted in a beaker over a water bath

at 58 ± 2 °C and LV was added under magnetic stirring. The aqueous phase was prepared in another beaker, containing water and the surfactant, heated on a hot plate under magnetic stirring and this solution was added to the lipid phase under mixing, 12,000 rpm for 3 min, in an Ultraturrax blender (IKA® T18 basic, Germany) using the S18N-19G dispersing tool. This emulsion was then sonicated using a tip sonicator (Vibracell, Sonics & Materials Inc., USA) fitted with a 3 mm probe. The following conditions of processing were used: power 130 W and 20 kHz nominal frequency; cycling of 30 s (on/off) for 30 min at an amplitude of 50 %. The dispersion was then cooled to 25 °C over an ice bath and stored at room temperature protected from the light.

3.6.2.7. Determination of hydrodynamic diameter (z-average), dispersity (PdI) and zeta potential (ZP)

Z-average size was determined by Dynamic Light Scattering (DLS) (Zetasizer Nano ZS90, Malvern Instruments ltd, UK), at a 90° scattering angle and 25 °C, using a disposable polystyrene cuvette, with samples diluted to 1:200 in sodium chloride 10 mM or milliQ water (refraction index 1.332 – viscosity 0.8910 cP) to reach an adequate correlation coefficient (between 0.7 and 1). The zeta potential (ZP) of these diluted samples was determined by the same instrument, measuring the electrophoretic mobility using a disposable polystyrene cuvette model DTS1070 with electrodes. The samples were measured in triplicate and results presented as mean ± standard deviation.

3.6.2.8. Determination of LV concentration by high performance liquid chromatography (HPLC)

LV was measured using HPLC, as described in the United States Pharmacopoeia (USP) monograph for Levofloxacin Tablets ("Levofloxacin," 2017). The analyses were performed using the Prominence-i LC2030C, Shimadzu HPLC system (Shimadzu, Japan), Hitachi LaChrom Elite HPLC System (Merck-Hitachi, Japan) and a Waters 2695 Alliance HPLC System with a PDA detector (USA). The mobile phase consisted of a mixture of 7 parts v/v of buffer (8.5 g/L of ammonium acetate, 1.25 g/L of cupric sulfate, pentahydrate, and 1.3 g/L of l-isoleucine in water) and 3 parts v/v of methanol with a column containing the L1 packing (Waters Symmetry C18 250 mm × 4.6 mm i.d. column, 5 µm particle size). The following conditions of

separation were used: the oven temperature was 45 °C, the mobile phase flow rate of 0.8 mL/min (isocratic) and the injection volume was 25 µL. UV detection was carried out at 360 nm with the total running time of 26 min. The quantification method was based on a calibration curve using LV standard, in a concentration range from 5 µg/mL to 200 µg/mL (r2 = 0.9999) Limits of detection and quantification were 1.97 µg/mL and 5.97 µg/mL, respectively. The same method was applied to run the standard of levofloxacin N-oxide (LNO) to identify its peak in both the raw material and the NLC formulations. For degradation analysis, the total amount of impurities, as percentage of area in the chromatograms, was considered and not only LNO. A normalization procedure based on the signal-to-noise ratio was used to determine the quantitation limit of impurities (Fig. S1).

3.6.2.9. Determination of total drug content, drug loading and entrapment efficiency (EE)

The determination of the total drug content was done by transferring 500 µL of the NLC suspension to a 50 mL volumetric flask, and then adding 1 mL of THF to partially dissolve the matrix. The resulting suspension was vortex mixed in a Quimis mixer, model Q220M (Brazil), for 2 min, to which 30 mL of the mobile phase was added, and the flask was sonicated in an ultrasonic bath for 5 min, with vigorous shaking every-two minutes. After cooling down to room temperature, the volume of the liquid was made up to 50 mL in a volumetric flask, and the resulting solution was filtered through a PVDF membrane syringe filter Sartorius Minisart®, 25 mm in diameter and 0.45 µm pore size, discarding the first 2 mL of the filtrate.

EE was determined indirectly by the ultrafiltration method, using centrifugal filter tubes (Millex, Millipore, USA) with a 30 kDa molecular weight cut-off (Beraldo-de-Araújo et al., 2019). A volume of 500 µL of NLC suspensions were centrifuged at 4100 × g for 20 min in an Eppendorf 5418 centrifuge (Germany). Free LV in the supernatant was diluted 25x in the mobile phase and quantified according the HPLC method. EE was calculated based on the difference between the drug content in the formulations and the amount detected in the filtrate, applying Eq. (1):

$$\text{EE (\%)} = \frac{\text{Total amount of drug} - \text{free drug}}{\text{Total amount of drug}} * 100 \quad (1)$$

Drug loading was calculated using Equation 2 (Papadimitriou e Bikiaris 2009):

$$\mathrm{DL}\ (\%) = \frac{\text{weight of entrapped drug in nanoparticles}}{\text{weight of nanoparticles (drug+excipien)}} * 100 \quad (2)$$

3.6.2.10. Formulation stability

The stability of the optimized formulation with and without LV was evaluated at pre-determined time points. The samples were stored in a stability chamber (40 °C and 75 % RH) and parameters measured by DLS (z-average, PdI and zeta potential) in triplicate and results presented as mean ± standard deviation. Drug recovery, EE and total impurities were also evaluated by HPLC.

3.6.2.11. Dynamic vapor sorption (DVS)

First, 1 – 2 mL of the optimized nanosuspensions NLC_LV (with LV) and NLC_BL (blank, without LV) were poured into 20 mL open glass tubes. They were dried at room temperature inside a desiccator with silica gel for approximately 60 days before DVS studies. DVS analyses were performed using an Advantage-1 automated gravimetric vapor sorption analyzer (Surface Measurement Systems ltd., UK) at 25.0 ± 0.1 °C, with nitrogen as a dry carrier gas. Approximately 20 mg of the sample in the sample basket was placed in the instrument and equilibrated at 0 % relative humidity (RH) overnight. The reference mass was recorded, and sorption − desorption analysis was then carried out between 0 and 90 % RH, in steps of 10 % RH. At each stage, the sample mass was equilibrated (dm/dt ≤ 0.002 mg/min for at least 10 min and the maximum equilibration time was set as 480 min) before the RH was changed. An isotherm was calculated from the complete sorption and desorption profile (Mesallati et al., 2017). Water distribution within the samples was evaluated by Young-Nelson model as described previously (Mesallati et al., 2019).

3.6.2.12. Drug release profiles

Drug release was assessed by two methods, since there is no consensus about the most appropriate approach for nanoparticulates. Therefore, release studies were performed using Franz cells and carried out in 7 mL static vertical diffusion cells with automatic sampling (Microette Plus®, Hanson Research, USA). The receptor chamber was filled with PBS pH 7.4, covered with the cellulose membrane and the donor chamber was filled with 1 mL sample in PBS. The available diffusion surface area was 1.76 cm2 and a clamp was used to hold the compartments together. Two

diffusion cells were prepared for each sample tested. The receptor medium, maintained at 37 ± 1 °C, was constantly mixed (magnetic stirring at 700 rpm), except during the periods of sample collection. Aliquots of 2.5 mL (with 1 mL accounting for purging and 1.5 mL used for analysis) were withdrawn at specific time intervals and collected into HPLC vials. The aliquots withdrawn from the receptor chamber were immediately replaced with the blank receptor medium at the same temperature. The LV concentrations were accordingly corrected considering the replenished volumes. The collected samples were analyzed by HPLC as already described above.

A non-membrane release method was adapted from (Magenheim et al., 1993) without the use of a membrane that separates the colloidal formulation from the release medium. The optimized LV-loaded NLC (100 µL) was poured into 2 mL-capped plastic tubes containing 900 µL of PBS 0.01 M pH = 7.4. The samples were placed in a shaking water bath (100 rpm, 37 °C) and every time point was run in quadruplicate. Every 0.08, 0.25, 0.5, 0.75 1.0, 1.5, 2, 2.5, 3, 4, 6 and 24 h, 500 µL of the samples were withdrawn and centrifuged immediately using 30 kDa Amicon centrifuge filters (4100 × g, 15 min, 21 °C). The supernatant was diluted 4x with the mobile phase and LV quantified by HPLC. There was one sample tube for each time point, avoiding the withdrawal of aliquots of LV together with nanoparticles from the samples and interfering with results of the next time points. Samples with the same concentration of free LV (0.5 mg/mL) were prepared by adding 20 mL of PBS into 10 mg of LV in 50 mL-capped plastic tubes at the same conditions as NLCs and analyzed by HPLC at the same time points to evaluate drug dissolution rate.

3.6.2.13. Statistical analysis

Samples were evaluated as mean ± standard deviation. The statistical significance in the differences between samples was determined using a one-way analysis of variance (ANOVA). The differences were considered significant at $p < 0.05$. DoE analysis was made with the help of software Minitab® 17.1.0.

3.7. Results and discussion

3.7.1. Preformulation studies on NLC formulation components

We previously described the importance on evaluating critical formulation parameters (CQAs) to reach a good NLC, such as lipid type and amount, crystallinity and drug properties (Beraldo-de-Araújo et al., 2019). For this reason, we started with a preliminary visual evaluation of LV solubility in different lipids. The qualitative results are given in Table 1. It was expected that the lipids, in which LV dissolved better, can incorporate more the drug in the lipidic core (Bhalekar et al., 2017).

Table 1. Solubility of LV in lipids. ("-" did not dissolve; "±" partially dissolved; "+" completely dissolved).

Lipid type + Drug (%)	15 min	30 min	45 min	60 min
Beeswax + LV 1	–	±	±	±
Beeswax + LV 5	–	–	–	–
Dynasan 116 + LV 1	–	–	–	–
Dynasan 116 + LV 5	–	–	–	–
Gelucire 50/13 + LV 1	–	–	±	±
Gelucire 50/13 + LV 5	–	–	–	–
Geleol mono and diglycerides + LV 1	–	±	+	+
Geleol mono and diglycerides + LV 5	–	–	±	±
Cetyl Palmitate + LV 1	–	–	±	±
Cetyl Palmitate + LV 5	–	–	–	–
Precirol® ATO 5 + LV 1	+	+	+	+
Precirol® ATO 5 + LV 2.5	±	+	+	+
Precirol® ATO 5 + LV 5	–	–	±	±
Tego care 450 (Stearyl glucoside) + LV 1	–	–	–	±
Tego care 450 (Stearyl glucoside) + LV 5	–	–	–	–
Dynasan 118 + LV 1	–	±	±	±
Dynasan 118 + LV 5	–	–	±	±
Biogapress vegetal BM297 ATO + LV 1	–	+	+	+
Biogapress vegetal BM297 ATO + LV 5	–	–	±	±
Compritol® 888 ATO + LV 1	±	+	+	+
Compritol® 888 ATO + LV 5	–	±	±	±
Stearic acid + LV 1	+	+	+	+
Stearic acid + LV 5	–	–	–	–
Oleic acid + LV 1	±	+	+	+

Lipid type + Drug (%)	15 min	30 min	45 min	60 min
Oleic acid + LV 5	–	±	±	±

It was noticed that LV at the higher loading (5 % w/w) was not completely soluble at any of the lipids, with incomplete solubilization in Geleol, Precirol, Dynasan, Biogapress, Compritol and oleic acid, typically achieved after at least of 30 min of thermal treatment. However, LV, at 1 % w/w level, dissolved entirely in Precirol and stearic acid after 15 min, followed by Compritol and oleic acid, with a partial solubilization at the same time point, but a complete dissolution after 30 min, as well as Biogapress. As the other lipids did not dissolve LV completely, they were therefore not included in further studies going forward. Since this test allows us to predict the success of drug incorporated in lipid carriers, we considered that it would be better to embedded LV in the lipids that solubilized the drug the most. Therefore, we have decided to prepare nanostructured lipid carriers (NLCs) with Precirol and/or stearic acid as solid lipids, and oleic acid as a liquid lipid. Compritol was dismissed because of its high melting point, which could impair the production by the proposed method, due to evaporation of the aqueous phase.

Thermal properties of the bulk ingredients and physical mixtures of excipients with 5 % LV were determined using DSC and TGA (Fig. 1A and B). Since the chosen method of NLC production involves heat, we also evaluated the binary mixtures with thermal treatment at the condition of NLC production (58 °C, 30 min).

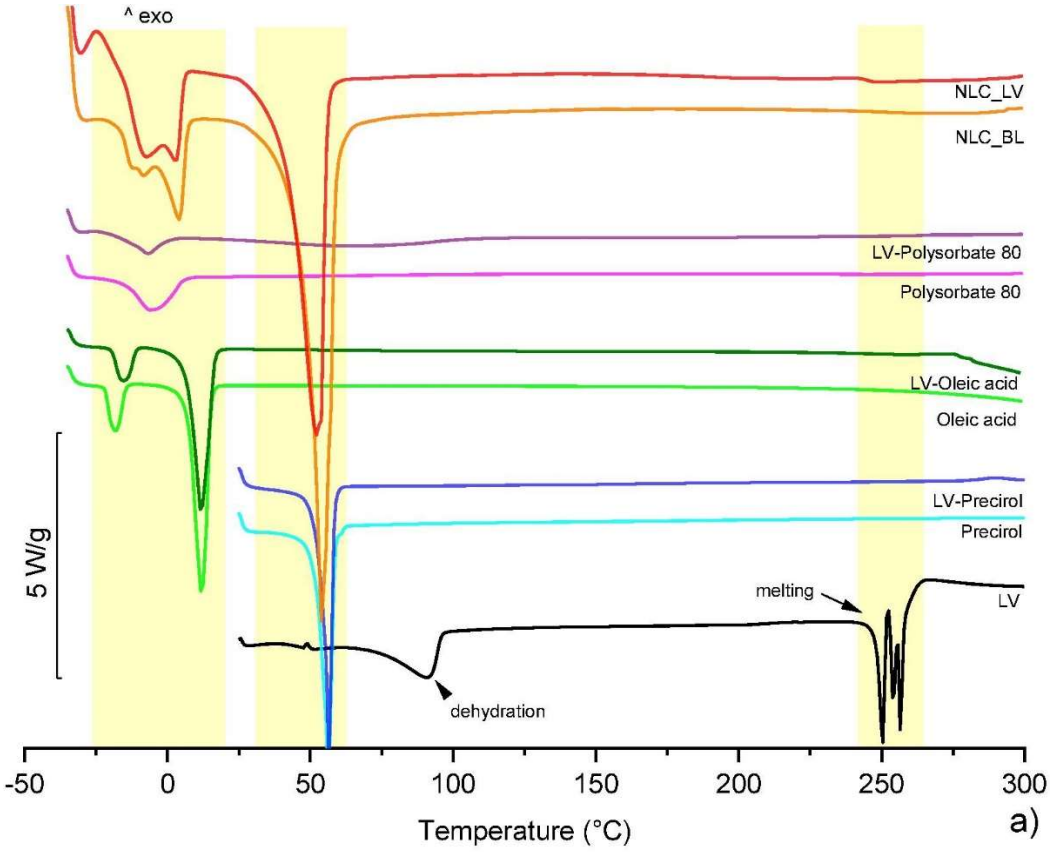
^ exo
NLC_LV
NLC_BL
LV-Polysorbate 80
Polysorbate 80
LV-Oleic acid
Oleic acid
LV-Precirol
Precirol
melting
LV
dehydration
5 W/g
-50
0
50
100
150
200
250
300
Temperature (°C)
a)

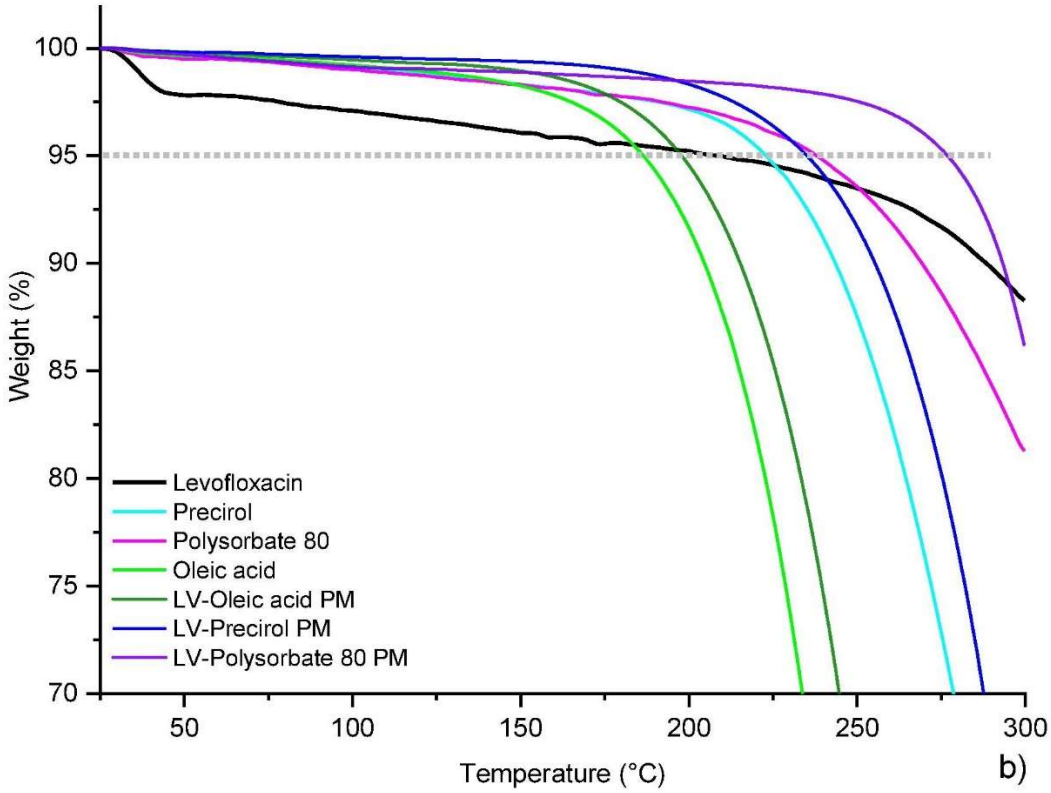
100
95
90
85
80
75
70
Weight (%)
Levofloxacin
Precirol
Polysorbate 80
Oleic acid
LV-Oleic acid PM
LV-Precirol PM
LV-Polysorbate 80 PM
50
100
150
200
250
300
Temperature (°C)
b)

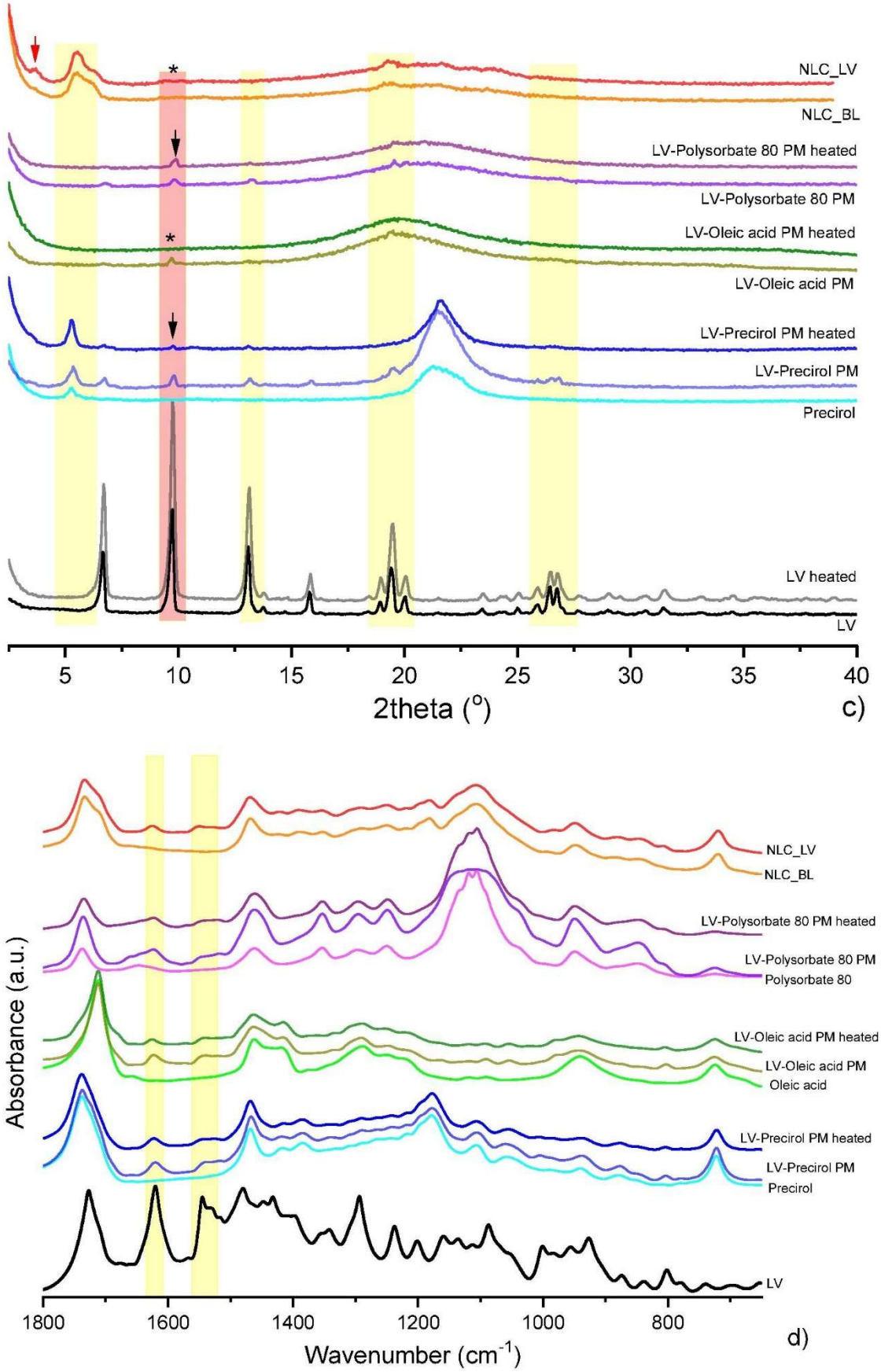

Fig. 1. DSC (A), TGA (B), XRD (C) and FTIR (D) data of levofloxacin (LV), the chosen excipients to produce NLCs and their mixtures (5 % LV + excipient), at

room temperature or after thermal treatment (58 °C, 30 min), and the optimized NLC with and without LV (NLC_LV and NLC_BL, respectively). Yellow rectangles indicate areas characteristic of LV and/or excipients (DSC). Black arrows indicate the presence of LV and stars disappearance of the LV Bragg peak in the heated samples; the red arrow shows the peak position suggesting a liquid crystalline arrangement of the NPs (XRD).

TGA presents decomposition of the samples on heating. Clearly, oleic acid and its mixture with LV have the lower decomposition temperatures, starting at 195–200 °C and being the least thermally stable mixtures (Fig. 1B and Table 2). Degradation also appears in the DSC mixture LV-oleic acid (~275 °C, Fig. 1A). All the physical mixtures have the onset of the decomposition temperature (at 5 % weight loss) higher than for the ingredients alone.

Table 2. Thermal characterization of levofloxacin (LV), the excipients, physical mixtures and optimized NLC (placebo and with LV). Degradation temperature is the temperature at which up to 5% weigh loss occurred.

		DSC		
Ingredient	**Degradation temperature (°C)**	**T_{Onset} (°C)**	**ΔH normalized (J/g)**	**Probable event**
Levofloxacin	145–150	48.6	−76.4	dehydration[1]
		224.6	N/A	γ form melting[1]
		229.5	N/A	β form melting[1]
		232.3	N/A	α form melting[1]
Precirol	**220–225**	51.6	−137.4	melting[2]
Oleic acid	185–190	−21.9	−27.1	γ to α polymorph[3]
		7.0	−135.6	α form melting[3]
Polysorbate 80	235–240	−15.4	−57.2	
		225.8	−3.2	
LV-Precirol	235–240	54.2	−122.6	Precirol melting
		282.0	2.9	possible LV degradation
LV-Oleic acid	195–200	−19,5	−24.0	γ to α polymorph
		6,6	−126.9	

		DSC		
LV-Polysorbate 80	275–280	−16.2	–23.8	
		17.0	−53.9	
NLC_LV (dried at RT)	190–195	−20.9	−39.2	
		41.2	−80.7	Precirol melting
NLC_BL (dried at RT)	190–195	−6.7	−29.2	
		48.9	−102.5	Precirol melting

*Events based on the literature reports: [1] from (Kitaoka et al., 1995); [2] from (Jannin et al., 2006); [3] from (Inoue et al., 2004).

DSC thermograms present the melting points of each component in accordance with the literature (Table 2). Specifically, LV has an endothermic transition due to dehydration with an onset at 48.6 °C and a broad temperature range (40–75 °C) (Fig. 1A). It can also be seen in TGA (~3% weight loss until 50–55 °C, in agreement with the stoichiometric amount of water loss in hemihydrate LV molecules, 2.43 % w/w) (Gorman et al., 2012) (Fig. 1B). Melting, at app. 224.6 °C, followed by extensive decomposition was then observed, with a possible underlying polymorphic transformation (Gorman et al., 2012, Nisar et al., 2020). XRD analysis showed that LV hemihydrate was crystalline in accordance with literature (Wei et al., 2019) and it maintained crystallinity after heating (Fig. 1C).

Precirol presents only one endothermic melting event at 51.6 °C (Table 2) in agreement with the values published before (Hamdani et al., 2003). The same transition occurred in both pure sample and mixture with LV 5 % (Fig. 1A), but no event due to LV melting, was found, suggesting that LV may dissolved in the lipid matrix (Abdel Hady et al., 2020). XRD presented that Precirol had a semi-crystalline structure with a Bragg peak at app. 5.3 °2θ and a broad “halo” between 20 and 23 °2θ. The diffractogram of the physical mixture of this excipient with 5 % w/w LV displayed weak intensity peaks characteristic of the drug, which reduced in intensity following heating to 58 °C and cooling to RT. Thus, LV partially dissolved in this lipid as expected from the qualitative solubility studies. Oleic acid had two endothermic events, corresponding to the solid–solid transition from γ to α form (-21.9 °C) and then the α form melting (7.0 °C). The solid–solid transition temperature is lower than that found in the literature for pure and dry oleic acid (between −3 to −5.7 and 12.2 to 13 °C, respectively) (Inoue et al., 2004, Wartewig et al., 1998), maybe because we used the super refined grade of this excipient. Mixing oleic acid with LV 5 % did not change its transitions on heating

and no LV melting event was seen, suggesting that the drug dissolved in the liquid (Fig. 1A). XRD confirmed that oleic acid was a good solvent for LV, as no peaks of the drug were seen in the mixtures that was heated and then cooled to RT (Fig. 1C). LV at this concentration was detected by XRD as seen for the Precirol system. Polysorbate 80 presented a broad melting range temperature with an onset at −15.4 °C and a broader event when mixed with 5 % LV starting at 17.0 °C, which could be dehydration. Again, no peaks of LV were found. From XRD analysis, we can conclude that the LV did not completely dissolve in the surfactant, but there was evidence of partial solubility (Fig. 1C).

Supporting thermal analysis and XRD studies, IR clearly showed the presence of LV in the mixtures with excipients. The most characteristic were stretching vibrations of the ring carbonyl group (C = O) at 1620 cm−1 and (C = C) of the ring at 1541 cm−1. These principal LV absorptions shifted slightly following heating with oleic acid and Polysorbate 80, to 1623 and 1539 cm−1 as well as 1624 and 1550 cm−1, respectively, with larger deviations seen for the mix with Polysorbate 80. It could suggest weak intermolecular interactions between the components. There were no band shifts for LV in Precirol. Collectively, based on the above studies, LV showed the ability of not only solubilize in the selected excipients, but also to interact with them at molecular level, potentially affecting the NLC formation and their structure. This finding is supported by the work of Ortiz-Collazos et al. showing that LV was able to increase the thickness of the acyl tails in 1,2-dipalmitoyl-sn-glycero-3-phosphocholine monolayers (Ortiz-Collazos et al., 2019). A related molecule, ciprofloxacin, has been asserted to interact with oleic acid via ionic chemical interactions and/or hydrogen bonds (Torge et al., 2017). As a result of preformulation studies presented in this section, the key CMAs were determined.

3.7.2. Optimization of NLCs

Based on our previous experience and reports published by other groups (Beraldo-de-Araújo et al., 2019, Ferreira et al., 2015, Hejri et al., 2013, Kelidari et al., 2017, Subramaniam et al., 2020), optimization of the NLC process and formulation aspects was carried out. Several attributes were investigated: the key excipients and their proportion as well as the process parameters. Following on preformulation studies, pilot NLCs were fabricated with Precirol and stearic acid as prospective solid lipids and oleic acid as a liquid lipid. While both preliminary NLCs showed good LV

incorporation and parameters (NLC with stearic acid: 589 ± 22 nm mean particle size, PdI 0.32 ± 0.01, EE 62 %; NLC with Precirol: 180 ± 30 nm mean size, PdI 0.23 ± 0.03 and EE 57 %), the formulation containing stearic acid became very viscous after 24 h, therefore this formulation prototype was excluded from further studies. A similar behavior was observed by Umerska and co-workers when the nanocapsules with stearic acid solidified after preparation (Umerska et al., 2016).

Having determined the NLC composition, a full factorial design of experiments 2^3 was performed to choose the proportion of excipients, which would ensure the optimum formulation in terms of physicochemical properties. The following targets were determined: z-average of around 200 nm, to avoid reticule-endothelial rejection (Martins et al., 2012, Wang et al., 2020), PdI ≤ 0.3 to reduce e.g. Ostwald ripening (Wooster et al., 2008), high absolute zeta potential values to ensure physical stability and high EE. The inputs (factors) for each of the formulations and the obtained responses are presented in Table 3. Theoretical drug loading (TDL) was also provided for comparisons.

Table 3. Full factorial 23 design of experiment with triplicate of the center point. TDL: theoretical drug loading. Factors: total lipids (TL), amount of surfactant (% w/v) and total proportion of solid lipid (SL) compared to liquid lipid (% w/w). Responses: z-average, polydispersity index (PdI), zeta potential (ZP, measured using milliQ water as the diluent) and EE.

Formulation composition			Factors				Responses		
Code	TDL (%)	Lipid/aqueous phase ratio (g/g)	TL (mg)	Surfactant (% w/v)	Total SL (% w/w)	z-average (nm)	PdI	ZP (mV)	EE (%)
S1	3.86	0.5/10	500	2	70_30	144 ± 2	0.238 ± 0.008	−40 ± 0.7	73.3
S2	2.95	1/10	1000	2	70_30	199 ± 4	0.317 ± 0.025	−44 ± 1	85.6
S3	2.99	0.5/10	500	4	70_30	71 ± 3	0.368 ± 0.067	−43 ± 4	56.8
S4	2.76	1/10	1000	4	70_30	162 ± 0.3	0.242 ± 0.008	−40 ± 0.8	80.1
S5	2.21	0.5/10	500	2	90_10	126 ± 0.4	0.202 ± 0.013	−42 ± 2	41.9
S6	2.27	1/10	1000	2	90_10	234 ± 1	0.288 ± 0.036	−41 ± 2	65.9
S7	1.23	0.5/10	500	4	90_10	87 ± 0.6	0.207 ± 0.003	−31 ± 1.1	23.3
S8	2.28	1/10	1000	4	90_10	143 ± 0.6	0.242 ± 0.002	−38 ± 0.7	66.2
S9_1	2.50	0.75/10	750	3	80_20	152 ± 2	0.210 ± 0.011	−40 ± 0.7	59.9
S9_2	2.86	0.75/10	750	3	80_20	141 ± 0.6	0.222 ± 0.002	−42 ± 0.5	68.7
S9_3	2.70	0.75/10	750	3	80_20	150 ± 1	0.260 ± 0.036	−41 ± 2	64.7

The linear model provided a good explanation of the z-average parameter (r2 = 0.996). The contour z-average plot (Fig. 2A) shows the positive and negative influence of TL and surfactant, respectively, on nanoparticle size indicating that the higher amount of TL and the lower amount of surfactant, the greater nanoparticle size. Pareto charts show that TL has a significant influence on z-average (Fig. 2E), which is reasonable, because of the abundant availability of excipients in the formulation, which allows the constitution of bigger nanoparticles (Das et al., 2011, Martins et al., 2012). On the other hand, the amount of surfactant has a negative influence, which means that the highest the surfactant concentration, the smaller nanoparticle size (Martins et al., 2012). This may be due to the coating effect of the surfactant, as the more surfactant available, the more lipid nanodroplets would be coated and be smaller and/or lowering surface tension.

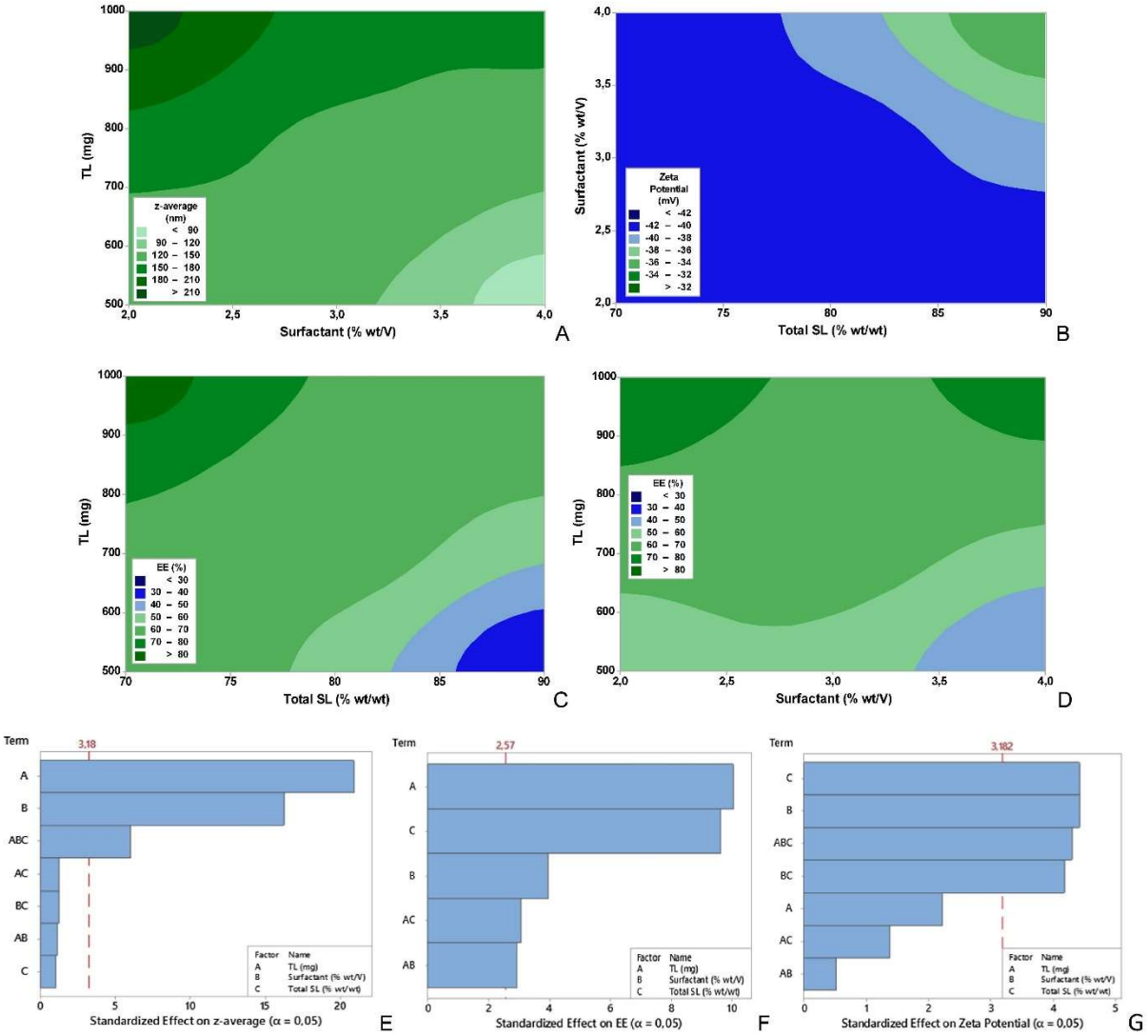

Fig. 2. Contour plots (A-D) and Pareto charts (E-G) with outputs under the significant influence of DoE factors (α = 0.05). The contour plots illustrate how two factors may affected the outputs (z-average (A), zeta potential (B) and EE (C and D)). Pareto charts show the factors that have influenced the outputs (bars that exceed the threshold red lines for z-average (E), EE (F) and zeta potential (G).

Determination of zeta potential depends on the surface charge and it is important when comes to predicting the colloidal stability of nanoparticles in a suspension (Rasmussen et al., 2020). This response was influenced by all the factors in the DoE (r2 = 0.9647), except by TL alone (Fig. 2B and 2G). The difference in the total amount of lipids did not change, on its own, the surface charge of nanoparticles, which occurred when we varied the concentrations of each excipient. To illustrate, Fig. 2B presents that the increased amount of total SL and surfactant lead to an increase in zeta potential (less negative). On the other hand, the interaction of the three factors has a negative effect, resulting on the zeta potential values being more negative. There was no factor with a significant influence on PdI.

Finally, an increasing amount of TL resulted in an increase in EE (Fig. 2C, 2D, 2F), most likely due to greater amount of lipids able to entrap more LV (Das et al., 2011). But increasing the quantity of solid lipid had the opposite impact, the EE values decreased, most likely because LV has more affinity to the liquid lipid, as suggested by DSC, XRD and FTIR results (Fig. 1 A, C and D, respectively). When there was more liquid lipid (30 % of LL) in the formulation, more LV got incorporated in the NLCs and with lower quantities of LL (10 %), lower EE values were obtained. The surfactant led to a decrease in EE, probably because it increased LV solubility in the aqueous phase. However, at the higher amounts of TL, the higher concentration of surfactant did not affect the EE (r^2 = 0.9784).

The formulation S1 presented the highest theoretical drug loading (3.86 %, Table 3), but its EE was not the highest, as expected for formulations with a low TL level. On the other hand, S2 had the highest EE, but solidified on storage, perhaps due to its low level of surfactant (2 %). For these reasons, the subsequent experiments with performed using the composition of the formulation S4 due to its high EE (high levels of TL and the liquid lipid) and the physical stability of the dispersion (high surfactant concentration, 4 %). Preliminary stability tests on the S4 dispersion carried out at room temperature showed that this system was stable for 15 days. The formulation on day

15 had the following characteristics: z-average 176 ± 2 nm; PdI 0.188 ± 0.010; zeta potential −44.8 ± 0.7 mV, and no visual changes in viscosity or homogeneity were noticed. A replicate was produced, and its zeta potential was evaluated after dilution in 10 mM NaCl instead of milliQ water. The change of the dilution medium was introduced as it is more physiological than ultrapure water. This protocol changed the zeta potential value of the samples from around −40 to nearly −20 mV, expected due to screening of the surface charge by NaCl (Skoglund et al., 2017).

The initial process parameters used in the above DoE were based on our previous experiments (Beraldo-de-Araújo et al., 2019) (30 min of sonication at 50 % amplitude) and selecting the process temperature of 58 °C to ensure full melting of the solid lipid. However, after optimizing the proportion of excipients to ensure the best physicochemical properties of LV formulation, we discovered an indication of drug degradation, of around 4 % of total impurities, when performing HPLC analysis for EE. Since the limit of total impurities for LV according to United States Pharmacopeia is 0.5 % ("Levofloxacin," 2017), a new full factorial 2^3 design was designed and performed, introducing process variations to improve NPs with acceptable values of total impurities (Table 4). The analytical grade oleic acid was replaced by Super Refined™ oleic acid, as this change was related with the decrease of LV impurities, mainly LNO, in further tests of LV-excipients compatibility (data not shown). The level of peroxides in pharmaceutical excipients has been known to affect the purity levels of drugs, such as disulfiram (Chen et al., 2015) and others (Khanum and Thevanayagam, 2017).

Table 4. Full factorial 23 design of experiment with triplicate in center point, containing the inputs: temperature (T), sonication time and sonication amplitude. TDL: Theoretical drug loading. The outputs are z-average (measured using 10 mM NaCl as the diluent), polydispersity index (PdI), zeta potential (ZP), entrapment efficiency (EE) and total impurities (SD = standard deviation; n = 3).

Formulation		Factors			Responses				
Formulation #	TDL (%)	T (°C)	Sonic. time (min)	Sonic. amplitude (%)	z-average ± SD (nm)	PdI ± SD	ZP ± SD (mV)	EE (%)	Total impurities (%)
F1	3.48	38	10	30	168 ± 2	0.317 ± 0.036	−24 ± 0.8	75.9	0.37
F2	3.46	78	10	30	183 ± 4	0.353 ± 0.033	–22 ± 0.8	77.5	0.75
F3	3.51	38	30	30	156 ± 3	0.271 ± 0.01	−24 ± 1	75.5	0.43
F4	3.48	78	30	30	169 ± 6	0.322 ± 0.029	−24 ± 0.9	75.4	1.09

Formulation		Factors			Responses				
Formulation #	TDL (%)	T (°C)	Sonic. time (min)	Sonic. amplitude (%)	z-average ± SD (nm)	PdI ± SD	ZP ± SD (mV)	EE (%)	Total impurities (%)
F5	3.47	38	10	70	138 ± 1	0.266 ± 0.025	−21 ± 0.7	73.9	0.56
F6	3.42	78	10	70	163 ± 1	0.256 ± 0.007	–22 ± 1	72.2	0.74
F7	3.52	38	30	70	132 ± 1	0.227 ± 0.017	−21 ± 0.7	74.7	0.53
F8	3.47	78	30	70	164 ± 1	0.267 ± 0.006	−21 ± 0.4	78.9	1.13
F9_1	3.49	58	20	50	140 ± 2	0.238 ± 0.007	−21 ± 0.4	77.7	0.48
F9_2	3.43	58	20	50	138 ± 2	0.247 ± 0.005	−21 ± 0.8	71.9	0.53
F9_3	3.45	58	20	50	142 ± 0.2	0.281 ± 0.032	−21 ± 0.6	75.2	0.63

After analyzing the outcomes, we were able to determine that temperature and sonication amplitude had the most impact on the z-average values, with the highest values of temperature resulting in larger NP sizes, while the highest amplitude gave smaller NP sizes, followed by the sonication time (longer sonication gave smaller nanoparticles) (r2 = 0.9917) (Fig. 3A). The sonication amplitude was the only factor affecting PdI (lower PdI values were obtained with higher sonication amplitude, r2 = 0.5072) (Fig. 3B). Zeta potential appeared to be dependent on a multitude of factors and their interactions (r2 = 1), but, from a practical point of view, the values of zeta potential were all acceptable (around −20 mV) and, in addition, polysorbate 80 is a nonionic surfactant providing steric stabilization to the nanoparticles. The backward elimination (α = 0.05) removed all terms from the model pertaining to EE, thus it was not possible to determine the significant factors impacting the EE values. Importantly, the highest content of total impurities was related to the highest levels of temperature and sonication time (r2 = 0.9641) (Fig. 3D).

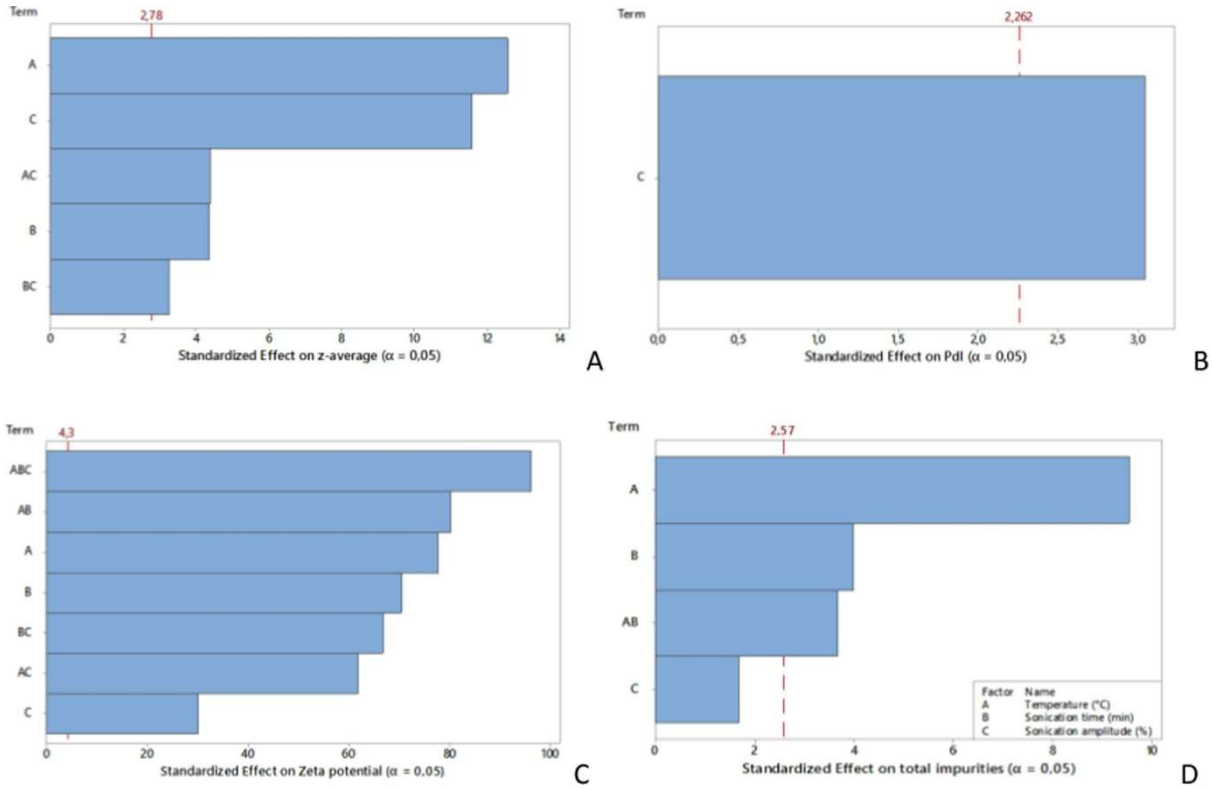

Fig. 3. Pareto charts of the effect of the factors on the dependent variables z-average (A), PdI (B), zeta potential (C) and total impurities (D). The bars correspond to the factors or their interactions. The bars that surpassed the Bonferroni limits have a relevant interference on the respective outputs.

Regarding the process parameters, we focused on total impurities and PdI, since all the particle size values were < 200 nm, zeta potential below −20 mV and EE was not statistically influenced by any DoE factor. Therefore, it was decided to avoid the highest temperature and longest sonication time to prevent LV degradation. However, working with these two parameters at the lowest levels lead to formulations with higher apparent viscosity, thus it was decided to work with their intermediate levels (58 °C and 20 min, respectively). As there was a weak correlation (r2 = 0.5072) between high amplitude of sonication and low PdI, then this value was fixed it at 50 %. In summary, the only change introduced to the process conditions was the duration of the sonication process, reduced from 30 to 20 min.

Overall, superior formulations were designed as guided by the DoEs, with greater EE values than those published for lipid nanocarriers. There is only one account that reports on the maximum of entrapped LV of ~ 56 % that could be incorporated in NLCs (Islan et al., 2016). Another study loaded almost the same amount of LV on solid lipid nanoparticles (SLN) as that reported in the Islan et al. study

(Islan et al., 2016), however, SLNs are known as not an optimum option for an entrapped drug in terms of the long term stability (Abdel Hady et al., 2020). Polymeric nanoparticles were the most chosen carriers to deliver LV, including the PLGA-based systems. The success in terms of obtaining high EE values seems to depend on the type of polymer and the method of nanoparticle production, and could reach between ~ 3 % with chitosan (Ameeduzzafar et al., 2018) and ~ 91 % with PLGA (Shah et al., 2020). Although polymeric and lipid nanoparticles have been applied to carry LV, the natural and biological source of lipids yield nanoparticles potentially less toxic than polymeric NPs, depending on the polymer (natural, semisynthetic or synthetic origin), and easier to scale up (Müller et al., 2000, Rezigue, 2020).

3.7.3. Solid state properties of optimized NLCs

Following the optimization of the composition and process condition, thermal properties of the LV loaded NLC (NLC_LV) were compared to the unloaded carrier equivalent (NLC_BL). The thermograms of both were comparable, showing a range of endothermal peaks up to 25 °C, as the ones of oleic acid and Polysorbate 80. The melting peaks of Precirol were broader and shifted to lower temperatures, being affected by the liquid oleic acid and Polysorbate 80 (highlighted on Fig. 1A). In addition, a very low intensity endotherm at around 250 °C was noted for NLC_LV, most likely of LV. The heating improved LV solubilization in the excipient mixture, and in the optimized NLC_LV one could see the presence of a faint crystalline LV peak at ~ 18-20° 2θ that may be due to the non-solubilized drug (Fig. 1(c)). This peak was absent in NLC_BL. This is in accordance with the further EE determination and the presence of ~ 25 % free LV (Table 3). Interestingly, in both NLC samples an extra, low intensity peak was seen at 3.7° 2θ, absent from diffraction patterns of the components and it was not caused by a polymorphic transformation of LV occurring on heating. It might be due to the liquid crystalline arrangements of NLC components and this periodicity was estimated to be approximately 2 nm (Nonomura et al., 2009).

The partial solubility of LV in the NLC mixture along with the possible intriguing lamellar structure of the NLC prompted further investigations by DVS. The isotherm plots of NLC_LV and NLC_BL were similar (Fig. 4 A). The desorption data followed sorption data. At the end of the sorption cycle both NLC_LV and NLC_BL sorbed the same amount of water (approximately 9 %). At the end of the desorption cycle, the mass was similar to the initial mass (change in mass was smaller than 0.05

%). Both samples sorbed approximately 5.7 % of water at 80 % RH, so they can be considered as moderately hygroscopic, considering their lipidic constitution (2–15 % w/w of water uptake at 25 °C/80 RH, (Newman et al., 2008)).

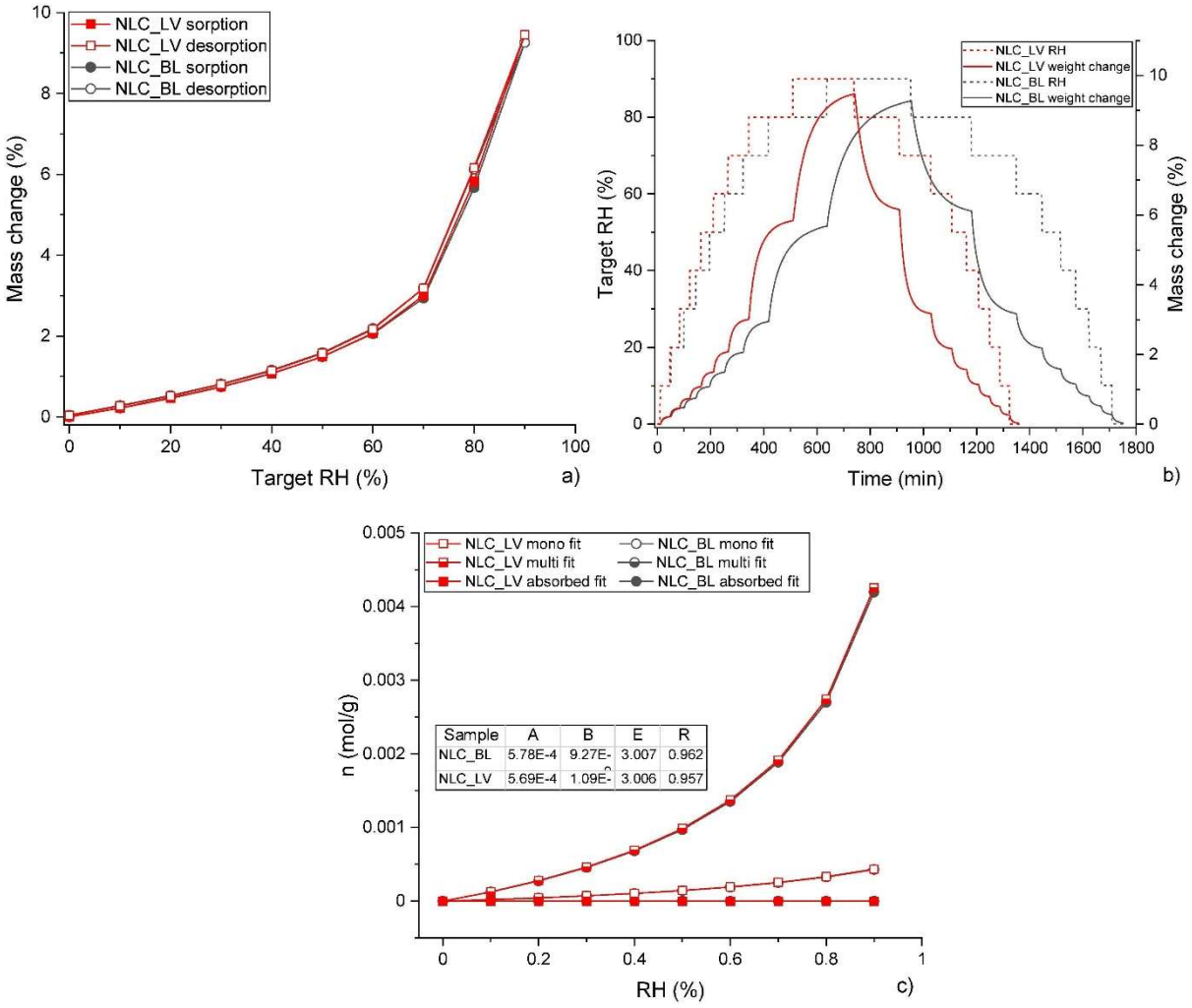

Fig. 4. (A) Moisture sorption and desorption isotherm plots of NLCs at 25 °C, (B) Moisture sorption and desorption kinetic plots of NLCs at 25 °C. Broken lines show RH variations during sorption (0 – 90 % RH) and desorption (90 – 0 % RH), while solid lines show mass change (%) during the same conditions of sorption and desorption, (C) Water distribution patterns according to the Young-Nelson model in NLCs (mono fit refers to a monomolecular adsorption layer; multi fit refers to an adsorption as a multilayer and adsorbed fit refers to adsorption into the interior of nanoparticles) with parameters estimated from the Young-Nelson model for dried NLCs presented in the table: A - fraction of adsorbed water (mol/g), B - fraction of absorbed water (mol/g), E - Young-Nelson equilibrium constant, R: regression coefficient. NLC_BL: blank lipid NPs and NLC_LV: levofloxacin-loaded lipid NPs.

The only difference between the loaded and unloaded NLCs was seen in the kinetic DVS plots (Fig. 4B), indicating that after exposure to 0–90 % RH at all RH steps the equilibrium was established, and that moisture sorption and desorption occurred rapidly at low RH and became slower at higher RH (80–90 %). The incorporation of LV shortened both, sorption and desorption cycles: the sorption cycle lasted approximately 13 h and 15.5 h for NLC_LV and NLC_BL, respectively, whereas the completion of both, sorption and desorption cycles (0–90-0 % RH) took approximately 23.5 and 28.5 h, respectively.

Considering the very similar isotherms for NLC_LV and NLC_BL, it was of no surprise that the water distribution patterns, according to the Young-Nelson model (Mesallati et al., 2019), were also alike (Fig. 4C). According to this model, water can be taken up by a sample in three different ways: adsorbed as a monomolecular layer, adsorbed as a multilayer, or absorbed into the interior of the sample (Young and Nelson, 1967). Most water taken up by the NLCs was bound to their exterior surfaces as a multilayer (Fig. 4C). A small part of water taken up by the particles was adsorbed as a monolayer. The water did not penetrate to the interior of the nanoparticles, as reflected by the value of fraction of absorbed water, which was 4–5 orders of magnitude lower than the fraction of adsorbed water (Fig. 4C). This is consistent with the hydrophobic nature of the NLC core, which does not allow water penetration.

Therefore, this analysis showed that NLCs has a lipidic core with part of LV solubilized in this lipidic core, while the outside possibly had a more hydrophilic, lamellar-like construction with the remaining LV molecules dispersed throughout.

3.7.4. Drug release

The dissolution of free LV was carried out for 24 h and compared to the drug release profile from NLC_LV at the same conditions (Fig. 5). The free LV had a fast and complete dissolution in the PBS medium, as expected of a class I BCS drug (high solubility and high permeability) (Koeppe et al., 2011). Around 85 % of the entrapped drug released after 15 min with the remaining LV amount contained in the nanoparticles within the timeframe of the experiment (24 h). The entrapped LV may be bound to the lipids, as hypothesized above, since no degradation was detected by HPLC. We also performed a release experiment using the Franz cell apparatus, which has a cellulose membrane separating the donor from the acceptor compartments. Free

LV presented a slow permeation rate through the membrane with a longer release time when compared to the results of the test with no membrane. The drug from NLC_LV had a delayed release profile in the Franz cell method when compared to the free drug in the same setup, resulting in nearly 50 % release after 5 h. At the end of the test, approximately 10 % was also retained in NLC.

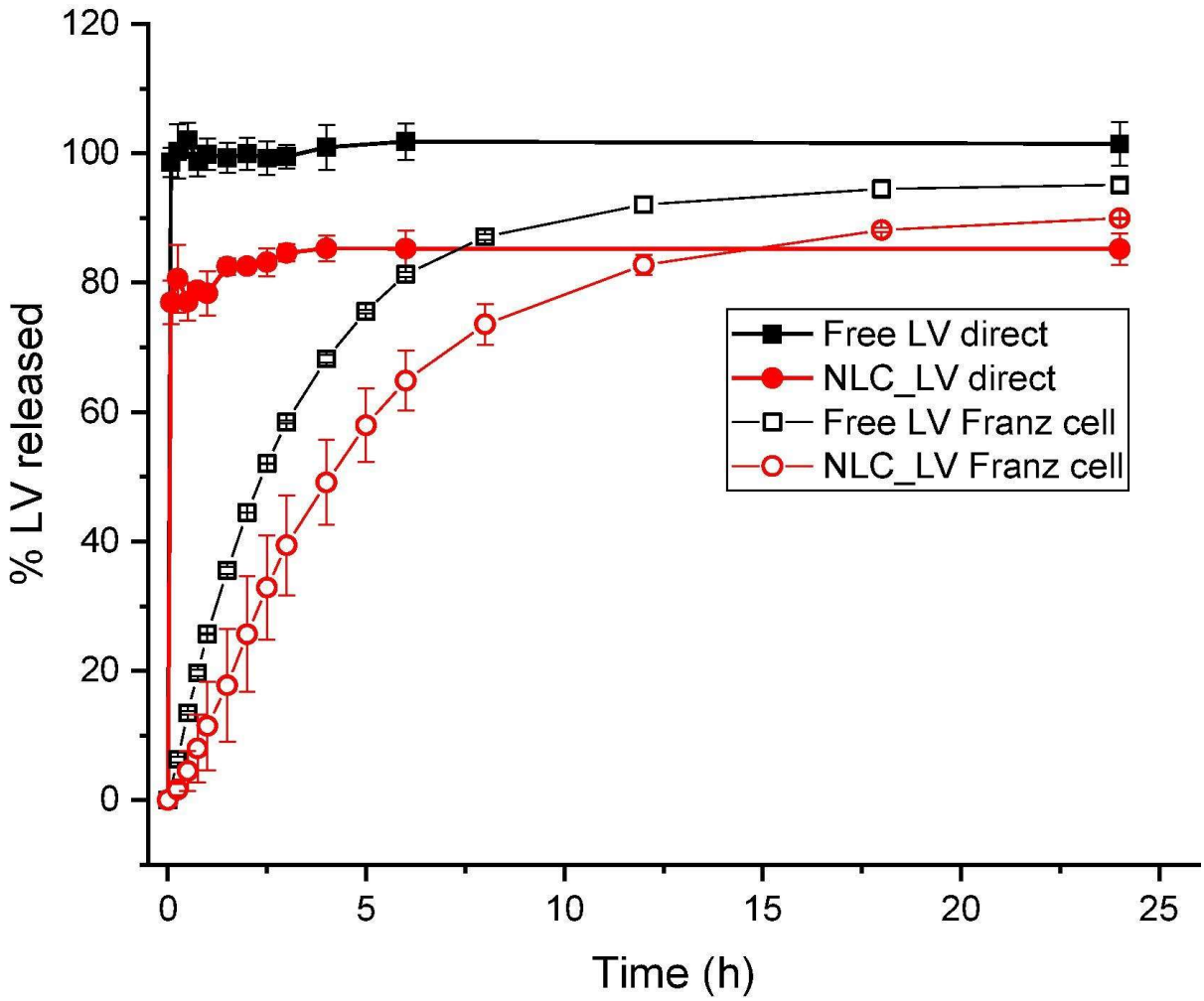

Fig. 5. LV release profiles. Free LV dissolution (black filled squares, n = 4), LV from NLC_LV using the direct method (red filled circles, n = 4), free LV in the Franz cell apparatus (black open squares, n = 2) and LV from NLC_LV in the Franz cell apparatus (red open circles, n = 2), The medium in the direct method and the acceptor compartment in the Franz cell method was PBS 0.1 M, pH 7.4.

Abdel Hady and co-workers incorporated LV and doxycycline in SLNs and performed drug release by the dialysis bag method (Abdel Hady et al., 2020). They found that 50 % of LV released after 5 h from the SLN with the intermediate amount of

surfactant (2.125 % of Span 60), which is in line with our results. Other researchers produced NLCs of LV with DNAse and also assessed the release profile by the dialysis method. They found nearly 60 % release after 5 h, close to our results, at the same timepoint (Islan et al., 2016). Noteworthy, both studies did not present the corresponding release profiles of free LV, therefore we cannot compare the differences in the LV permeation rate based on the literature data.

The rapid LV release from NLC_LV upon direct dilution in PBS could indicate a fast release in an intravenous application. In contrast, the cellulose membrane studies showed a slower release. The membrane test is closer to a mucosal application, such as nasal and pulmonary routes of administration, where the local fluids have a small volume suggesting that these NLCs with modified release might be valuable for LV administration on mucosal surfaces. In addition, the non-released amount of LV from the NLCs corresponds to approximately 400 µg/mL, which is sufficient to inhibit bacteria that are susceptible to this drug (Grillon et al., 2016). Since NLCs have been shown to enhance internalization of several drugs (Barbosa et al., 2016, Garbuzenko et al., 2019) and LV has a limited efficacy of intracellular bacterial killing (Nguyen et al., 2006), our formulation has potential to enhance LV activity against intracellular bacteria, regardless of the administration route.

3.7.5. Accelerated stability test

Accelerated stability tests with both free and LV-loaded optimized samples (NLC_LV and NLC_BL) were performed. The samples were kept in a stability chamber for 30 days at 40 °C and 75 % RH, which might correspond to 4 months of long-term stability, according to the Arrhenius equation (Nicoletti et al., 2009). The parameters evaluated before and after the incubation were z-average, PdI, zeta potential, EE, drug recovery and total impurities.

NLC_BL increases in size and PdI, followed by an increase in zeta potential. After 30 days of incubation, the apparent viscosity considerably increased, probably related to the strength of the interfacial film (Fang et al., 2008). On the other hand, NLC_LV presented acceptable physical stability, keeping the size constant between 138 and 145 nm, which is in a range required to avoid reticule-endothelial rejection (100–300 nm) (Wang et al., 2020). The PdI (0.241–0.223) and zeta potential (-18.1 to −15.9 mV) values presented slight fluctuations which did not impact on the stability or the formulation dispersity. The particles in the mentioned size range and negatively

charged are adequate, for example, for a pulmonary route of administration, being able to penetrate lung mucus barrier (Finbloom et al., 2020). EE and drug recovery values were also maintained (1.2 % and 2 % variation, respectively), while total impurities increased by a 1.7-fold in relation to the initial amount. But, as the greatest amount of impurities were detected outside the NPs (the filtrate), the carrier probably protected the incorporated drug from degradation.

These findings have shown the significance of performing formulation and process studies with a drug stability indicating method. To avoid LV degradation, NPs could be dried following the formulation process suing a secondary pharmaceutical process. The complexation of LV to cations could help to stabilize LV, as suggested by Brillaut et al., for another fluoroquinolone, ciprofloxacin, which resulted in decrease in drug permeability, a desirable feature for pulmonary administration and local action (Brillault et al., 2017). Noteworthy, Seedher and Agarwal reported that this complex with LV may reduce antibiotic activity due to altered albumin-binding rates, which should be considered when planning intravenous or oral administrations, but it would not be an issue to a non-systemic route of delivery such as pulmonary (Seedher and Agarwal, 2010). Thus, the incorporation of LV in NLC enhances drug stability, protects the drug from degradation and have adequate characteristics for various routes of administration (Ghasemiyeh and Mohammadi-Samani, 2018, Thapa et al., 2021), including the inhalation route (Gelperina et al., 2005).

3.8. Conclusions

In this study, we investigated the CMAs for the levofloxacin lipid-based nanoparticles, selecting biodegradable and non-toxic excipients. Further, we optimized the excipient composition for compatibility and solubility, incorporating higher amounts of levofloxacin in NLC than that described for lipid nanoparticles in the published literature. Solid state analysis indicated that the NLCs had a lipid core with most LV solubilized in it, and the outside was more hydrophilic, containing the remaining LV molecules dispersed in a lamellar-like construction. From the process DoE we found that LV impurities, mainly LNO, could be present in different concentrations in the NLCs depending on the CPPs (sonication time, amplitude and temperature). The LNO degradation product has no antimicrobial activity and could affect the final drug dose, which highlights the need for stability indicating methods when formulating LV.

We prepared an optimized NLC with the adjusted process parameters (58 °C, 20 min sonication time and 50 % sonication amplitude) and accelerated studies revealed that LV-loaded NLC was stable according to the preset CQAs for 30 days (40 °C/75 % RH) with no significant changes in the particle size, polydispersibility, zeta potential and EE. Total impurities increased 1.7-fold after 30 days at accelerated stability conditions, but it was mainly LV degradation from non-entrapped drug, indicating the drug-protective action of NLC. LV presented a fast release from NLC upon dilution in buffer, but sustained release by the Franz cell method, indicating a preferential use in mucous membranes, such as administration by pulmonary or nasal routes. Independent of the release method, approximately 10–15 % of LV remained in the NLCs, which can boost LV internalization and consequently improve intracellular bacterial killing.

CRediT authorship contribution statement

Viviane Lucia Beraldo de Araújo: Conceptualization, Methodology, Formal analysis, Investigation, Resources, Writing – original draft, Visualization. Ana Flávia Siqueira Vicente: Methodology, Formal analysis, Investigation, Writing – original draft. Marcelo van Vliet Lima: Methodology, Validation, Formal analysis, Investigation, Writing – original draft, Visualization. Anita Umerska: Conceptualization, Methodology, Formal analysis, Investigation, Writing – original draft, Visualization. Eliana Barbosa Souto: Conceptualization, Resources, Writing – original draft, Supervision. Lidia Tajber: Conceptualization, Formal analysis, Resources, Writing – review & editing, Visualization, Supervision, Project administration, Funding acquisition. Laura de Oliveira Nascimento: Conceptualization, Formal analysis, Resources, Writing – review & editing, Visualization, Supervision, Project administration, Funding acquisition.

Declaration of Competing Interest

The authors declare that they have no known competing financial interests or personal relationships that could have appeared to influence the work reported in this paper.

Acknowledgements

This study was part-financed by the Coordenação de Aperfeiçoamento de Pessoal de Nível Superior - Brasil (CAPES) - Finance Code 001, CAPES-PrInt, Santander – Program of International Mobility number 31/2018 and Sao Paulo Research Foundation (FAPESP) grant numbers 2018/03666-3, 2019/09719-4 and 2020/08059-8. LT and AU acknowledge funding from Science Foundation Ireland, grants 15/CDA/3602 and 12/RC/2275_P2.

3.9. References

M. Abdel Hady, O.M. Sayed, M.A. Akl
Brain uptake and accumulation of new levofloxacin-doxycycline combination through the use of solid lipid nanoparticles: formulation; optimization and in-vivo evaluation
Colloids Surf. B Biointerfaces, 193 (2020), Article 111076, 10.1016/j.colsurfb.2020.111076
Ameeduzzafar, S.S. Imam, S.N. Abbas Bukhari, J. Ahmad, A. Ali
Formulation and optimization of levofloxacin loaded chitosan nanoparticle for ocular delivery: in-vitro characterization, ocular tolerance and antibacterial activity
Int. J. Biol. Macromol., 108 (2018), pp. 650-659
J.P. Barbosa, A.R. Neves, A.M. Silva, M.A. Barbosa, M. Salette Reis, S.G. Santos
Nanostructured lipid carriers loaded with resveratrol modulate human dendritic cells
Int. J. Nanomedicine, 11 (2016), pp. 3501-3516, 10.2147/IJN.S108694
V.L. Beraldo-de-Araújo, A. Beraldo-de-Araújo, J.S.R. Costa, A.C.M. Pelegrine, L.N.M. Ribeiro, E. de Paula, L. Oliveira-Nascimento
Excipient-excipient interactions in the development of nanocarriers: an innovative statistical approach for formulation decisions
Sci. Rep., 9 (2019), p. 10738, 10.1038/s41598-019-47270-w
M. Bhalekar, P. Upadhaya, A. Madgulkar
Formulation and characterization of solid lipid nanoparticles for an anti-retroviral drug darunavir
Appl. Nanosci., 7 (2017), pp. 47-57, 10.1007/s13204-017-0547-1
J. Brillault, F. Tewes, W. Couet, J.C. Olivier
In vitro biopharmaceutical evaluation of ciprofloxacin/metal cation complexes for pulmonary administration
Eur. J. Pharm. Sci., 97 (2017), pp. 92-98, 10.1016/j.ejps.2016.11.011
X. Chen, L. Zhang, X. Hu, X. Lin, Y. Zhang, X. Tang
Formulation and preparation of a stable intravenous disulfiram-loaded lipid emulsion
Eur. J. Lipid Sci. Technol., 117 (2015), pp. 869-878, 10.1002/ejlt.201400278
S. Cunha, C.P. Costa, J.N. Moreira, J.M. Sousa Lobo, A.C. Silva
Using the quality by design (QbD) approach to optimize formulations of lipid nanoparticles and nanoemulsions: a review
Nanomed. Nanotechnol. Biol. Med., 28 (2020), Article 102206, 10.1016/j.nano.2020.102206
A. Czyrski, K. Anusiak, A. Teżyk
The degradation of levofloxacin in infusions exposed to daylight with an identification of a degradation product with HPLC-MS
Sci. Rep., 9 (2019), p. 3621, 10.1038/s41598-019-40201-9
S. Das, W.K. Ng, P. Kanaujia, S. Kim, R.B.H. Tan
Formulation design, preparation and physicochemical characterizations of solid lipid nanoparticles containing a hydrophobic drug: Effects of process variables
Colloids Surf. B Biointerfaces, 88 (2011), pp. 483-489, 10.1016/j.colsurfb.2011.07.036
N. Dhiman, R. Awasthi, B. Sharma, H. Kharkwal, G.T. Kulkarni

Lipid nanoparticles as carriers for bioactive delivery
Front. Chem., 9 (2021), Article 580118, 10.3389/fchem.2021.580118
J.Y. Fang, C.L. Fang, C.H. Liu, Y.H. Su
Lipid nanoparticles as vehicles for topical psoralen delivery: solid lipid nanoparticles (SLN) versus nanostructured lipid carriers (NLC)
Eur. J. Pharm. Biopharm., 70 (2008), pp. 633-640, 10.1016/j.ejpb.2008.05.008
M. Ferreira, L.L. Chaves, S.A.C. Lima, S. Reis
Optimization of nanostructured lipid carriers loaded with methotrexate: a tool for inflammatory and cancer therapy
Int. J. Pharm., 492 (2015), pp. 65-72, 10.1016/j.ijpharm.2015.07.013
J.A. Finbloom, F. Sousa, M.M. Stevens, T.A. Desai
Engineering the drug carrier biointerface to overcome biological barriers to drug delivery
Adv. Drug Deliv. Rev., 167 (2020), pp. 89-108, 10.1016/j.addr.2020.06.007
O.B. Garbuzenko, A. Kuzmov, O. Taratula, S.R. Pine, T. Minko
Strategy to enhance lung cancer treatment by five essential elements: Inhalation delivery, nanotechnology, tumor-receptor targeting, chemo- and gene therapy
Theranostics, 9 (2019), pp. 8362-8376, 10.7150/thno.39816
S. Gelperina, K. Kisich, M.D. Iseman, L. Heifets
The potential advantages of nanoparticle drug delivery systems in chemotherapy of tuberculosis
Am. J. Respir. Crit. Care Med., 172 (2005), pp. 1487-1490, 10.1164/rccm.200504-613PP
P. Ghasemiyeh, S. Mohammadi-Samani
Solid lipid nanoparticles and nanostructured lipid carriers as novel drug delivery systems: applications, advantages and disadvantages
Res. Pharm. Sci., 13 (2018), pp. 288-303, 10.4103/1735-5362.235156
E.M. Gorman, B. Samas, E.J. Munson
Understanding the dehydration of levofloxacin hemihydrate
J. Pharm. Sci., 101 (2012), pp. 3319-3330, 10.1002/jps.23200
A. Grillon, F. Schramm, M. Kleinberg, F. Jehl, M.H. Nguyen
Comparative activity of ciprofloxacin, levofloxacin and moxifloxacin against Klebsiella pneumoniae, Pseudomonas aeruginosa and Stenotrophomonas maltophilia assessed by minimum inhibitory concentrations and time-kill studies
PLoS ONE, 11 (6) (2016), p. e0156690
J. Hamdani, A.J. Moës, K. Amighi
Physical and thermal characterisation of Precirol® and Compritol® as lipophilic glycerides used for the preparation of controlled-release matrix pellets
Int. J. Pharm., 260 (2003), pp. 47-57, 10.1016/S0378-5173(03)00229-1
A. Hejri, A. Khosravi, K. Gharanjig, M. Hejazi
Optimisation of the formulation of β-carotene loaded nanostructured lipid carriers prepared by solvent diffusion method
Food Chem., 141 (2013), pp. 117-123, 10.1016/j.foodchem.2013.02.080
T. Inoue, Y. Hisatsugu, R. Yamamoto, M. Suzuki

Solid-liquid phase behavior of binary fatty acid mixtures: 1. Oleic acid/stearic acid and oleic acid/behenic acid mixtures
Chem. Phys. Lipids, 127 (2004), pp. 143-152, 10.1016/j.chemphyslip.2003.09.014
G.A. Islan, P.C. Tornello, G.A. Abraham, N. Duran, G.R. Castro
Smart lipid nanoparticles containing levofloxacin and DNase for lung delivery. Design and characterization
Colloids Surf. B Biointerfaces, 143 (2016), pp. 168-176, 10.1016/j.colsurfb.2016.03.040
V. Jannin, E. Pochard, O. Chambin
Influence of poloxamers on the dissolution performance and stability of controlled-release formulations containing Precirol® ATO 5
Int. J. Pharm., 309 (2006), pp. 6-15, 10.1016/j.ijpharm.2005.10.042
H.R. Kelidari, M. Saeedi, J. Akbari, K. Morteza-semnani, H. Valizadeh, M. Maniruzzaman, A. Farmoudeh, A. Nokhodchi
Development and optimisation of spironolactone nanoparticles for enhanced dissolution rates and stability
AAPS PharmSciTech, 18 (2017), pp. 1469-1474, 10.1208/s12249-016-0621-0
R. Khanum, H. Thevanayagam
Lipid peroxidation: Its effects on the formulation and use of pharmaceutical emulsions
Asian J. Pharm. Sci., 12 (2017), pp. 401-411, 10.1016/j.ajps.2017.05.003
H. Kitaoka, C. Wada, R. Moroi, H. Hakusui
Effect of dehydration on the formation of levofloxacin pseudopolymorphs
Chem. Pharm. Bull., 43 (1995), pp. 649-653, 10.1248/cpb.43.649
M.O. Koeppe, R. Cristofoletti, E.F. Fernandes, S. Storpirtis, H.E. Junginger, S. Kopp, K.K. Midha, V.P. Shah, S. Stavchansky, J.B. Dressman, D.M. Barends
Biowaiver monographs for immediate release solid oral dosage forms: levofloxacin
J. Pharm. Sci., 100 (2011), pp. 1628-1636, 10.1002/jps.22413
G. Kumar, S. Sharma, N. Shafiq, G.K. Khuller, S. Malhotra
Optimization, in vitro-in vivo evaluation, and short-term tolerability of novel levofloxacin-loaded PLGA nanoparticle formulation
J. Pharm. Sci., 101 (2012), pp. 2165-2176, 10.1002/jps.23087
Levofloxacin, 2017, in: Unites States Pharmacopeia. pp. 4831–4833. https://doi.org/10.1001/jama.1950.02910390046012.
J. Li, Y. Qiao, Z. Wu
Nanosystem trends in drug delivery using quality-by-design concept
J. Control. Release, 256 (2017), pp. 9-18, 10.1016/j.jconrel.2017.04.019
H.H. Liu
Safety profile of the fluoroquinolones: Focus on levofloxacin
Drug Saf., 33 (2010), pp. 353-369, 10.2165/11536360-000000000-00000
Y. Liu, Q. He, M. Wu
Levofloxacin-induced crystal nephropathy
Nephrology, 20 (2015), pp. 437-438, 10.1111/nep.12405
B. Magenheim, M.Y. Levy, S. Benita

A new in vitro technique for the evaluation of drug release profile from colloidal carriers - ultrafiltration technique at low pressure
Int. J. Pharm., 94 (1993), pp. 115-123, 10.1016/0378-5173(93)90015-8
S. Martins, I. Tho, E. Souto, D. Ferreira, M. Brandl
Multivariate design for the evaluation of lipid and surfactant composition effect for optimisation of lipid nanoparticles
Eur. J. Pharm. Sci., 45 (2012), pp. 613-623, 10.1016/j.ejps.2011.12.015
H. Mesallati, A. Umerska, K.J. Paluch, L. Tajber
Amorphous polymeric drug salts as ionic solid dispersion forms of ciprofloxacin
Mol. Pharm., 14 (2017), pp. 2209-2223, 10.1021/acs.molpharmaceut.7b00039
H. Mesallati, A. Umerska, L. Tajber
Fluoroquinolone amorphous polymeric salts and dispersions for veterinary uses
Pharmaceutics, 11 (6) (2019), p. 268
R.H. Müller, K. Mäder, S. Gohla
Solid lipid nanoparticles (SLN) for controlled drug delivery - A review of the state of the art
Eur. J. Pharm. Biopharm., 50 (2000), pp. 161-177, 10.1016/S0939-6411(00)00087-4
A.W. Newman, S.M. Reutzel-Edens, G. Zografi
Characterization of the “hygroscopic” properties of active pharmaceutical ingredients
J. Pharm. Sci., 97 (2008), pp. 1047-1059, 10.1002/jps.21033
H.A. Nguyen, J. Grellet, D. Paillard, V. Dubois, C. Quentin, M.-C. Saux
Factors influencing the intracellular activity of fluoroquinolones: a study using levofloxacin in a Staphylococcus aureus THP-1 monocyte model
J. Antimicrob. Chemother., 57 (2006), pp. 883-890, 10.1093/jac/dkl079
M.A. Nicoletti, E.L. Siqueira, A.C. Bombana, G.G. de Oliveira
Shelf-life of a 2.5% sodium hypochlorite solution as determined by arrhenius equation
Braz. Dent. J., 20 (2009), pp. 27-31, 10.1590/s0103-64402009000100004
J. Nisar, M. Iqbal, M. Iqbal, A. Shah, M.S. Akhter, Sirajuddin, R.A. Khan, I. Uddin, L.A. Shah, M.S. Khan
Decomposition kinetics of levofloxacin: drug-excipient interaction
Zeitschrift fur Phys. Chemie, 234 (1) (2020), pp. 117-128
Y. Nonomura, K. Nakayama, Y. Aoki, A. Fujimori
Phase behavior of bile acid/lipid/water systems containing model dietary lipids
J. Colloid Interface Sci., 339 (2009), pp. 222-229, 10.1016/j.jcis.2009.07.030
S. Ortiz-Collazos, P.H.S. Picciani, O.N. Oliveira, A.S. Pimentel, K.J. Edler
Influence of levofloxacin and clarithromycin on the structure of DPPC monolayers
Biochim. Biophys. Acta - Biomembr., 1861 (10) (2019), p. 182994
S. Papadimitriou, D. Bikiaris
Novel self-assembled core-shell nanoparticles based on crystalline amorphous moieties of aliphatic copolyesters for efficient controlled drug release
J. Control. Release, 138 (2009), pp. 177-184, 10.1016/j.jconrel.2009.05.013
M.K. Rasmussen, J.N. Pedersen, R. Marie
Size and surface charge characterization of nanoparticles with a salt gradient
Nat. Commun., 11 (2020), p. 2337, 10.1038/s41467-020-15889-3

Rezigue, M., 2020. Lipid and polymeric nanoparticles: drug delivery applications. pp. 167–230. https://doi.org/10.1007/978-3-030-36260-7_7.
C. Schwarz, W. Mehnert, J.S. Lucks, R.H. Müller
Solid lipid nanoparticles (SLN) for controlled drug delivery. I. Production, characterization and sterilization
J. Control. Release, 30 (1994), pp. 83-96, 10.1016/0168-3659(94)90047-7
N. Seedher, P. Agarwal
Effect of metal ions on some pharmacologically relevant interactions involving fl uoroquinolone antibiotics
Drug Metabol. Drug Interact., 25 (2010), pp. 17-24, 10.1515/DMDI.2010.003
S.R. Shah, H.R. Prajapati, D.B. Sheth, E.M. Gondaliya, A.J. Vyas, M.M. Soniwala, J.R. Chavda
Pharmacokinetics and in vivo distribution of optimized PLGA nanoparticles for pulmonary delivery of levofloxacin
J. Pharm. Pharmacol., 72 (2020), pp. 1026-1037, 10.1111/jphp.13275
S. Skoglund, J. Hedberg, E. Yunda, A. Godymchuk, E. Blomberg, I. Odnevall Wallinder, Y.K. Mishra
Difficulties and flaws in performing accurate determinations of zeta potentials of metal nanoparticles in complex solutions - Four case studies
PLoS ONE, 12 (7) (2017), p. e0181735
B. Subramaniam, Z.H. Siddik, N.H. Nagoor
Optimization of nanostructured lipid carriers: understanding the types, designs, and parameters in the process of formulations
J. Nanoparticle Res., 22 (2020), p. 141, 10.1007/s11051-020-04848-0
F. Tamjidi, M. Shahedi, J. Varshosaz, A. Nasirpour
EDTA and α-tocopherol improve the chemical stability of astaxanthin loaded into nanostructured lipid carriers
Eur. J. Lipid Sci. Technol., 116 (2014), pp. 968-977, 10.1002/ejlt.201300509
R.K. Thapa, D.B. Diep, H.H. Tønnesen
Nanomedicine-based antimicrobial peptide delivery for bacterial infections: recent advances and future prospects
J. Pharm. Investig., 51 (2021), pp. 377-398, 10.1007/s40005-021-00525-z
A. Torge, S. Wagner, P.S. Chaves, E.G. Oliveira, S.S. Guterres, A.R. Pohlmann, A. Titz, M. Schneider, R.C.R. Beck
Ciprofloxacin-loaded lipid-core nanocapsules as mucus penetrating drug delivery system intended for the treatment of bacterial infections in cystic fibrosis
Int. J. Pharm., 527 (2017), pp. 92-102, 10.1016/j.ijpharm.2017.05.013
A. Umerska, V. Cassisa, N. Matougui, M.L. Joly-Guillou, M. Eveillard, P. Saulnier
Antibacterial action of lipid nanocapsules containing fatty acids or monoglycerides as co-surfactants
Eur. J. Pharm. Biopharm., 108 (2016), pp. 100-110, 10.1016/j.ejpb.2016.09.001
A. Umerska, K. Bialek, J. Zotova, M. Skotnicki, L. Tajber
Anticrystal engineering of ketoprofen and ester local anesthetics: Ionic liquids or deep eutectic mixtures?

Pharmaceutics, 12 (2020), p. 368, 10.3390/pharmaceutics12040368
A. Umerska, N.A. Mugheirbi, A. Kasprzak, P. Saulnier, L. Tajber
Carbohydrate-based Trojan microparticles as carriers for pulmonary delivery of lipid nanocapsules using dry powder inhalation
Powder Technol., 364 (2020), pp. 507-521, 10.1016/j.powtec.2020.02.028
D.Y. Wang, H.C. van der Mei, Y. Ren, H.J. Busscher, L. Shi
Lipid-based antimicrobial delivery-systems for the treatment of bacterial infections
Front. Chem., 7 (2020), p. 872, 10.3389/fchem.2019.00872
S. Wartewig, R. Neubert, W. Rettig, K. Hesse
Structure of stratum corneum lipids characterized by FT-Raman spectroscopy and DSC. IV. Mixtures of ceramides and oleic acid
Chem. Phys. Lipids, 91 (1998), pp. 145-152, 10.1016/S0009-3084(97)00105-9
N. Wei, L. Jia, Z. Shang, J. Gong, J. Gong, S. Wu, J. Wang, W. Tang
Polymorphism of levofloxacin: Structure, properties and phase transformation
CrystEngComm, 21 (2019), pp. 6196-6207, 10.1039/c9ce00847k
T.J. Wooster, M. Golding, P. Sanguansri
Impact of oil type on nanoemulsion formation and ostwald ripening stability
Langmuir, 24 (2008), pp. 12758-12765, 10.1021/la801685v
J.H. Young, G.L. Nelson
Theory of hysteresis between sorption and desorption isotherms in biological materials
Trans. ASAE, 10 (1967), pp. 0260-0263, 10.13031/2013.39649
C. Zhang, W. Zhao, C. Bian, X. Hou, B. Deng, D.W. McComb, X. Chen, Y. Dong
Antibiotic-derived lipid nanoparticles to treat intracellular staphylococcus aureus
ACS Appl. Bio Mater., 2 (2019), pp. 1270-1277, 10.1021/acsabm.8b00821

3.10. Appendix A. Supplementary material

The following are the Supplementary data to this article:

Supporting Information file:

Levofloxacin in nanostructured lipid carriers: preformulation and critical process parameters for a highly incorporated formulation

Viviane Lucia Beraldo-Araújo, Ana Flávia Siqueira Vicente, Marcelo van Vliet Lima, Anita Umerska, Eliana B. Souto, Lidia Tajber, Laura Oliveira-Nascimento

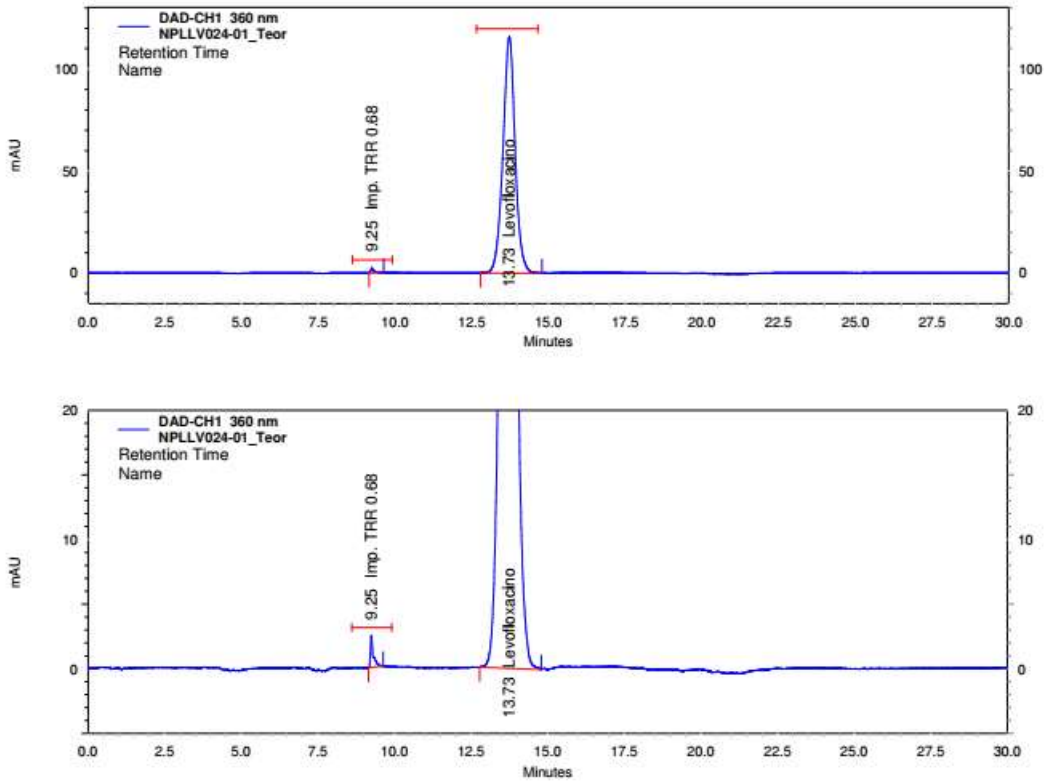

DAD-CH1
360 nm Results

Nome	TR	Área	Theoretical plates (USP)	Asymmetry	S/R	S/N (ASTM)
Imp. TRR 0.68	9.25	61648	84174	3.24	**17.4**	**36.4**
Levofloxacino	13.73	12759626	5796	1.01	**817.9**	**2666.6**

a)

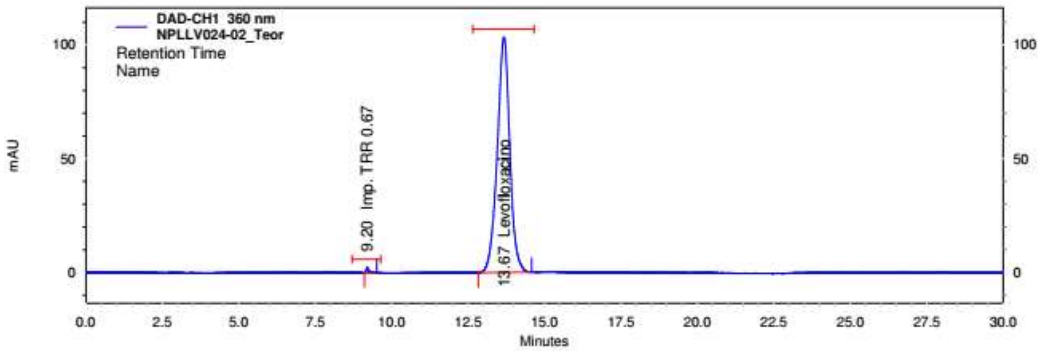

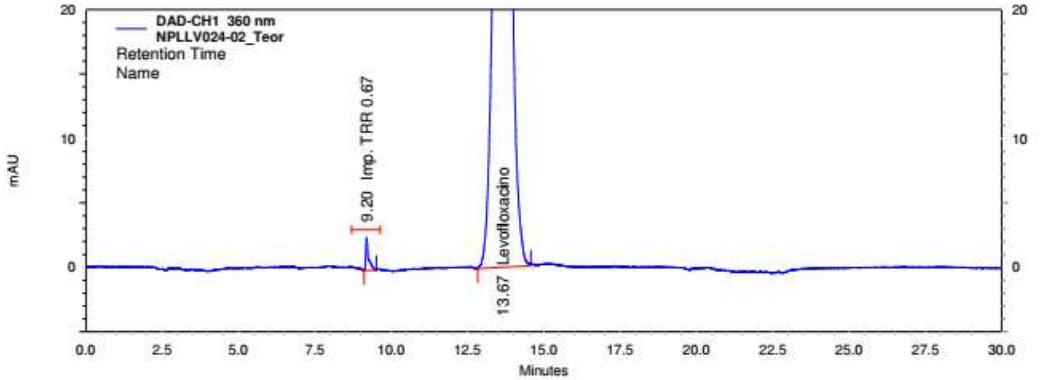

DAD-CH1
360 nm Results

Nome	TR	Área	Theoretical plates (USP)	Asymmetry	S/R	S/N (ASTM)
Imp. TRR 0.67	9.20	62965	81073	2.54	**30.1**	**36.6**
Levofloxacino	13.67	11803288	5353	0.99	**1236.5**	**1814.6**

b)

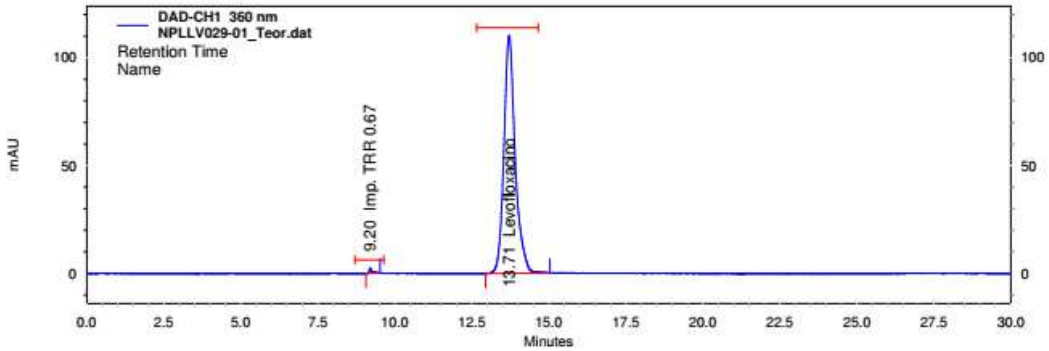

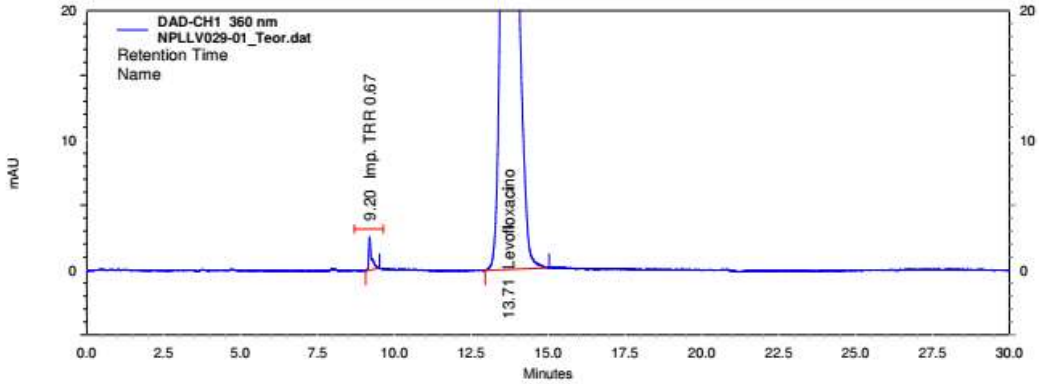

DAD-CH1
360 nm Results

Nome	TR	Área	Theoretical plates (USP)	Asymmetry	S/R	S/N (ASTM)
Imp. TRR 0.67	9.20	63139	84422	3.03	**58.6**	**43.5**
Levofloxacino	13.71	11203254	7281	1.24	**2546.1**	**2527.7**

c)

Fig. S1 Sample chromatographs showing separation of levofloxacin and the degradation products.

4. CHAPTER 3 – NANOSTRUCTURED LIPID CARRIERS LOADING LEVOFLOXACIN: *IN VITRO* BIOLOGICAL EFFECTS OF DIFFERENT SURFACTANT COATINGS FOR REACHING AN OPTIMIZED PULMONARY FORMULATION

4.1. Authors

Viviane Lucia Beraldo-Araújo [a, *], Marcelo van Vliet Lima [a, b], Samira Elisa Alves Geraldo [a], Gabriel da Silva Cordeiro [c], João Paulo Guarnieri [a], Marcelo Lancellotti [a], Karina Cogo Muller [a], Catarina Raposo [a, c], Laura Oliveira-Nascimento [a]

[a] Faculty of Pharmaceutical Sciences, State University of Campinas, Campinas, Brazil

[b] Sanofi Medley Farmacêutica Ltda, Campinas, Brazil

[c] Department of Structural and Functional Biology, Biology Institute, State University of Campinas, Campinas, Brazil

* Corresponding author: vivi.beraldo@gmail.com

4.2. Abstract

Surfactants play a key role as coating agents of nanoparticles, influencing their physicochemical and biological characteristics. Since they have distinct structures, molecular weight, charge, and hydrophilic-lipophilic balance values (HLB), their coating provides different long-term stability conditions and physicochemical features for the particulate carriers, which may interfere with their interactions in body fluids and mucus permeability. We formulated and characterized three levofloxacin-loaded nanostructured lipid carriers (NPLLV), with different non-ionic surfactants: polysorbate 80, poloxamers 407 and 188 (NPLLV_033, NPLLV_034 and NPLLV_035, respectively). Physicochemical characteristics among the NLCs remained similar: nanoparticle size (100-200 nm), size distribution (polydispersity < 0.3), negative zeta potential (-4 to -16 mV), LV entrapment efficiency (> 80%), morphology (rounded) - measured by DLS, NTA, HPLC and electron microscopy. Then, they were evaluated in *in vitro* assays. Their antimicrobial activity *in vitro* was like the activity of the free levofloxacin (LV) against *Klebsiella pneumoniae* and *Staphylococcus aureus*. The Calu-3 cell viability assays brought NPLLV_034 as the safest formulation for non-differentiated cells (50 μg/mL). Besides the good viability profile, NPLLV_034 was able to reduce IL-8 production caused by lipopolysaccharide, compared to free LV. The three formulations had haemolytic activity in 100x-diluted nanoparticles (corresponding to LV 50 μg/mL), with non-haemolytic NPLLV_034 at 400x dilution. Despite of similar physicochemical and antimicrobial profiles, NPLLV_034 presented enhanced cellular viability and potential anti-inflammatory activity. Our findings pointed out this formulation as a promising one to be delivered by the pulmonary route.

Keywords: Nanostructured lipid carrier, levofloxacin, surfactant, Calu-3, pulmonary drug delivery

4.3. Introduction

The lung serves as a gateway between the external and internal environments, rendering it highly susceptible to infections caused by viruses, bacteria, and fungi. Such respiratory tract infections are a major cause of mortality and morbidity worldwide, with *Streptococcus pneumoniae, Staphylococcus aureus,* and *Klebsiella pneumoniae* being the most common bacterial species detected in microbiological diagnoses (Kradin e Digumarthy 2017). In the case of cystic fibrosis patients, *Pseudomonas aeruginosa* is the primary causative agent (Derbali et al. 2019). Unfortunately, the misuse and overuse of antibiotics to treat lung infections have contributed to the development of antibiotic resistance.

Systemic therapies for lung diseases have limitations such as low drug concentrations at the site and side effects due to drug distribution to other organs (Derbali et al. 2019). The lung is a favourable delivery site for local therapy due to a low rate of drug metabolism and rapid onset of therapeutic effects (Elmowafy e Al-Sanea 2021). However, it faces challenges such as the endogenous defence mechanisms, involving proinflammatory responses and particle size related expelling. Some pulmonary diseases that can benefit from local therapy are asthma, chronic obstructive pulmonary disease, cystic fibrosis, pulmonary hypertension, and infections such as pneumonia and tuberculosis (Brunaugh, Smyth, e Williams III 2019).

Although antibiotics are typically administered orally or intravenously, pulmonary drug delivery has been gaining popularity, with Tobramycin, Amikacin sulphate, and Aztreonam being FDA-approved for this route (Li, Zheng, e Leung 2022). Inhaled levofloxacin (LV) has also been approved for use in the European Union and Canada for pseudomonas infection in cystic fibrosis patients.

LV is a broad-spectrum fluoroquinolone antibacterial agent that is commonly used to treat respiratory, genitourinary, and topical infections. In particular, it works against both penicillin-susceptible and penicillin-resistant *Streptococcus pneumoniae*, one of the main etiological agents of the community-acquired pneumonia. The bactericidal action of LV happens by inhibiting bacterial DNA gyrase and topoisomerase IV, facilitated by a rapid absorption after oral administration, good biodistribution, and some tissue accumulation, like in the lungs, prostate gland, and skin. (Croom e Goa 2003; Hurst et al. 2002). Reported side effects of its oral

administration include nausea, diarrhoea, loss of appetite, besides tendon effects and ultimately tendon rupture.

Pulmonary delivery of LV allows dosage split with efficient bacterial clearance, diminishing plasma concentration and consequent side effects. However, it can cause dysgeusia (taste disturbance) and cough as a common side effect not seen in oral administration (Flume et al. 2016). Of note, commercial pulmonary LV has magnesium chloride, which presents a bitter taste (Lawless et al. 2003) and may be involved in the dysgeusia effect.

Studies have demonstrated positive outcomes in the use of nanoparticles for the delivery of LV. For instance, anionic liposomes loaded with LV and delivered through the pulmonary route showed extended release, with sustained antibacterial activity against *P. aeruginosa*. The formulation remained stable during nebulization, leading to deep lung deposition where the infection occurs (Derbali et al. 2019). Furthermore, NLCs carrying LV have shown favourable characteristics, such as good encapsulation, controlled release profile, and effective antimicrobial activity against *P. aeruginosa* and *S. aureus*, as well as reducing bacterial biofilm formation (Islan et al. 2016).

The significance of the surfactant type utilized in NLC stabilization is extensively documented in the literature (Elmowafy e Al-Sanea 2021). Some of the most common types are poloxamer 188, 407, and polysorbate 80 (P188, P407 and P80, respectively) (Liu et al. 2012; Elmowafy e Al-Sanea 2021). P80 coats and facilitates transport of nanoparticles across the blood-brain-barrier (BBB), being helpful for parenteral drug delivery administration targeting the brain (Ravichandran et al. 2021). On the other hand, poloxamers 407 and 188 avoid that serum proteins adsorption to the nanoparticles, increasing their residence time in circulation (Shubhra et al. 2014; Jackson et al. 2000).

The three surfactants are non-ionic and bring less potential toxicity than ionic surfactants (Sonia e Sharma 2014; Miyazawa et al. 2021). Besides, they can be a useful strategy to the drug delivery interfaces, being able to modify drug absorption in the lungs, produce large porous particles (P80 and P407), for example, or stabilize inhalable particles, enhancing powder aerodynamics (P188) (Cortés et al. 2021; Morales, Peters, e Williams 2011).

P407 has mucus-penetrant capacity and would be helpful to a pulmonary drug delivery. Huang et al., 2022 presented a study to enhance mucus penetration and

lung absorption of an inhalable nanomaterial and showed that P407 had a better performance than P80. This behaviour was related to the charge of the coating nanomaterial. As the lung mucus tend to trap and remove nanoparticles by different interactions (hydrogen-bonding, hydrophobic and electrostatic interactions), the nanomaterial with negative potential would have an electrostatic repulsion due to the negative-charged mucin, summed to the hydrophilic surface of the coated-nanoparticle that could avoid this trapping and penetrate the mucus layer (Huang et al. 2022). As P188 is the most hydrophilic surfactant of this study (P188 = HLB 29, P80 = HLB 15 and P407 = HLB 22), it would be promisor to penetrate lung mucus.

Therefore, the aim of this paper was to produce 3 types of NLC, each with one type of surfactant (P80, P407 and P188), and to evaluate their effect in the physicochemical parameters (nanoparticle size, morphology, concentration and distribution, zeta potential, entrapment efficiency), haemolytic capacity and microbial activity against bacteria that provoke lung infections. In addition, cell viability was verified in non-differentiated and differentiated Calu-3 lung cells, together with secretion of the proinflammatory cytokine IL-8 upon formulation contact.

4.4. Material and methods

4.4.1. Material

Levofloxacin hemihydrate (LV, (2S)-7-fluoro-2-methyl-6-(4-methylpiperazin-1-yl)-10-oxo-4-oxa-1-azatricyclo [7.3.1.05,13] trideca-5(13),6,8,11-tetraene-11-carboxylic acid hemihydrate) was gently donated from Sanofi-Medley Farmacêutica Ltda from Brazil. Super Refined™ polysorbate-80, Super Refined™ oleic acid, were donated by Croda (Brazil). Precirol® ATO 5, was donated by Gattefossé (France). Kolliphor® P 188 Geismar (Poloxamer 188, P188) was gently donated by BASF (Brazil). Pluracare F 127 NF (Poloxamer 407, P407) was donated by Chemspecs (Brazil). Trypticasein soy agar (TSA) was purchased from KASVI (Brazil). Mueller Hinton Broth (MHB) was purchased from BD Difco™ (Brazil). All other chemicals and solvents were of analytical grade. Lipopolysaccharides (LPS) from *Escherichia coli* were obtained from Invitrogen (USA). Human IL-8/CXCL8 DuoSet® ELISA DY208-05 kit was purchased from R&D Systems, USA. DMEM with 4500 mg/L glucose, L-glutamine, sodium pyruvate, and sodium bicarbonate (Sigma-Aldrich® code D6429) and MEM non-essential aminoacids solution was purchased from Merck (Brazil). Foetal bovine serum (FBS) was purchased from Cultilab (Brazil). Fresh lamb blood was obtained from Anilab (Brazil). Gibco™ Trypsin-EDTA (0.25%) solution was purchased from ThermoFisher Scientific (Germany). Hank's balanced salt solution (code H8264) was purchased from Sigma-Aldrich®.

Bacterial strains and cell line: *Klebsiella pneumoniae* (strains ATCC BAA 1705 and ATCC 700603) and *Staphylococcus aureus* (strains ATCC 29213 and ATCC 33591) were used to conduct microbiological assessments. Calu-3 was purchased from Banco de Células do Rio de Janeiro – BCRJ (Brazil) (BCRJ code 0264, reference ATCC HTB-55). Calu-3 is an epithelial cell from human bronchial adenocarcinoma cell line used as pulmonary cell model (passages: 40 – 49)

4.4.2. NLC production

NLCs were prepared via hot emulsification-ultrasonication method, as described in (Beraldo-Araújo et al. 2022). The lipid phase (70 % w/w of precirol and 30 % w/w of oleic acid, totalling 10 % w/w of the final formulation) was heated in a beaker in a water bath at 58 ± 1 °C under magnetic stirring (300 rpm) until solid melting, and 0.5 % w/w of LV was added and solubilised to this phase. The aqueous phase (P80,

P407 or P188 at 4 % w/w in ultrapure water), was prepared in another beaker, heated under the same conditions as the lipid phase. Aqueous phase was added to the lipid phase under mixing in an Ultraturrax blender (IKA® T18 basic, Germany) at 12,000 rpm for 3 min using the S18N-19G dispersing tool. This emulsion was sonicated to reach nanometric and homogeneous particles size, using a tip sonicator (Vibracell, Sonics & Materials Inc., USA) fitted with a 3 mm probe, with power 130 W and 20 kHz nominal frequency. Sonication lasted 20 min, in cycles of 30 s (on/off) at an amplitude of 50 %. Final dispersion was cooled over an ice bath to 25 °C and stored at room temperature protected from the light.

4.4.3. NLC physicochemical characterization

4.4.3.1. Determination of hydrodynamic diameter (z-average), polydispersity index (PdI), zeta potential (ZP) and nanoparticle concentration

NLCs were analysed by Dynamic Light Scattering, DLS (Zetasizer Nano ZS90, Malvern Instruments ltd, UK), at a 90° scattering angle and 25 °C, using a disposable polystyrene cuvette for z-average and PdI determinations. Samples were diluted to 1:200 in sodium chloride 10 mM to reach an adequate correlation coefficient (between 0.7 and 1). The zeta potential (ZP) of the same diluted samples was determined by measuring the electrophoretic mobility, using a disposable polystyrene cuvette model DTS1070 with electrodes. All the samples were measured in triplicate and results presented as mean ± standard deviation.

Nanoparticle Tracking Analysis, NTA (Nanosight, Malvern Instruments Ltd) was also utilized at 25 °C. Captures during 30 s of five different populations of each NLC were made, with samples diluted in ultrapure water until reach 30-100 particles per frame and 10^7-10^9 particles per mL (dilution factor: 15000x). NTA allowed the determination of nanoparticle concentration (nanoparticles per mL). D10/D50 and D90 were also determined.

4.4.3.2. Drug content and entrapment efficiency (EE)

The LV was quantified by high performance liquid chromatography (HPLC) as outlined in the United States Pharmacopoeia (USP) monograph for Levofloxacin Tablets ("Levofloxacin monograph." 2017). A Shimadzu HPLC system (Prominence-i LC2030C, Shimadzu, Japan) was used for the analysis. The mobile phase consisted

of a buffer (made up of 8.5 g/L of ammonium acetate, 1.25 g/L of cupric sulfate, pentahydrate, and 1.3 g/L of l-isoleucine in water) and methanol in a ratio of 7:3. The column contained the L1 packing (Waters Symmetry C18 250 mm × 4.6 mm i.d. column, 5 µm particle size). The separation conditions included an oven temperature of 45 °C, a mobile phase flow rate of 0.8 mL/min (isocratic), and an injection volume of 25 µL. UV detection was performed at 360 nm and the total running time was 26 minutes. The quantification of LV was based on a calibration curve using LV standard within a concentration range of 5 µg/mL to 200 µg/mL (r2 = 0.9999). The limits of detection and quantification were found to be 1.97 µg/mL and 5.97 µg/mL, respectively (Beraldo-Araújo et al. 2022).

To determine drug content in nanoparticle dispersions, 250 µL of NLC was mixed with 500 µL of THF in a 25 mL volumetric flask to dissolve the matrix. The mixture was vortexed for 2 minutes using a Quimis mixer, model Q220M (Brazil). Then, 20 mL of the mobile phase was added, and the flask was sonicated in an ultrasonic bath for 5 minutes, with vigorous shaking every two minutes. After completing the volumetric flask with mobile phase, the resulting solution was filtered through a 25 mm diameter and 0.45 µm pore size PVDF membrane syringe filter (Sartorius Minisart®), discarding the first 2 mL of the filtrate.

The entrapment efficiency (EE) was indirectly determined using the ultrafiltration method, which involved centrifuging a volume of 500 µL of NLC suspension at 4100 × g for 20 minutes in an Eppendorf 5418 centrifuge (Germany), using centrifugal filter tubes (Millex, Millipore, USA) with a 30 kDa molecular weight cut-off (Beraldo-Araújo et al. 2022). The amount of free LV in the supernatant was diluted 25 times in the mobile phase and quantified using the HPLC method. EE was calculated by subtracting the amount of drug detected in the filtrate from the drug content in the formulations, using equation (1):

$$\mathrm{EE}\ (\%) = \frac{\text{Total amount of drug} - \text{free drug}}{\text{Total amount of drug}} * 100 \quad (1)$$

Drug loading was calculated using equation 2 (Papadimitriou e Bikiaris 2009):

$$\mathrm{DL}\ (\%) = \frac{\text{weight of entrapped drug in nanoparticles}}{\text{weight of nanoparticles (drug + excipients)}} * 100 \quad (2)$$

4.4.3.3. Morphology and integrity characterization of NLC by electron microscopy

NLCs were submitted to TEM analysis by diluting them 100x in ultrapure water and depositing 10 µL onto copper grids coated with carbon film (200 mesh). Sample excess was removed using a filter paper and water was evaporated for 1h at room temperature. Grids were treated with 20 µL of uranyl acetate 2% for 1 min to give contrast to the samples, followed by excess removal. Grids were then washed with 20 µL of ultrapure water for 1 min, dried with filter paper and resting at room temperature for 24 h before analysis. Micrographs were obtained using a Tecnai G2 Spirit BioTWIN transmission electron microscope, operated at 80 kV and magnification of 30000x and 68000x (adapted from (Beraldo-de-Araújo et al. 2019)).

Cryo-TEM were applied to have the most realistic images of NLCs' morphology, size and integrity in their diluted state, by a fast-freezing sample step. Copper grids with carbon film type Lacey, 300 mesh (#01895-F, Ted Pella, EUA) were treated with a charge of 25 mA per 50 seconds, in the EasiGlow (I) (Ted Pella, EUA). Then, the grids were put into the sample vitrification robot Vitrobot Mark IV (Thermo, EUA). Non-diluted samples were applied onto the grid and excess removed by Blot time 4 and blot force -3. The grids were immediately frozen in liquid ethane and kept in liquid nitrogen until the analysis in the microscope. Images were acquired in a TEM model Talos Arctica (Thermo, EUA), operated at 200kV. The microscope is equipped with a Ceta 16M 4k x 4k camera (Thermo, EUA) for acquisition of digital images.

4.4.3.4. LV Release Profile

LV drug release was assessed by using Franz-diffusion cells apparatus, with 7 mL static vertical diffusion cells and automatic sampling (Microette Plus®, Hanson Research, USA). The receptor chamber was filled with simulated interstitial lung fluid (SILF), prepared with 17 mg $MgCl_2 \cdot 6H_2O$, 594 mg NaCl, 36 mg KCl, 15 mg Na_2HPO_4, 6.7 mg Na_2SO_4, 35 mg $CaCl_2 \cdot 2H_2O$, 96 mg $CH_3COONa \cdot 3H_2O$, 262 mg $NaHCO_3$ and 8 mg sodium citrate dihydrate in 100 mL of ultrapure water (Derbali et al. 2019). The chamber was covered with a cellulose membrane (Spectrapore, 12000 - 14000 Da) and the donor chamber was filled with 1 mL of sample. The available diffusion surface area was 1.76 cm^2 and a clamp was used to hold properly both

compartments. Two diffusion cells were prepared for each sample tested. The receptor medium (SILF) was maintained at 37 ± 1 °C and magnetic stirring at 700 rpm, except during aliquots collection. Aliquots of 2.5 mL (1 mL for purging and 1.5 mL for analysis) were withdrawn at specific time intervals and collected into HPLC vials. The aliquots withdrawn from the receptor chamber were immediately replaced with SILF at the same temperature. The LV concentrations were analysed by HPLC and corrected considering the replenished volumes. Turkey's multiple comparisons test were run, with individual variances from each group computed for each comparison.

4.4.4. Determination of minimum inhibitory concentration (MIC)

All bacteria were cultivated in 37°C for 24h in the appropriate agar medium before the experiments (trypticasein soy agar, TSA). Then, isolated colonies were dispersed in of NaCl 0.9 % to perform MIC tests according to the microdilution method described by the Clinical and Laboratory Standards Institute (CLSI) (CLSI 2018). All tests were made in triplicates, and at least two independent replicates, in the appropriate culture medium (Mulller Hinton Broth - MHB). The assay dilutions of LV and NLCs stock solutions were made in MHB to obtain the same corresponding LV concentration. Stimuli were plated in serial dilutions (1:1) in the 96-wells microplate, followed by $5x10^4$ CFU/well of bacteria. After the incubation period (24h, 37°C), optical density readings were made on a Multiskan™ GO microplate spectrophotometer at 570 nm wavelength (Thermo Fisher Scientific, Inc., Waltham, MA, USA) to verify the turbidity and then stained with an aqueous solution of resazurin 0.01% (30 µL/well), incubated for 2h, for the visualization of bacterial growth/ inhibition (pink and blue, respectively) and MIC determination. MIC assays were run in triplicate, in at least two independent experiments.

4.4.5. Calu-3 cell assays

4.4.5.1. Calu-3 undifferentiated assays

Calu-3 was cultivated in DMEM (code D6429) supplemented with 10 % (V/V) FBS (Cultilab, Brazil) and 1% (V/V) non-essential aminoacids solution. Calu-3 was cultivated in cell culture flasks of 75 cm^2 surface area, incubated at 37 °C, 5% CO_2 and 90% of relative humidity. Medium was changed every 2-3 days and subcultured

after reaching ~ 80% of confluency, using a Trypsin-EDTA (0.25%) solution. Passages used in the experiments: 40 – 49 (maximum 8th passage post-thaw).

For viability assays, Calu-3 cells were seeded in the 96-well microplate at a density of 5×10^4 cells/well (100 μL) and incubated for 24h at 37°C, 5% CO_2 and 90% relative humidity. Then, cells were exposed to different treatments (LV aqueous solution, NPLBL, NPLLV, P80, P407 and P188) at different concentrations diluted in cell culture medium. Viable cell control was evaluated with cell culture medium and death cell control with DMSO 30% in cell culture medium. Cell viability was evaluated after 24 or 48h, by two different approaches: cell mitochondrial activity via MTT assay and cell membrane integrity, via neutral red assay. (n = 4 replicates, and a minimum of two independent experiments).

For the MTT assay, medium was removed from the treated cells and replaced by 110 μL of MTT 0.5 mg/mL in cell culture medium, followed by 3h at 37°C, 5% CO_2 and 90% relative humidity. Then, the reagent was removed and replaced by 100 μL of isopropanol to dissolve the formazan crystals. The absorbance was read using a Multiskan™ GO microplate spectrophotometer at 570 nm wavelength (Thermo Fisher Scientific, Inc., Waltham, MA, USA).(Chen et al. 2021; Riss et al. 2004).

For the Neutral Red assay, medium was removed from the treated cells and each well was washed with phosphate buffer saline (PBS) 150 μL/well. Further, 200 μL/well of neutral red solution (50 μg/mL, diluted in cell culture medium) were added and incubated for 3 h. Cells were washed with PBS again (150 μL/well) and treated with 150 μL of acidic-ethanol solution (made up with 1% of glacial acetic acid, 50% of 96% ethanol and 49% of ultrapure water) to solubilize the cell-incorporated dye. The microplate was agitated for 10 min, at 150 rpm and 37 °C in a shaker incubator. Absorbance was read in a Multiskan™ GO microplate spectrophotometer at 540 nm wavelength (Thermo Fisher Scientific, Inc., Waltham, MA, USA). This protocol was adapted from (Chen et al. 2021; Repetto, del Peso, e Zurita 2008).

4.4.5.2. Calu-3 differentiation and viability assays

Calu-3 differentiation was performed to confirm cell viability (neutral red assay) and cell secretion of IL-8 cytokine, and characterized by scanning electron microscopy and Hoechst nuclei stain. Differentiation followed the literature descriptions (Jeong et al. 2019; Haghi et al. 2010, 3; Lee, Lethem, e Lansley 2021; Chen et al.

2021) in Transwell-Clear™ inserts (6.5 mm, 0.4 µm diameter size pore, polyester membrane, 0.33cm^2 effective area for growth), over a 24-well microplate (Corning Costar, Cambridge, MA). Before cell seeding, inserts were washed with PBS, and 600 µL of cell culture medium were added on the basolateral compartment. Then, 100 µL of Calu-3 were seeded onto the apical compartment at a density of 5 x 10^5 cells/cm^2 (approximately 1.5 x 10^5 cells/insert).

Cells were incubated (37 °C, 5 % CO_2, 90 % relative humidity) and the culture medium changed every other day until cell monolayer was reached and confirmed by transepithelial electrical resistance (TEER) measurements using a Merck Millicell®-ERS2 (Electrical Resistance System Volt-Ohm meter, Germany) according to a previous report (Nafee et al. 2018) that stablished TEER ≥ 300 Ω cm^2 as indicative of a tight monolayer (Foster et al. 2000). Then, the medium was aspirated from the apical compartment and kept only in the basolateral compartment. Cells were incubated under air-liquid interface (ALI) for 12-16 days to allow differentiation. TEER was measured before and after treatments, by replacing culture medium by PBS (500 µL basolateral + 200 µL apical) and pre-incubated 30 min at 37°C to stabilize the cell monolayer prior measurements. TEER values were corrected by subtracting the mean resistance of PBS-blank porous membranes (Kreft et al. 2015) (Eq. (3)). Cell culture medium from basolateral compartment was changed every 2-3 days and apical compartment washed with 100 µL/insert of PBS to remove excess of mucus.

$$\text{TEER (ohm x cm}^2) = \{\text{TEER cells (ohm) - TEER blank (ohm)}\} \text{ x } 0{,}33 \text{ (cm}^2) \quad (3)$$

For cell viability, neutral red assay was performed to verify whether the results were consistent with those from non-differentiated Calu-3 (stimulated with LV aqueous solution, NPLLV_034, NPLBL_034). Cell viable control was evaluated with culture medium. 100 µL of each treatment were plated onto the apical compartment and incubated for 48 h (37 °C, 5 % CO_2, 90 % relative humidity). The following steps were likewise for the non-differentiated cells, except for shaker agitation that was increased to 200 rpm for better homogenization of the neutral red. 100 µL of the final content were transferred to a 96-well microplate to read absorbance at 540 nm wavelength (Thermo Fisher Scientific, Inc., Waltham, MA, USA). Adapted from (Chen et al. 2021; Repetto, del Peso, e Zurita 2008).

4.4.5.3. IL-8 cytokine quantification by Enzyme-Linked Immunosorbent Assay (ELISA)

Cytokine production of Interleukin 8 (IL-8) present in cell culture medium of treated non-differentiated Calu-3 cells (supernatant) and differentiated cells (apical and basolateral compartments) was quantified using immunoassay kits according to the manufacturer's instructions (Human IL-8/CXCL8 R&D Systems DuoSet ELISA - DY208-05). In brief, monoclonal antibody against IL-8 was previously incubated overnight in the 96-well microplate. Standard curves, controls and samples were added to the wells in duplicates and cytokines were bound to the immobilized antibody. When necessary, sample dilutions were made in cell culture medium. After plate washing, a substrate solution was added. The values were read by the standard curve in a Multiskan™ GO microplate spectrophotometer at 540 nm wavelength (Thermo Fisher Scientific, Inc., Waltham, MA, USA) in duplicates and two independent experiments.

The Calu-3 secretion of IL-8 was compared among control, treated with formulations (free LV solution, NPLLV, NPLBL, P80, P407 and P188) and stimulated cells with lipopolysaccharide (LPS) (with and without the treatments). First, we screened the best concentration and exposure time of Calu-3 to LPS (1 and 10 µg/mL, for 24 and 48h). After selecting LPS 1 µg/mL and 48h of incubation time, we rerun the treatments with the respective concentration of LPS per cell (for non-differentiated cells, we used LPS 0.5 µg/mL, for differentiated cells, 1 µg/mL).

4.4.6. NLC haemolytic activity

This method was adapted from (Filipczak et al. 2023). Fresh lamb blood (Anilab, Brazil) was gently homogenized, and an aliquot of 2 mL diluted in 18 mL of NaCl 0.9 %. This suspension was centrifuged for 5 min at 500 x g. The supernatant was discarded, and the process was repeated twice with the pellet of erythrocytes. Then, the erythrocyte pellet was resuspended in saline solution to reach a concentration of 5 % (w/w). 100 µL of each treatment (LV aqueous solution, NPLBL, NPLLV, P80, P407 and P188) were pipetted in triplicate into wells of the first row of a 96-well round-bottom microplate. 50 µL of NaCl 0.9 % were pipetted into the other wells followed by a serial dilution of the samples (1:1, from 100x to 3200x dilution). Finally, 100 µL of erythrocytes were pipetted in all the wells. NaCl 0.9 % was used as negative control, and an aqueous solution of Triton X-100 0.2 % (V/V) was used as

positive control of haemolysis. The microplate was incubated at 37 °C per 1 hour. Then, the microplate was centrifuged at 500 x g per 10 min. Supernatants were carefully transferred to a 96-well flat-bottom microplate and analysed in a Multiskan™ GO microplate spectrophotometer at 540 nm wavelength (Thermo Fisher Scientific, Inc., Waltham, MA, USA). The percentage (%) of haemolysis was calculated in comparison with the positive control values, which were considered as 100 % of haemolysis. Results were presented as mean ± standard deviation (n = 6, triplicates of two independent replicates for each treatment).

4.4.7. Statistical analysis

Results were expressed as mean ± standard deviation. The number of replicates and independent experiments were specified in each experiment. For analysis involving two groups, unpaired *t*-test, or one-way analysis of variance (ANOVA) was used. All data was analysed by GraphPad Prism 8.0.1 software (GraphPad Software, San Diego, CA, USA). The differences were considered significant at $p < 0.05$ or mentioned when different from this value.

4.5. Results and discussion

4.5.1. NLC production and characterization

NLCs were produced with different surfactants (polysorbate 80 (P80), poloxamer 407 (P407) and poloxamer 188 (P188)) to evaluate if this variation would interfere in physicochemical characteristics, microbiological and cellular behaviour. At first, they were characterized by different techniques to measure their particle size and size distribution (z-average size, PdI and D10, D50 and D90). (Tables 1 and 2).

Table 1. Physicochemical characterization of nanoparticles by DLS and HPLC.

Surfactant	Formulation Tracking code	Size (nm)	PdI	Zeta Potential (mV)	D10 (nm)	D50 (nm)	D90 (nm)	Drug content (%)	EE (%)
P80	NPLBL_033	186 ± 2	0.239 ± 0.011	-9 ± 4	101 ± 5	199 ± 5	416 ± 19	-	-
P80	NPLLV_033	133 ± 0.2	0.226 ± 0.003	-16 ± 0.3	73 ± 2	148 ± 6	308 ± 23	92 ± 10	80,1 ± 0.5
P407	NPLBL_034	143 ± 0.1	0.169 ± 0.022	-4 ± 2	85 ± 5	161 ± 5	284 ± 14	-	-
P407	NPLLV_034	112 ± 1	0.116 ± 0.018	-7 ± 1	72 ± 2	120 ± 1	199 ± 11	96.9 ± 0.2	84,0 ± 0.2
P188	NPLBL_035	145 ± 1	0.218 ± 0.017	-7 ± 1	80 ± 2	165 ± 5	337 ± 45	-	-
P188	NPLLV_035	130 ± 1	0.166 ± 0.018	-11 ± 0.4	79 ± 3	143 ± 4	260 ± 22	110 ± 1	83,8 ± 0.2

NPLBL = blank nanoparticles. NPLLV= levofloxacin-loaded nanoparticles. Number in tracking codes relates to Lot number of nanoparticles (NP). Size (Z-average) = hydrodynamic diameter; PdI = polydispersity index of the diameter. D10, D50 and D90 correspond to the particle size below which 10, 50 or 90 % of the nanoparticles are smaller, respectively (n = 3). EE = Entrapment efficiency, and drug content (n = 2). All analyses are expressed as mean ± standard deviation. Graphs are added to the supplementary material.

Table 2. Physical characterization of nanoparticles by NTA.

Surfactant	Formulation Tracking code	Mean ± SD (nm)	D10 ± SD (nm)	D50 ± SD (nm)	D90 ± SD (nm)	Span	Concentration (n° particles/ mL)
P80	NPLBL_033	122 ± 4	78 ± 3	109 ± 6	188 ± 5	1.01	4.31E+17
P80	NPLLV_033	126 ± 8	77 ± 6	113 ± 7	189 ± 17	0.99	1.37E+13
P407	NPLBL_034	100 ± 1	67 ± 2	87 ± 2	153 ± 4	0.99	1.85E+17
P407	NPLLV_034	114 ± 6	73 ± 7	105 ± 9	169 ± 11	0.91	6.98E+16
P188	NPLBL_035	135 ± 4	92 ± 4	129 ± 2	183 ± 9	0.71	2.45E+17
P188	NPLLV_035	134 ± 1	98 ± 1	122 ± 1	188 ± 7	0.74	3.05E+17

NPLBL = blank nanoparticles. NPLLV= levofloxacin-loaded nanoparticles. Number in tracking codes relates to Lot number of nanoparticles (NP). Mean = hydrodynamics diameter; D10, D50 and D90 correspond to the particle size below which 10, 50 or 90 % of the nanoparticles are smaller, respectively (n = 5). All analyses are expressed as mean ± standard deviation. All analyses are expressed as mean ± standard deviation. Span = (D90 – D10)/D50. Graphs are added to the supplementary material.

Despite of the surfactant type, the tree of NLCs had high EE values (> 80 %), being similar between the poloxamers-NLCs. We can hypothesize that these surfactants with higher hydrophilic-lipophilic balance (HLB) values favoured higher EE values.

DLS results presented monodispersed NLCs (PdI < 0.3), in an acceptable size range for different administration routes (100 – 300 nm) (Beraldo-Araújo et al. 2022). Although DLS points to a general decrease in mean sizes due to LV incorporation, this trend is not observed in NTA. Both techniques indicate a broader size distribution for the P80 compared to the other surfactants (PDI, Span). Since P80 has the lowest molecular weight but the same mass in the NLCs than the others, P80 has a molar concentration more than 10 times higher than P407 and P188 (66 mmol/L, 3 mmol/L and 4 mmol/L, respectively). Thus, the highest number of molecules may have saturated the NLC surface and caused particle size increments.

D10/D50/D90 values from DLS presented a broader range than those from NTA (Table 2), which can be due to the light scattering of a population skewed to larger particles, and not individual nanoparticles. Thus, mean size and consequent D90 tends to be smaller than the ones measured by DLS. In DLS case, it is possible to occur interference in the measurement due to the presence of dust in the solvent used to dilute the nanoparticles, suggesting the obtention of a population with micrometric particle size, but we critically analysed the representation of the DLS results (Supplementary Figure 1), it is possible to identify the interference of particles in the micrometric range, which elevates D90 of NLCs made with P80, for example. For similar situations, it is important to analyse particle size distribution by more than one technique, e.g., NTA. According to NTA results (Table 2), it is possible to understand the individual contribution of the nanoparticles to the mean particle size. Thus, mean size tends to be smaller than that measured by DLS. It is clear that when a technique uses an individual particle size measurement, the D10/D50/D90 values of a monodisperse suspension are in a narrow range. In addition, NTA gives the concentration of nanoparticles, an important data to design other experiments such as TEM analysis.

The zeta potential is a parameter that indicate and predicts colloidal stability of nanoparticles. Generally, a nanosuspension is considered physically stabilized when it presents zeta potential values higher than |20 mV|. However, for nanoparticles stabilized by a non-ionic surfactant, steric effect prevails to the electrostatic effect, and

they can be stable with a zeta potential value below |20 mV| (Bhakay et al. 2018). We noticed (Table 1) higher zeta potential values in module in NPLLVs than the respective NPLBLs, suggesting a contribution of LV to the nanoparticle surface charge due to surface adsorption.

Based on formulation studies from our previous paper (Beraldo-Araújo et al. 2022), we saw that, regarding drug stability assays, NPLLV_033 was stimulating the production of LV degradation product. The stability tests showed that the NLCs formulated with both poloxamers somehow were keeping LV protected from degradation (data not shown – stability tests in progress, where we are evaluating NLC drug content and EE, and observed a chromatographic peak correspondent to the levofloxacin N-oxide, a degradation product of LV, which is greater at high storage temperature (40 °C)). These findings led to the followed biological assays to compare the three NLCs.

Electron-microscopy

To evaluate particle morphology, we analysed the samples by transmission electron microscopy (TEM) and cryogenic transmission electron microscopy (Cryo-TEM). Cryo-TEM analysis of blank and LV loaded nanoparticles with P80 (Figure 1) showed round-shaped nanoparticles with similar sizes to that found by DLS. The lamellar structure of the NLCs corroborates with our previous results using the sorption and desorption analysis and X-ray diffraction (Beraldo-Araújo et al. 2022). NLCs presented smaller sizes in TEM compared to Cryo-TEM due to the sample preparation process, which could shrink NLCs upon drying.

TEM analysis (Figure 1, letter c, d and e) identified that all samples presented a high electron density on the edges, which could indicate the lamellar structure arranged by the surfactants coating and visualized in Cryo-Tem. There are also bright vesicles in the lipid matrix, corresponding to the accommodation of the liquid lipid, which is not clear on Cryo-TEM images because samples were not contrasted with a stain. In summary there is no indicative of structural difference among different surfactants, and the three NLCs were of multiple type.

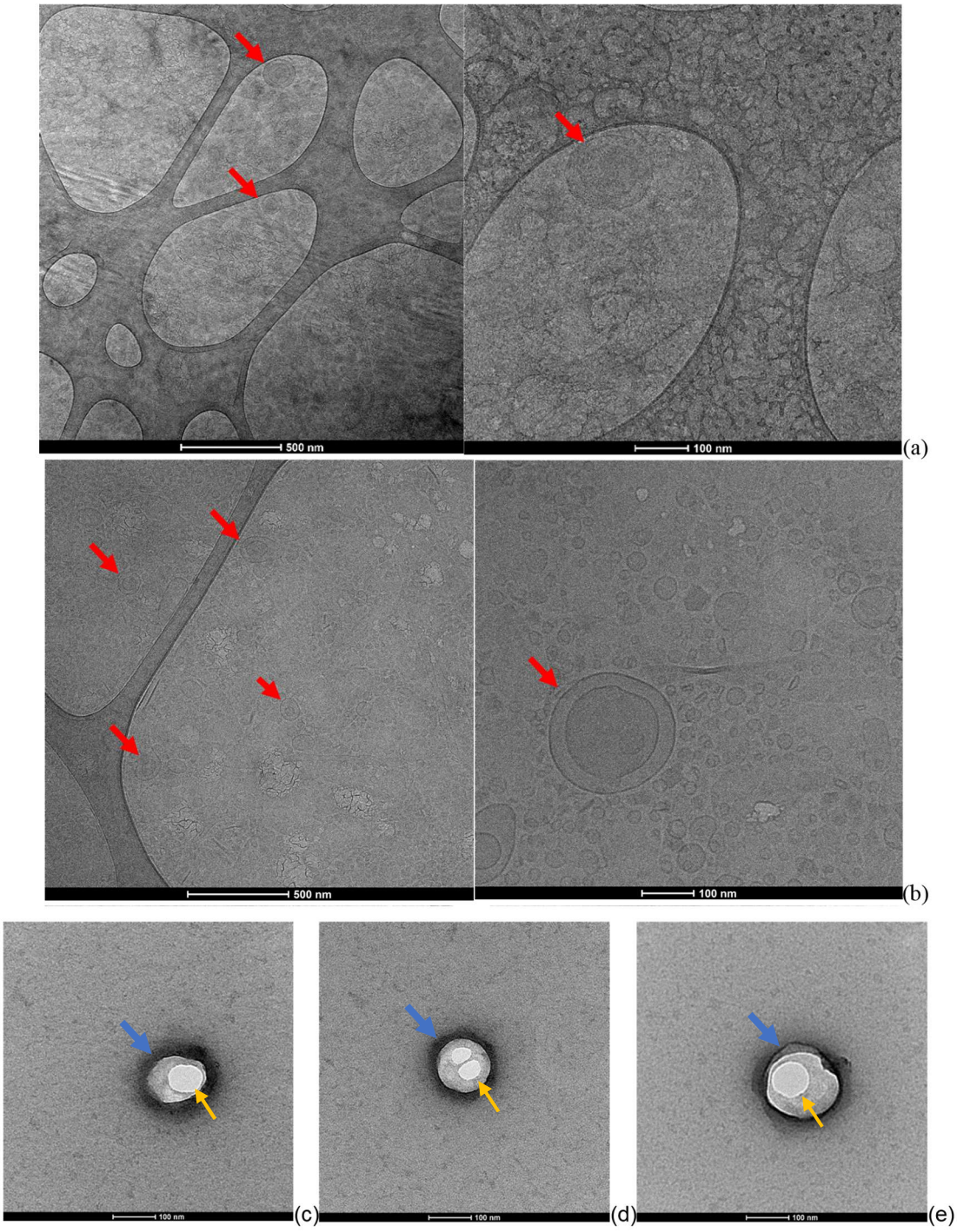

Figure 1. Transmission Electron Microscopy images of NLCs. Cryogenic-TEM images of non-diluted and non-stained (a) NPLBL_033 (without levofloxacin) and (b) NPLLV_033 (with levofloxacin), NLCs made with polysorbate 80. Red arrows indicate NLCs, suggesting a multilamellar structure. TEM images of (c) NPLLV_033, (d) NPLLV_034 and (e) NPLLV_035, made with polysorbate 80, poloxamer 407 and poloxamer 188, respectively. NLCs diluted 100x and contrasted with uranyl acetate 2%. 68000x magnification. Blue arrows indicate high electron-density regions, corresponding to the surfactant coating. Yellow arrows indicate vesicular structures in the lipid matrix, corresponding to the liquid lipid.

LV release profile

We performed LV release assay from the formulations using the Franz diffusion cell apparatus, and artificial simulated interstitial lung fluid (SILF) to reproduce the ionic conditions of the lung. All samples presented quite similar release behaviour, with a burst release in the first hours, which could be related to the adsorbed-LV on the NLCs, reaching 80-90 % drug release after 24 hours (Figure 2). NPLLV_033 did not differ from Free LV ($p > 0.05$), which is in contrast with our previous publication (Beraldo-Araújo et al. 2022). However, our previous test was performed in PBS, and this difference highlighted the importance of using biorelevant media related with the intended delivery route (Figure 2). NPLLV_035 presented a slower LV release in the first 12 hours, having a different release profile from the others ($p < 0.001$). As an example, free LV had 30 % of drug released after 1,5h, while NPLLV_035 released 2.5 times less LV (12 ± 2 %). It is possible that the surfactants promoted faster LV release rate from NPLLV_033 and NPLLV_034 because of P80 and P407 ability to enhance drug permeation across membranes in general.

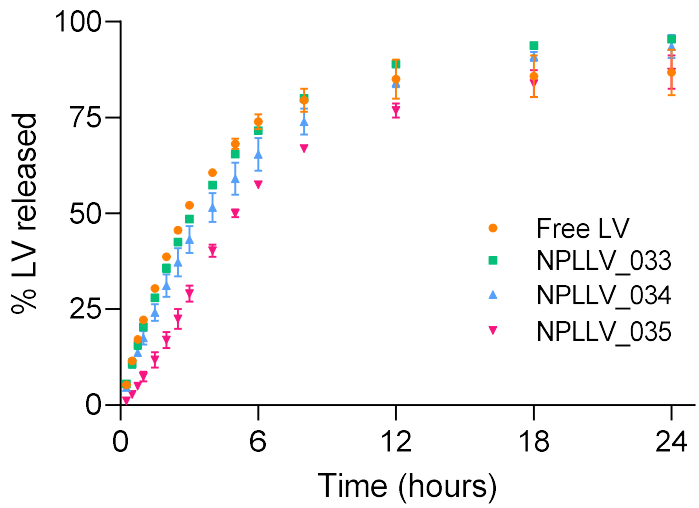

Figure 2. LV release profiles in Franz cell apparatus, from free LV (orange filled circles, n = 2), NPLLV_033 (green filled squares, n = 2), NPLLV_034 (blue filled triangles, n = 2), and NPLLV_035 (magenta filled inverted triangles, n = 2). The medium in the acceptor compartment was simulated interstitial lung fluid (SILF). Turkey's multiple comparisons test were performed, with individual variances computed for each group comparison.

4.5.2. Microbiological studies

Samples were submitted to MIC tests to evaluate their impact on growth of bacterial strains that infect lungs. *K. pneumoniae* strain BAA 1705 presented resistance to LV, whereas strain ATCC 700603 was susceptible and within the literature range of 40 strains against LV, with MICs in an interval from 0.094 to 8 µg/mL (Grillon et al. 2016).

The MIC values reported for strains of *S. aureus* were among 0.5 and 4 µg/mL of LV (Lister 2001). In our test, both strains, ATCC 29213 and ATCC 33591 presented a MIC of 0.19 µg/mL for all the treatments. No NPLBL presented antimicrobial activity for none of the bacterial strains tested.

There was no variation in MIC between free LV and NPLLVs, indicating that LV does not lose its activity when incorporated into the produced nanoparticles. The presence of the three surfactants at the interface between the nanoparticle and the external medium had no impact on the necessary drug concentration to inhibit the growth of the bacteria tested (Table 3).

Table 3. Minimum Inhibitory Concentration (MIC).

Bacterial strain	LV (µg/mL)	NPLLV_033 (µg/mL)	NPLLV_034 (µg/mL)	NPLLV_035 (µg/mL)
K. pneumoniae 700603	0.78	0.78	0.78	0.78
K. pneumoniae BAA 1705	125	125	125	125
S. aureus ATCC 29213	0.19	0.19	0.19	0.19
S. aureus ATCC 33591	0.19	0.19	0.19	0.19

Bacteria treated with Levofloxacin (LV), nanoparticles with levofloxacin (NPLLV) and without LV (NPLBL, not shown). n = 3 replicates, at least two independent experiments. Blank nanoparticles did not inhibit bacterial growth on the same dilutions used for the ones loaded with LV.

4.5.3. Calu-3 cell viability

Tests with the Calu-3 cell line were chosen since it is considered a model for lung and nasal epithelial cells to evaluate drug cytotoxicity and trans-epithelial transport of drugs (Chen et al. 2021; Zhang et al. 2016). The stimuli dilutions refer to the concentration of LV at 1, 10, and 100 µg/mL. The values were based on studies with A549 lung cells exposed to free or nano-encapsulated LV, (Derbali et al. 2019)

and related to the minimum inhibitory concentration (MIC) obtained for *Klebsiella pneumoniae* ATCC 700603 (0.78 µg/mL), being equivalent to 1.3, 13, and 130 times the determined MIC (Figure 3).

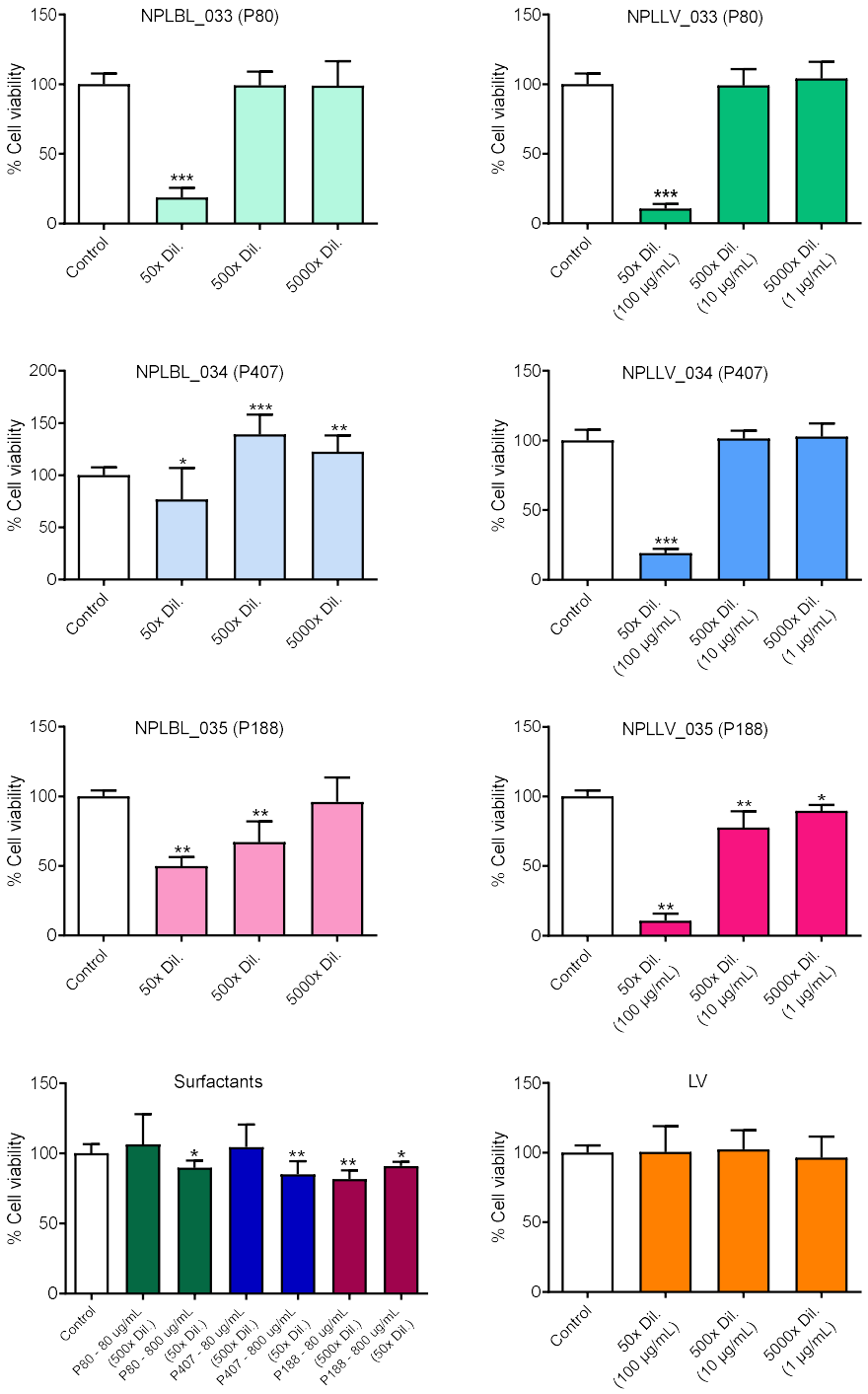

Figure 3. Cell viability assay (MTT reduction) of non-differentiated Calu-3 cell line. Cell viability (%) was evaluated after 24h treatment with samples in 96-well microplates (5 x 10^4 cells/well). Positive control: DMEM medium, white bars. Samples: blank (NPLBL) and LV-loaded nanoparticles (NPLLV) prepared with P80 (green bars), P407 (blue bars), and P188 (pink bars); LV aqueous solution (orange bars); aqueous solutions of the surfactants (green, purple and red bars). Results are expressed as mean ± standard deviation, obtained from at least 2 independent assays, with n ≥ 3 replicates per assay. Symbols *, **, and *** represent statistical significance compared

to viable cell control ($p < 0.05$, $p < 0.005$, and $p < 0.0005$, respectively), determined by the non-parametric Mann-Whitney test.

We verified that LV in aqueous solution did not alter the viability of Calu-3 at any of the three tested concentrations (Figure 3, LV). On the other hand, the three aqueous solutions of surfactants significantly reduced cell viability at a concentration of 800 µg/mL ($p < 0.05$), which corresponds to the dilution of the LV formulation at a concentration of 100 µg/mL (Figure 3, surfactants). When these solutions were diluted 50-times they did not influence cell viability, except for P188 ($p < 0.0005$). However, despite of the drop tendencies, Calu-3 reached averages higher than 80 % of viability, and the stimuli were considered non-cytotoxic to this cell (Steiner et al. 2019).

Regarding the NLCs, we found that the three blank formulations (Figure 3, NPLBL_033, NPLBL_034 and NPLBL_035) significantly reduced cell viability at the highest concentration (50-times diluted). As described by Allotey-Babington et al., this could be related to the high concentration of the nanoparticles in the formulation, which may alter the osmotic pressure of the system (Allotey-Babington et al. 2018). However, at 500-times diluted, they presented different behaviours: NPLBL_033 did not alter cell viability, NPLBL_034 seemed to somehow stimulate cell growth, and NPLBL_035 reduced viability.

When the NLCs are loading LV at a concentration of 100 µg/mL (50-times diluted), the reduction in cell viability increases (about 80 to 90 %, with the greatest reduction obtained with NPLLV_035 and the smallest reduction with NPLLV_034). NPLLV_033 and NPLLV_034 did not change cell viability at LV concentrations of 10, in agreement with the LV concentrations tested by (Derbali et al. 2019) with A549 cells. However, NPLLV_035 (with P188) significantly reduced Calu-3 viability when at LV concentration of 10 µg/mL (< 80 % cell viability).

These findings showed that in a certain manner P188 negatively influences Calu-3 cell viability in the MTT assay, while P407 is the surfactant that least reduced its viability. Instead, P407 enhanced the survival of Calu-3, as also noticed by Allotey-Babington et al., 2018, in specific types of cells (rat liver epithelial cells (WB), murine kidney cells (MDCK) and triple negative human breast cancer cells (MDA-MB231)) (Allotey-Babington et al. 2018). Another study applied low concentrations of P407 to improve tissue generation and to enhance gingival fibroblasts attachment and growth,

suggesting the necessity of deep examination to better comprehension on how poloxamer works (Dumortier et al. 2006).

To confirm the effect of stimuli in Calu-3 cell viability, we performed neutral red assay, which allowed the inference of cell viability through a different mechanism (cell membrane integrity, instead of mitochondrial activity (MTT)). Thus, we run assays only with LV-loaded NLCs, comparing to free-LV aqueous solution and positive control of cell viability. As shown in Figure 4, we confirmed that free LV did not interfere in Calu-3 cell viability and that NLCs prepared with the three different surfactants significantly reduced this cell viability at 50-times dilution ($p < 0.0005$), in accordance with MTT assays (reduction of 80 – 90 % of cell viability at the respective LV concentration of 100 µg/mL). We reached similar results for NPLLV_033 and NPLLV_034 at higher dilutions. For NPLLV_035, we did not find statistical difference in cell viability comparing to the control, differently to the MTT assay. Apart from the statistical relevance and considering ISO 10993-5 that standardizes *in vitro* cytotoxicity of medical devices, cell viability percentages higher than 80% are not considered cytotoxic. Therefore, we should be thorough when evaluating the biological cytotoxicity relevance of a formulation against each cell line (López-García et al. 2014; ISO 10993-5:2009 2009).

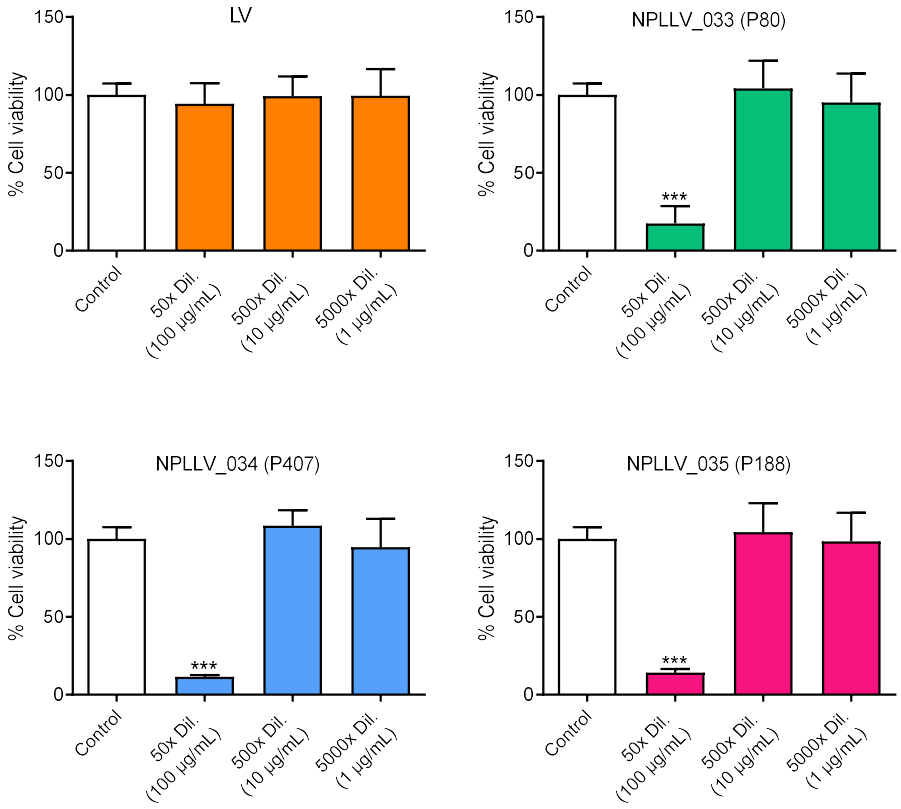

Figure 4. Cell viability after 24h-exposure to NLCs expressed as cell membrane integrity by neutral red evaluation in non-differentiated Calu-3 cell line. Graphs correspond to the percentage of Calu-3 cell viability after treatment with LV-loaded NLCs prepared with the three surfactants (NPLLV_033, with P80 (green bars), NPLLV_034, with P407 (blue bars), and NPLLV_035, with P188 (pink bars) and LV aqueous solution (orange bars) in three different concentrations (related to LV): 100, 10 or 1 µg/mL. All treatments were compared with the positive control (DMEM medium, white bars). Cell viability (%) was evaluated by the neutral red assay in 96-well microplates with a density of 5 x 10^4 cells/well, stimulated for 24 h. Results are expressed as mean ± standard deviation, obtained from at least 2 independent assays, with n ≥ 3 replicates per assay. Symbol *** represents statistical significance compared to viable cell control ($p < 0.0005$), determined by the non-parametric Mann-Whitney test.

We considered worthwhile to improve the respective LV concentrations to achieve a concentration higher than 10 µg/mL, to which would not be considered harmful to Calu-3. Then, we assayed the respective LV concentrations: 50, 25 and 10 µg/mL. Another modification on the viability assay was the stimulation time (from 24 to 48h), since the Calu-3 doubling-time is about 30 – 40 h (according to Cellosaurus.org website - variations may occur according to the medium and environmental conditions) and it is in our interest to examine how the stimuli affects cell proliferation too.

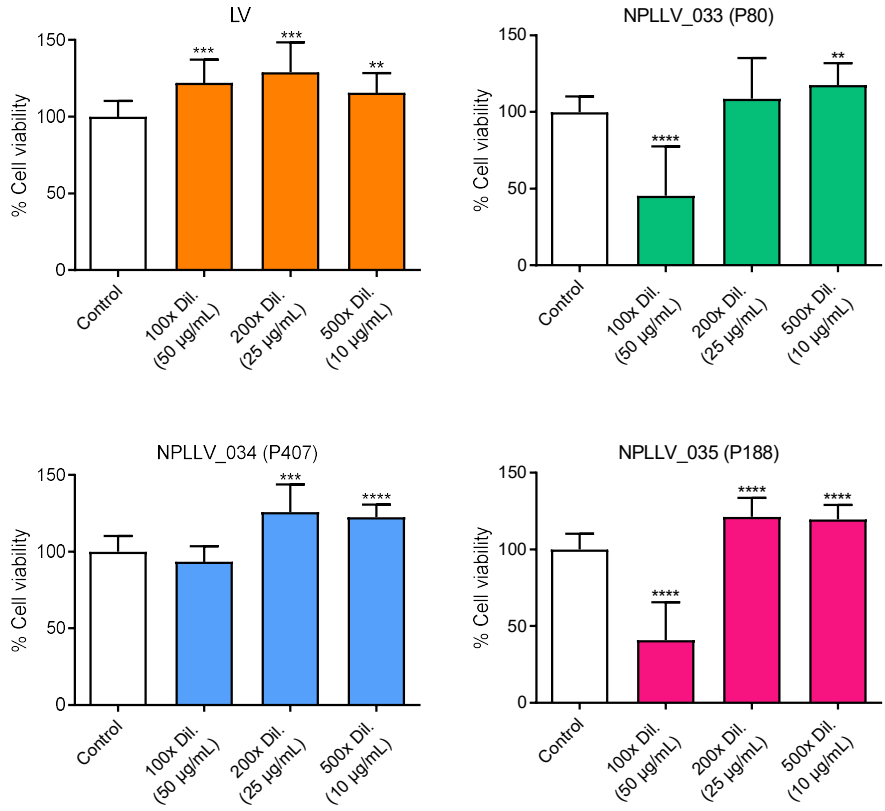

Figure 5. Cell viability after 48h-exposure to NLCs expressed as cell membrane integrity by neutral red evaluation in non-differentiated Calu-3 cell line. Graphs correspond to the percentage of Calu-3 cell viability after treatment with LV-loaded NLCs prepared with the three surfactants (NPLLV_033, with P80 (green bars), NPLLV_034, with P407 (blue bars), and NPLLV_035, with P188 (pink bars) and LV aqueous solution (orange bars) in three different concentrations (related to LV): 50, 25 or 10 µg/mL. All treatments were compared with the positive control (DMEM medium, white bars). Cell viability (%) was evaluated by the neutral red assay in 96-well microplates with a density of 5 x 10^4 cells/well, stimulated for 48 h. Results are expressed as mean ± standard deviation, obtained from 3 independent assays, with n ≥ 3 replicates per assay. Symbols **, ***, and **** represent statistical significance compared to viable cell control ($p < 0.005$, $p < 0.0005$, and $p < 0.00005$, respectively), determined by the non-parametric Mann-Whitney test.

The results (Figure 5) confirmed that free LV did not inhibit cell proliferation. NPLLV_033 and NPLLV_035 reduced cell viability at the highest concentration (50 µg/mL), which did not occur with NPLLV_034. The other LV-entrapped NLC concentrations (25 and 10 µg/mL) were not cytotoxic to Calu-3. Indeed, all NLCs in these concentrations seemed to stimulate cell proliferation, when compared to control. These results underlay the cell viability test in differentiated Calu-3 on transwell and

helped us to choose the NPLLV_034, as the less harmful NLC to test in the following experiments.

4.5.4. Cell viability in differentiated Calu-3

In addition to the cell viability assay on undifferentiated cells, we conducted the assay on differentiated Calu-3 cells, as their characteristics change and may alter their tolerance to different stimuli. The neutral red assay with NPLLV_034 50 µg/mL shown a 71 ± 6 % of cell viability (n = 2, data not shown), considered weakly cytotoxic (classification to the range of 60 – 80 % cell viability - (López-García et al. 2014)). For this reason and considering that differentiated cells are not only morphologically but also biochemically different, we deemed more appropriate to set the stimuli concentration at 25 µg/mL, being safer for this cell line treatment.

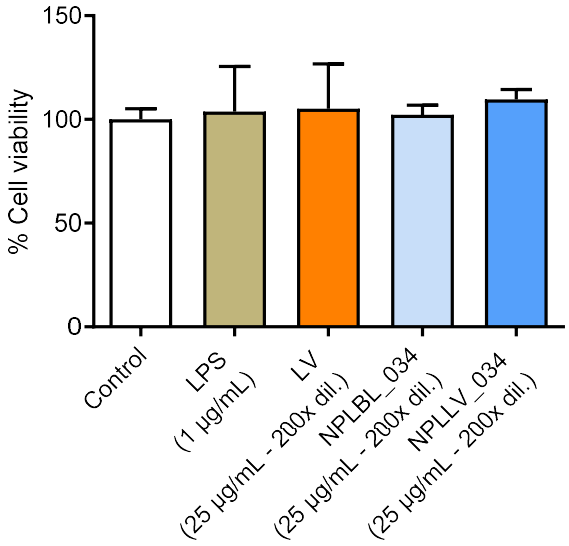

Figure 6. Cell viability after 48h-exposure to NLCs expressed as cell membrane integrity by neutral red evaluation in differentiated Calu-3 cell line. Graph correspond to the percentage of Calu-3 cell viability after treatment with lipopolysaccharide (LPS) 1 µg/mL (beige bar); LV aqueous solution (orange bar), NPLBL_034 (light blue bar) and NPLLV_034 (blue bar) at 25 µg/mL concentration. All treatments were compared with the positive control (DMEM medium, white bar). Cell viability (%) was evaluated by the neutral red assay in transwell inserts (6.5 mm, 0.4 µm diameter size pore, polyester membrane, 0.33cm^2 effective area for growth), in 24-well microplates with an initial density of 5 x 10^5 cells/well, stimulated for 48 h. Results are expressed as mean ± standard deviation, obtained from 2 independent assays, with n = 2 replicates per assay. There was no statistical significance between treatments and the control (non-parametric Mann-Whitney test).

We confirmed that 25 µg/mL was a safer concentration for differentiated Calu-3 cells after 48 h of exposition to the treatments (Figure 6). Also, we confirmed that lipopolysaccharide at the concentration of 1 µg/mL was not considered cytotoxic to the cells, being a useful result for the IL-8 cytokine secretion assay, stimulated by LPS. However, TEER measurements after 48-stimuli exposition shown a reduction the values compared to TEER after reaching the cell tight monolayer (reduction from ~ 792 $\Omega.cm^2$ to ~557 $\Omega.cm^2$), but this reduction did not compromise the integrity of the cell monolayer, as TEER values were > 500 $\Omega.cm^2$ (Chen et al. 2021). Also, cell viability was similar to the control, it is possible that the stimuli opened the tight junctions during the cell treatment without causing a cellular damage (Morales, Peters, e Williams 2011).

4.5.5. IL-8 cytokine secretion profile

Inflammatory interleukins are a group of cytokines that participate in the body's inflammatory response. Upon the introduction of the nano drug-loading system into the bloodstream, the secretion of inflammatory cytokines may be altered. TNF-α, IL-1β, IL-6, IL-8, and other cytokines are known to play important roles in this process (Guo et al. 2021). Hence, we decided to evaluate the effect of NLCs on Calu-3 cells regarding its secretion of the pro-inflammatory cytokine IL-8, as they are frequently used in studies of in vitro IL-8 release as a response to infection or injury (Darweesh e Sakagami 2018).

First, we screened the best LPS concentrations and periods of Calu-3 exposition to the stimuli formulations with LPS. We compared the basal secretion of IL-8 after 24h to that with LPS 1 µg/mL (24 and 48 h), LPS 10 µg/mL (24h), and treatments (LV and NPLLV_034 25 µg/mL) with LPS at the same periods and concentrations (Figure 7 (a)). The results indicated that the basal secretion of IL-8 by Calu-3 after 24h is insignificant, but it increased after stimulation with LPS. Lower levels of IL-8 were found with lower concentration and period of exposition to LPS, which increased after the double of the time of exposition, and get higher with LPS more concentrated in 24h. Increases were proportional and we decided to choose LPS 1 µg/mL and 48 h of exposition, to avoid reaching undetectable values of IL-8 or

exacerbated levels of the cytokine, resulting in potential tissue damage. This concentration was set for the transwell cell density, and LPS 0.5 µg/mL for Calu-3 non-differentiated in 96-wells microplate, in order to keep similar LPS doses per cell.

Despite the slight difference on the results of IL-8 secretion by non-differentiated Calu-3, they shown no statistical difference when compare the control to stimuli without LPS or control to LPS 0.5 µg/mL (Figure 7 (b)). Statistical relevance was present when compared the control to stimuli with LPS, showing that the treatments, alone, do not interfere in the basal secretion of IL-8. But, when they faced the enhancement of cytokine levels with LPS, they were not able to reduce its levels at the concentration of 25 µg/mL.

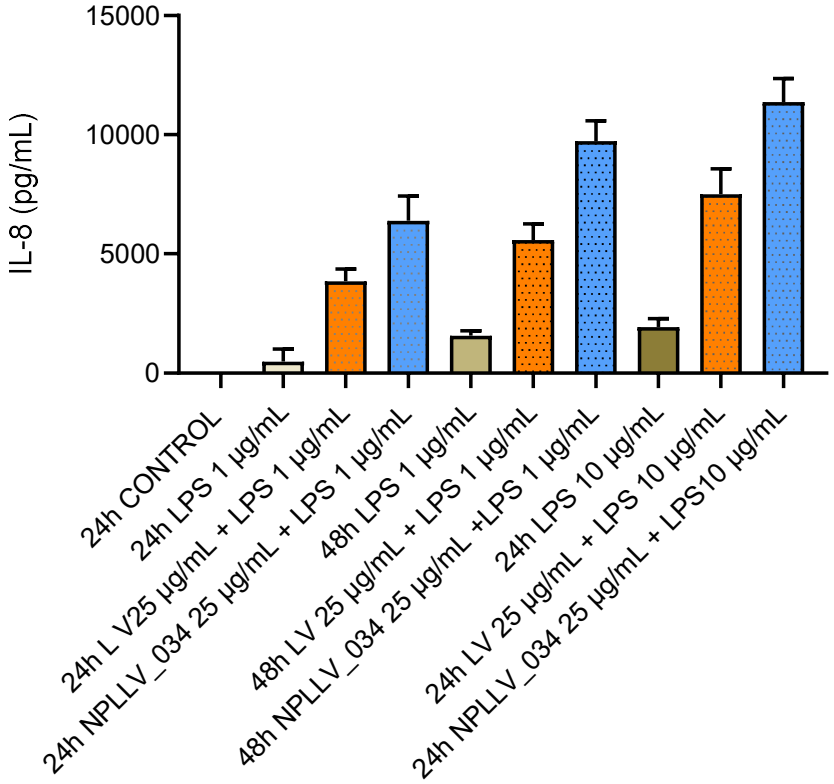

(a)

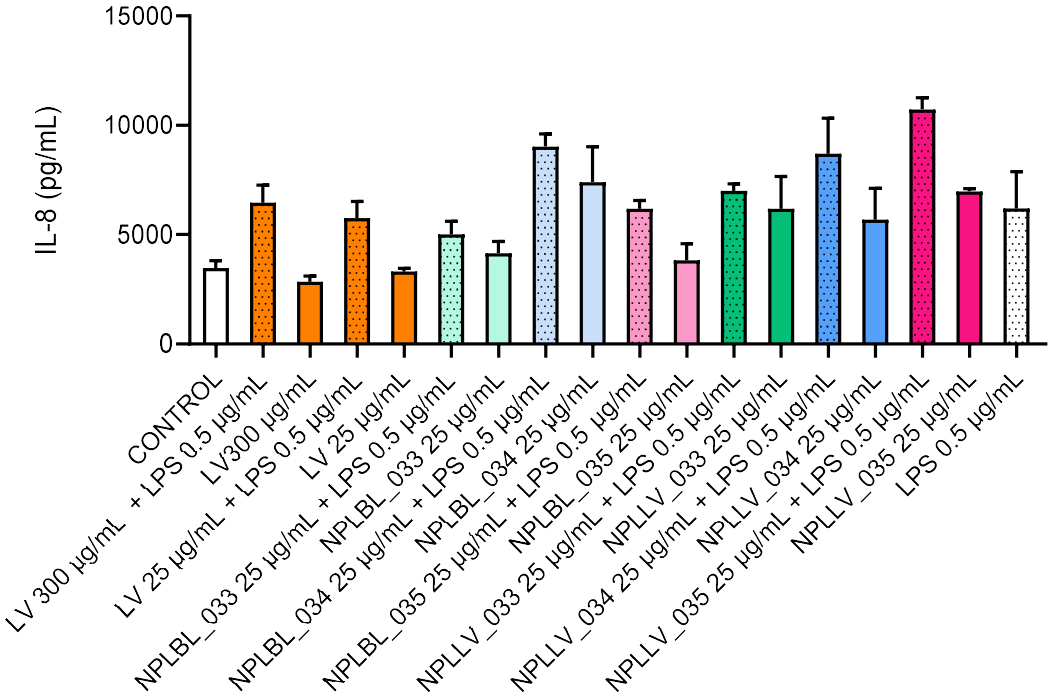

(b)

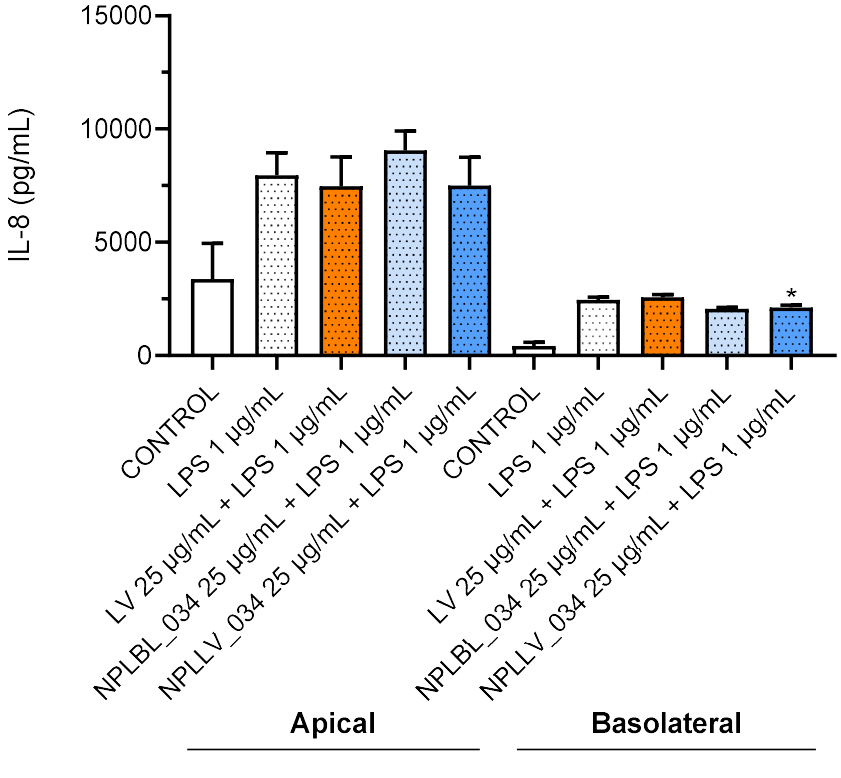

(c)

Figure 7. IL-8 cytokine secretion from (a) non-differentiated Calu-3 stimulated by LV and NPLLV_034 25 µg/mL in different periods of incubation (24 and 48 h) and with different concentrations of LPS (1 or 10 µg/mL); (b) non-differentiated and (c) differentiated Calu-3 cells. Non-differentiated cells were seeded into 96-wells

microplate at a density of 5 x 10^4 cells/well. After 72h, medium was withdrawn and cells treated with stimuli (LV solution 300 μg/mL and 25 μg/mL; NPLBL_033, _034 and _035 and NPLLV_033, _034 and _035 diluted to the respective LV concentration of 25 μg/mL) with or without LPS 0.5 μg/mL to stimulate inflammatory process. Stimuli were incubated during 48h and IL-8 secreted in the medium was measured using ELISA kit (n = 2). Differentiated Calu-3 were treated with stimuli after 14 ± 2 days of differentiation and TEER measured. Stimuli (LV solution, NPLBL_034 and NPLLV_034 25 μg/mL) with LPS 1 μg/mL were plated on the apical compartment of the transwell (n = 2, two independent experiments). Controls with cell culture medium with and without the respective concentration of LPS were used as parameter for basal and stimulated-IL-8 secretion from Calu-3.

Analysing IL-8 secretion by differentiated Calu-3 onto transwell inserts, there are higher concentrations of cytokine in the apical compartments than in basolateral ones (Figure 7 (c)). This can be due dilution of IL-8 (the volume on apical compartment is 100 μL, while on basolateral, this volume is 6 times larger. Apart from that, cells are polarized, and their behaviour are different on their apical and basal portions, therefore, they could secrete more IL-8 to the lumen of alveoli than systemically. Also, evaluating the compartments separately, there is an increase in IL-8 secretion with all stimuli with LPS 1 μg/mL compared to the controls. Not LV nor NLCs reverted or exacerbated IL-8 secretion. Interestingly, NPLLV_034 25 μg/mL reduced IL-8 compared to free LV at the same concentration ($p < 0.05$). Jackson et al., 2000 report that the use of P407 can prevent plasma proteins from adsorbing to microspheres surfaces and reduce the opsonization-induced activation of neutrophils, suggesting that this application of P407 may potentially decrease their inflammatory properties (Jackson et al. 2000). On the other hand, (Tsivkovskii et al. 2011) studied the potential anti-inflammatory action of LV, reducing IL-8 and IL-6 proinflammatory cytokines when LV was at concentrations > 100 μg/mL. According to then, LV at lower concentrations (10 and 30 μg/mL) was not sufficient to reduce cytokines secretion by NL20 cells, which we confirmed to Calu-3 cells.

4.5.6. Haemolytic activity of NLC formulations and surfactants

The haemolysis test is used to determine the extent of damage to red blood cells (RBCs) caused by a particular preparation or formulation. Depending on formulations concentration, they can lead to the rupture and dissolution of RBCs,

resulting in haemolysis caused by a shift in the osmotic concentration of the system. Since there is currently no standardized preclinical *in vivo* method to assess haemolytic reactions, toxicity studies should take into account the potential for haemolysis in the preparation.

This assay is performed by estimating the amount of haemoglobin released because of the RBCs damage. The most frequently used method to detect and measure oxygenated haemoglobin is spectrophotometry, although it can be influenced by several factors (e.g., centrifugation temperature, speed and auxiliary materials). Overall, the evaluation of haemolysis is crucial in the research of various types of nano preparations, especially for pulmonary delivery. This is due to the abundant vascularization on the surface of the alveoli and the potential for nanoparticle absorption (Guo et al. 2021).

While the thresholds for various forms of haemolysis differ - around 10% for humans, 10%-29% for dogs, and 0%-37% for rabbits - 10% and 25% are typically viewed as relative thresholds. If the level of haemolysis is less than 10%, it is classified as non-haemolytic, whereas levels exceeding 25% are considered haemolytic (Guo et al. 2021; Amin e Dannenfelser 2006).

It is clear that NLCs with different surfactants presented different haemolytic profiles (Figure 8). NLCs had high lipid content (10% w/w) and surfactant (4%). Therefore, a 200 times-dilution of all NLCs, including blank NLCs were considered haemolytic. NPLLV_034, was the less haemolytic (considered non-haemolytic with 400 times-dilution, with 5 ± 3 % haemolysis). NPLLV_033, were non-haemolytic at 800-times dilution (5 ± 3 % haemolysis), and the most haemolytic NLCs were NPLLV_035, requiring a 1600-times dilution to be considered non-haemolytic (7 ± 5 % haemolysis).

Comparing to a DNase formulation from the literature, used as a standard safety check, particles with a lipid concentration of 5 mg/mL were considered non-haemolytic, with 6 % of haemolysis (Filipczak et al. 2023). Our less haemolytic formulation has lower lipid concentration (0.25 mg/mL), but they are different formulations and therefore the haemolytic activity of a formulation is not related only to its lipid concentration. In our formulations, the surfactant type and concentration have a great importance related to this issue.

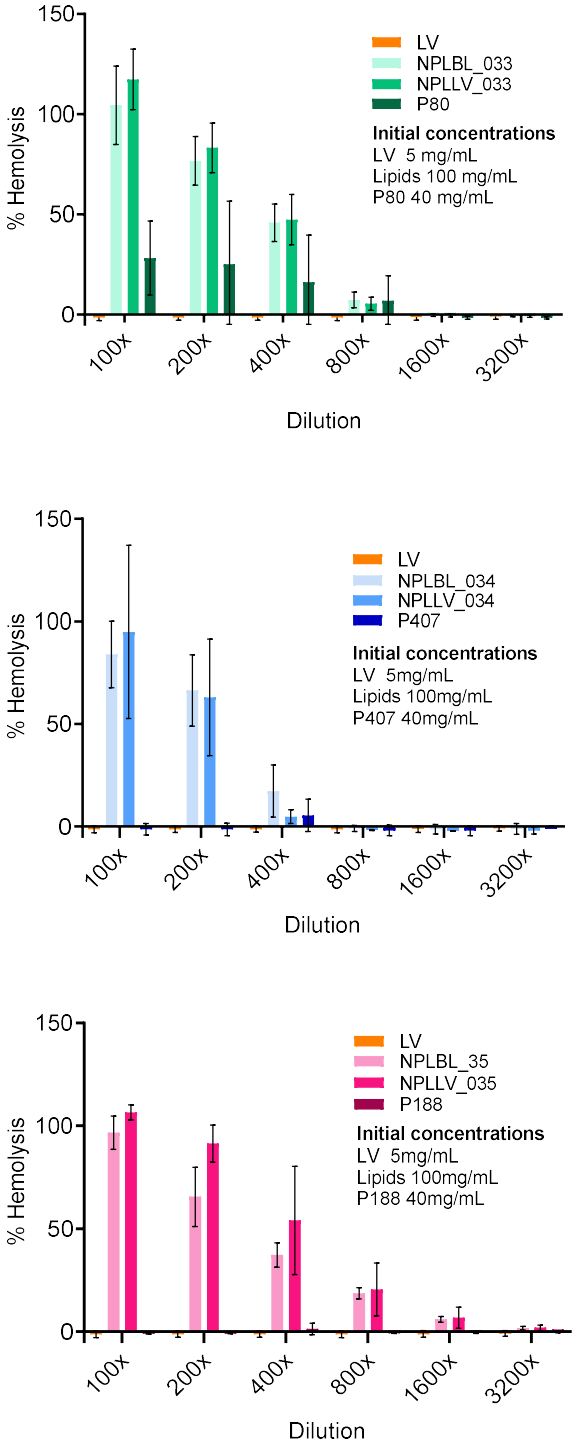

Figure 8. Haemolytic profiles from NLCs and respective excipients. Graphs expresses the percentage of haemolysis in different serial dilutions of groups of NLCs: the upper graph presents LV, NPLBL_033, NPLLV_033 and P80 data; the middle graph presents LV, NPLBL_034, NPLLV_034 and P407 data; and the bottom graph presents LV, NPLBL_035, NPLLV_035 and P188 data. n ≥ 2 for at least two independent experiments.

4.6. Conclusion

We formulated and evaluated physicochemical and drug stability of LV incorporated in NLCs coated with three different surfactants: NPLLV_033, NPLLV_034 and NPLLV_035 (coated with P80, P407 and P188, respectively). Apart from the good outcome for a pulmonary delivery, NPLLV_033 showed less protective activity to LV, promoting higher amount of drug degradation. The drug release profile in Franz diffusion cells showed that NPLLV_035 had the most sustained LV release, while NPLLV_033 did not differ from free LV release. Incorporating the three surfactants in the NLC did not have an impact on the antimicrobial activity of LV. Interestingly, the entrapped drug exhibited the same level of antimicrobial activity against *K. pneumoniae* as the free LV. In addition, a cell viability assay was conducted on undifferentiated and differentiated Calu-3 cells using the different formulations. This included comparing nanoparticles with and without LV (NPLBL and NPLLV, respectively) with the free LV and surfactants. The results showed that at a concentration of 100 µg/mL, both blank and loaded formulations exhibited cytotoxicity to Calu-3 cells. However, depending on the surfactant used in the NLC, a concentration of 50 µg/mL may not significantly reduce cell viability. Overall, NPLLV_035 demonstrated a tendency to decrease Calu-3 cell viability in the conducted assay, whereas NPLLV_034 showed a less pronounced effect among the three surfactants. The tested LV formulation did not exhibit any reduction in cell viability. Additionally, the exposure of Calu-3 cells to LPS did not lead to an exacerbation of IL-8 secretion. Interestingly, NPLLV_034 exhibited a decrease in IL-8 secretion compared to free LV, suggesting that this particular formulation holds promise for pulmonary drug delivery. Differences become greater when compared the haemolytic capacity of NLCs, showing that NPLLV_034 has a lower haemolytic profile (non-haemolytic when faced a 400-times dilution), while NPLLV_035 was the most haemolytic NLC. In conclusion, we successfully developed a well-characterized NLC formulation that effectively protected LV from degradation. This formulation demonstrated safe delivery of the drug, as it maintained the viability of epithelial cells and preserved the integrity of RBCs, at nanoparticle dilutions in the vascular tissue. Furthermore, the NLC formulation exhibited potential anti-inflammatory activity, which is advantageous for improving pulmonary infections. Overall, these findings highlight the promising potential of our NLC formulation for enhanced pulmonary drug delivery.

Acknowledgments:

This study was financed in part by the Coordenação de Aperfeiçoamento de Pessoal de Nível Superior - Brasil (CAPES) - Finance Code 001 and Sao Paulo Research Foundation (FAPESP) grant numbers 2018/03666-3, 2020/08059-8 and 2022/05047-4. We also thank the access to equipment and assistance provided by the Electron Microscope Laboratory (LME/UNICAMP) and Scanning Electron Microscope from Central Analitica (IQ/UNICAMP). This research used facilities of the Brazilian Nanotechnology National Laboratory (LNNano), part of the Brazilian Centre for Research in Energy and Materials (CNPEM), a private non-profit organization under the supervision of the Brazilian Ministry for Science, Technology, and Innovations (MCTI). The Cryo-EM staff is acknowledged for the assistance during the experiments 20220688 and 20220940.

Declaration of Competing Interest

The authors declare that they have no known competing financial interests or personal relationships that could have appeared to influence the work reported in this paper.

CRediT authorship contribution statement

Viviane Lucia Beraldo de Araújo: Conceptualization, Methodology, Formal analysis, Investigation, Resources, Writing – original draft, Visualization. Marcelo van Vliet Lima: Methodology, Investigation, Visualization. Samira Elisa Alves Geraldo: Methodology, Investigation, Visualization. Gabriel da Silva Cordeiro: Methodology, Formal analysis, Writing – original draft. João Paulo Guarnieri: Methodology, Formal analysis. Marcelo Lancellotti: Resources, Writing – review. Karina Cogo Muller: Resources. Catarina Raposo: Conceptualization, Resources, Writing – review. Laura de Oliveira Nascimento: Conceptualization, Formal analysis, Resources, Writing – review & editing, Visualization, Supervision, Project administration, Funding acquisition.

4.7. References

Allotey-Babington, Grace Lovia, Henry Nettey, Sucheta D'Sa, Kimberly Braz Gomes, e Martin J. D'Souza. 2018. "Cancer Chemotherapy: Effect of Poloxamer Modified Nanoparticles on Cellular Function". *Journal of Drug Delivery Science and Technology* 47 (outubro): 181–92. https://doi.org/10.1016/j.jddst.2018.06.012.

Amin, Ketan, e Rose-Marie Dannenfelser. 2006. "In Vitro Hemolysis: Guidance for the Pharmaceutical Scientist". *Journal of Pharmaceutical Sciences* 95 (6): 1173–76. https://doi.org/10.1002/jps.20627.

Beraldo-Araújo, Viviane Lucia, Ana Flávia Siqueira Vicente, Marcelo van Vliet Lima, Anita Umerska, Eliana B. Souto, Lidia Tajber, e Laura Oliveira-Nascimento. 2022. "Levofloxacin in Nanostructured Lipid Carriers: Preformulation and Critical Process Parameters for a Highly Incorporated Formulation". *International Journal of Pharmaceutics* 626 (outubro): 122193. https://doi.org/10.1016/j.ijpharm.2022.122193.

Beraldo-de-Araújo, Viviane Lucia, Anderson Beraldo-de-Araújo, Juliana Souza Ribeiro Costa, Ana Carolina Martins Pelegrine, Lígia Nunes Moraes Ribeiro, Eneida de Paula, e Laura Oliveira-Nascimento. 2019. "Excipient-Excipient Interactions in the Development of Nanocarriers: An Innovative Statistical Approach for Formulation Decisions". *Scientific Reports* 9 (1): 10738. https://doi.org/10.1038/s41598-019-47270-w.

Bhakay, Anagha, Mahbubur Rahman, Rajesh N. Dave, e Ecevit Bilgili. 2018. "Bioavailability Enhancement of Poorly Water-Soluble Drugs via Nanocomposites: Formulation–Processing Aspects and Challenges". *Pharmaceutics* 10 (3): 86. https://doi.org/10.3390/pharmaceutics10030086.

Brunaugh, Ashlee D., Hugh D. C. Smyth, e Robert O. Williams III. 2019. "Pulmonary Drug Delivery". Em *Essential Pharmaceutics*, editado por Ashlee D. Brunaugh, Hugh D. C. Smyth, e Robert O. Williams III, 163–81. AAPS Introductions in the Pharmaceutical Sciences. Cham: Springer International Publishing. https://doi.org/10.1007/978-3-030-31745-4_11.

Chen, Jianting, Maizbha U. Ahmed, Chune Zhu, Shihui Yu, Weisan Pan, Tony Velkov, Jian Li, e Qi (Tony) Zhou. 2021. "In Vitro Evaluation of Drug Delivery Behavior for Inhalable Amorphous Nanoparticle Formulations in a Human Lung Epithelial Cell Model". *International Journal of Pharmaceutics* 596 (março): 120211. https://doi.org/10.1016/j.ijpharm.2021.120211.

CLSI. 2018. *Methods for Dilution Antimicrobial Susceptibility Tests for Bacteria That Grow Aerobically*. 11th ed. Wayne, PA.

Cortés, Hernán, Héctor Hernández-Parra, Sergio A. Bernal-Chávez, María L. Del Prado-Audelo, Isaac H. Caballero-Florán, Fabiola V. Borbolla-Jiménez, Maykel González-Torres, Jonathan J. Magaña, e Gerardo Leyva-Gómez. 2021. "Non-Ionic Surfactants for Stabilization of Polymeric Nanoparticles for Biomedical Uses". *Materials* 14 (12): 3197. https://doi.org/10.3390/ma14123197.

Croom, Katherine F., e Karen L. Goa. 2003. "Levofloxacin: A Review of Its Use in the Treatment of Bacterial Infections in the United States". *Drugs* 63 (24): 2769–2802. https://doi.org/10.2165/00003495-200363240-00008.

Darweesh, Ruba S., e Masahiro Sakagami. 2018. "In Vitro Lung Epithelial Cell Transport and Anti-Interleukin-8 Releasing Activity of Liposomal Ciprofloxacin".

European Journal of Pharmaceutical Sciences 115 (março): 68–76. https://doi.org/10.1016/j.ejps.2018.01.018.

Derbali, Rabeb Mouna, Valery Aoun, Ghina Moussa, Giorgia Frei, Soudeh F. Tehrani, Juliana Campos Del'Orto, Patrice Hildgen, V. Gaëlle Roullin, e Jeanne Leblond Chain. 2019. "Tailored Nanocarriers for the Pulmonary Delivery of Levofloxacin against Pseudomonas aeruginosa: A Comparative Study". *Molecular Pharmaceutics* 16 (5): 1906–16. https://doi.org/10.1021/acs.molpharmaceut.8b01256.

Dumortier, Gilles, Jean Louis Grossiord, Florence Agnely, e Jean Claude Chaumeil. 2006. "A Review of Poloxamer 407 Pharmaceutical and Pharmacological Characteristics". *Pharmaceutical Research* 23 (12): 2709–28. https://doi.org/10.1007/s11095-006-9104-4.

Elmowafy, Mohammed, e Mohammad M. Al-Sanea. 2021. "Nanostructured lipid carriers (NLCs) as drug delivery platform: Advances in formulation and delivery strategies". *Saudi Pharmaceutical Journal : SPJ* 29 (9): 999–1012. https://doi.org/10.1016/j.jsps.2021.07.015.

Filipczak, Nina, Xiang Li, Gaurav Rajan Saawant, Satya Siva Kishan Yalamarty, Ed Luther, e Vladimir P. Torchilin. 2023. "Antibody-Modified DNase I Micelles Specifically Recognize the Neutrophil Extracellular Traps (NETs) and Promote Their Degradation". *Journal of Controlled Release* 354 (fevereiro): 109–19. https://doi.org/10.1016/j.jconrel.2022.12.062.

Flume, Patrick A., Donald R. VanDevanter, Elizabeth E. Morgan, Michael N. Dudley, Jeffery S. Loutit, Scott C. Bell, Eitan Kerem, et al. 2016. "A Phase 3, Multi-Center, Multinational, Randomized, Double-Blind, Placebo-Controlled Study to Evaluate the Efficacy and Safety of Levofloxacin Inhalation Solution (APT-1026) in Stable Cystic Fibrosis Patients". *Journal of Cystic Fibrosis* 15 (4): 495–502. https://doi.org/10.1016/j.jcf.2015.12.004.

Foster, K. A., M. L. Avery, M. Yazdanian, e K. L. Audus. 2000. "Characterization of the Calu-3 Cell Line as a Tool to Screen Pulmonary Drug Delivery". *International Journal of Pharmaceutics* 208 (1–2): 1–11. https://doi.org/10.1016/s0378-5173(00)00452-x.

Grillon, Antoine, Frédéric Schramm, Magali Kleinberg, e François Jehl. 2016. "Comparative Activity of Ciprofloxacin, Levofloxacin and Moxifloxacin against Klebsiella pneumoniae, Pseudomonas aeruginosa and Stenotrophomonas maltophilia Assessed by Minimum Inhibitory Concentrations and Time-Kill Studies". *PLoS ONE* 11 (6). https://doi.org/10.1371/journal.pone.0156690.

Guo, Shiqi, Yanan Shi, Yanzi Liang, Lanze Liu, Kaoxiang Sun, e Youxin Li. 2021. "Relationship and improvement strategies between drug nanocarrier characteristics and hemocompatibility: What can we learn from the literature". *Asian Journal of Pharmaceutical Sciences* 16 (5): 551–76. https://doi.org/10.1016/j.ajps.2020.12.002.

Haghi, Mehra, Paul M. Young, Daniela Traini, Ritu Jaiswal, Joyce Gong, e Mary Bebawy. 2010. "Time- and Passage-Dependent Characteristics of a Calu-3 Respiratory Epithelial Cell Model". *Drug Development and Industrial Pharmacy* 36 (10): 1207–14. https://doi.org/10.3109/03639041003695113.

Huang, Guiting, Shuyuan Shuai, Weicheng Zhou, Yingchong Chen, Baode Shen, e Pengfei Yue. 2022. "To Enhance Mucus Penetration and Lung Absorption of Drug by Inhalable Nanocrystals-In-Microparticles". *Pharmaceutics* 14 (3): 538. https://doi.org/10.3390/pharmaceutics14030538.

Hurst, Miriam, Harriet M. Lamb, Lesley J. Scott, e David P. Figgitt. 2002. “Levofloxacin: An Updated Review of Its Use in the Treatment of Bacterial Infections”. *Drugs* 62 (14): 2127–67. https://doi.org/10.2165/00003495-200262140-00013.

Islan, Germán A., Pablo Cortez Tornello, Gustavo A. Abraham, Nelson Duran, e Guillermo R. Castro. 2016. “Smart Lipid Nanoparticles Containing Levofloxacin and DNase for Lung Delivery. Design and Characterization”. *Colloids and Surfaces. B, Biointerfaces* 143 (julho): 168–76. https://doi.org/10.1016/j.colsurfb.2016.03.040.

ISO 10993-5:2009. 2009. “Biological Evaluation of Medical Devices — Part 5: Tests for in Vitro Cytotoxicity”. Geneva, Switzerland. https://www.iso.org/standard/36406.html.

Jackson, J. K., C. M. Springate, W. L. Hunter, e H. M. Burt. 2000. “Neutrophil Activation by Plasma Opsonized Polymeric Microspheres: Inhibitory Effect of Pluronic F127”. *Biomaterials* 21 (14): 1483–91. https://doi.org/10.1016/s0142-9612(00)00034-x.

Jeong, Mi Ho, Ha Ryong Kim, In Jae Bang, So Hee Yoo, Sang Jin Lee, Kyu Hong Lee, e Kyu Hyuck Chung. 2019. “In Vitro Model for Predicting Acute Inhalation Toxicity by Using a Calu-3 Epithelium Cytotoxicity Assay”. *Journal of Pharmacological and Toxicological Methods* 98 (julho): 106576. https://doi.org/10.1016/j.vascn.2019.04.002.

Kradin, Richard L., e Subbha Digumarthy. 2017. “The Pathology of Pulmonary Bacterial Infection”. *Seminars in Diagnostic Pathology* 34 (6): 498–509. https://doi.org/10.1053/j.semdp.2017.06.001.

Kreft, Mateja Erdani, Urška Dragin Jerman, Eva Lasič, Neli Hevir-Kene, Tea Lanišnik Rižner, Luka Peternel, e Katja Kristan. 2015. “The Characterization of the Human Cell Line Calu-3 under Different Culture Conditions and Its Use as an Optimized in Vitro Model to Investigate Bronchial Epithelial Function”. *European Journal of Pharmaceutical Sciences* 69 (março): 1–9. https://doi.org/10.1016/j.ejps.2014.12.017.

Lawless, Harry T., Frank Rapacki, John Horne, e April Hayes. 2003. “The Taste of Calcium and Magnesium Salts and Anionic Modifications”. *Food Quality and Preference* 14 (4): 319–25. https://doi.org/10.1016/S0950-3293(02)00128-3.

Lee, Diane F., Michael I. Lethem, e Alison B. Lansley. 2021. “A Comparison of Three Mucus-Secreting Airway Cell Lines (Calu-3, SPOC1 and UNCN3T) for Use as Biopharmaceutical Models of the Nose and Lung”. *European Journal of Pharmaceutics and Biopharmaceutics* 167 (outubro): 159–74. https://doi.org/10.1016/j.ejpb.2021.07.016.

“Levofloxacin monograph.” 2017. Em *UNITED States Pharmacopeia*, 40º ed, 4831–33.

Li, Jiaqi, Huangliang Zheng, e Sharon Shui Yee Leung. 2022. “Pulmonary Delivery of Emerging Antibacterials for Bacterial Lung Infections Treatment”. *Pharmaceutical Research*, setembro, 1–16. https://doi.org/10.1007/s11095-022-03379-8.

Lister, Philip D. 2001. “Pharmacodynamics of Moxifloxacin and Levofloxacin against Staphylococcus Aureus and Staphylococcus Epidermidis in an In Vitro Pharmacodynamic Model”. *Clinical Infectious Diseases* 32 (Supplement_1): S33–38. https://doi.org/10.1086/319374.

Liu, Rui, Zhidong Liu, Chengui Zhang, e Boli Zhang. 2012. “Nanostructured Lipid Carriers as Novel Ophthalmic Delivery System for Mangiferin: Improving in Vivo

Ocular Bioavailability". *Journal of Pharmaceutical Sciences* 101 (10): 3833–44. https://doi.org/10.1002/jps.23251.

López-García, Jorge, Marián Lehocký, Petr Humpolíček, e Petr Sáha. 2014. "HaCaT Keratinocytes Response on Antimicrobial Atelocollagen Substrates: Extent of Cytotoxicity, Cell Viability and Proliferation". *Journal of Functional Biomaterials* 5 (2): 43–57. https://doi.org/10.3390/jfb5020043.

Miyazawa, Taiki, Mayuko Itaya, Gregor C Burdeos, Kiyotaka Nakagawa, e Teruo Miyazawa. 2021. "A Critical Review of the Use of Surfactant-Coated Nanoparticles in Nanomedicine and Food Nanotechnology". *International Journal of Nanomedicine* 16 (junho): 3937–99. https://doi.org/10.2147/IJN.S298606.

Morales, Javier O., Jay I. Peters, e Robert O. Williams. 2011. "Surfactants: Their Critical Role in Enhancing Drug Delivery to the Lungs". *Therapeutic Delivery* 2 (5): 623–41. https://doi.org/10.4155/tde.11.15.

Nafee, N., K. Forier, K. Braeckmans, e M. Schneider. 2018. "Mucus-Penetrating Solid Lipid Nanoparticles for the Treatment of Cystic Fibrosis: Proof of Concept, Challenges and Pitfalls". *European Journal of Pharmaceutics and Biopharmaceutics: Official Journal of Arbeitsgemeinschaft Fur Pharmazeutische Verfahrenstechnik e.V* 124 (março): 125–37. https://doi.org/10.1016/j.ejpb.2017.12.017.

Papadimitriou, Sofia, e Dimitrios Bikiaris. 2009. "Novel self-assembled core-shell nanoparticles based on crystalline amorphous moieties of aliphatic copolyesters for efficient controlled drug release". *Journal of Controlled Release* 138 (2): 177–84. https://doi.org/10.1016/j.jconrel.2009.05.013.

Ravichandran, Vasanthan, Minjong Lee, Thuy Giang Nguyen Cao, e Min Suk Shim. 2021. "Polysorbate-Based Drug Formulations for Brain-Targeted Drug Delivery and Anticancer Therapy". *Applied Sciences* 11 (19): 9336. https://doi.org/10.3390/app11199336.

Repetto, Guillermo, Ana del Peso, e Jorge L. Zurita. 2008. "Neutral Red Uptake Assay for the Estimation of Cell Viability/Cytotoxicity". *Nature Protocols* 3 (7): 1125–31. https://doi.org/10.1038/nprot.2008.75.

Riss, Terry L., Richard A. Moravec, Andrew L. Niles, Sarah Duellman, Hélène A. Benink, Tracy J. Worzella, e Lisa Minor. 2004. "Cell Viability Assays". Em *Assay Guidance Manual*, editado por Sarine Markossian, Abigail Grossman, Kyle Brimacombe, Michelle Arkin, Douglas Auld, Chris Austin, Jonathan Baell, et al. Bethesda (MD): Eli Lilly & Company and the National Center for Advancing Translational Sciences. http://www.ncbi.nlm.nih.gov/books/NBK144065/.

Schwarz, C., W. Mehnert, J. S. Lucks, e R. H. Müller. 1994. "Solid lipid nanoparticles (SLN) for controlled drug delivery. I. Production, characterization and sterilization". *Journal of Controlled Release* 30 (1): 83–96. https://doi.org/10.1016/0168-3659(94)90047-7.

Shubhra, Quazi T. H., Judit Tóth, János Gyenis, e Tivadar Feczkó. 2014. "Surface Modification of HSA Containing Magnetic PLGA Nanoparticles by Poloxamer to Decrease Plasma Protein Adsorption". *Colloids and Surfaces. B, Biointerfaces* 122 (outubro): 529–36. https://doi.org/10.1016/j.colsurfb.2014.07.025.

Sonia, Thundiparambil Azeez, e Chandra P. Sharma. 2014. "5 - Lipids and Inorganic Nanoparticles in Oral Insulin Delivery". Em *Oral Delivery of Insulin*, editado por Thundiparambil Azeez Sonia e Chandra P. Sharma, 219–56. Woodhead Publishing Series in Biomedicine. Woodhead Publishing. https://doi.org/10.1533/9781908818683.219.

Steiner, Verena, Kristin Öhlinger, Carolina Corzo, Sharareh Salar-Behzadi, e Eleonore Fröhlich. 2019. “Cytotoxicity Screening of Emulsifiers for Pulmonary Application of Lipid Nanoparticles”. *European Journal of Pharmaceutical Sciences* 136 (agosto): 104968. https://doi.org/10.1016/j.ejps.2019.104968.

Tsivkovskii, Ruslan, Mojgan Sabet, Ziad Tarazi, David C. Griffith, Olga Lomovskaya, e Michael N. Dudley. 2011. “Levofloxacin reduces inflammatory cytokine levels in human bronchial epithelia cells: implications for aerosol MP-376 (levofloxacin solutionfor inhalation) treatment of chronic pulmonary infections”. *FEMS Immunology & Medical Microbiology* 61 (2): 141–46. https://doi.org/10.1111/j.1574-695X.2010.00755.x.

Zhang, Lin, Shou-Ying Du, Yang Lu, Chang Liu, Zhi-Hao Tian, Chang Yang, Hui-Chao Wu, e Zhen Wang. 2016. “Puerarin transport across a Calu-3 cell monolayer – an in vitro model of nasal mucosa permeability and the influence of paeoniflorin and menthol”. *Drug Design, Development and Therapy* 10 (julho): 2227–37. https://doi.org/10.2147/DDDT.S110247.

4.8. Appendix A. Supplementary material

The following are the Supplementary data to this article:

4.8.1. Particle size distribution by intensity measured by Dynamic light scattering

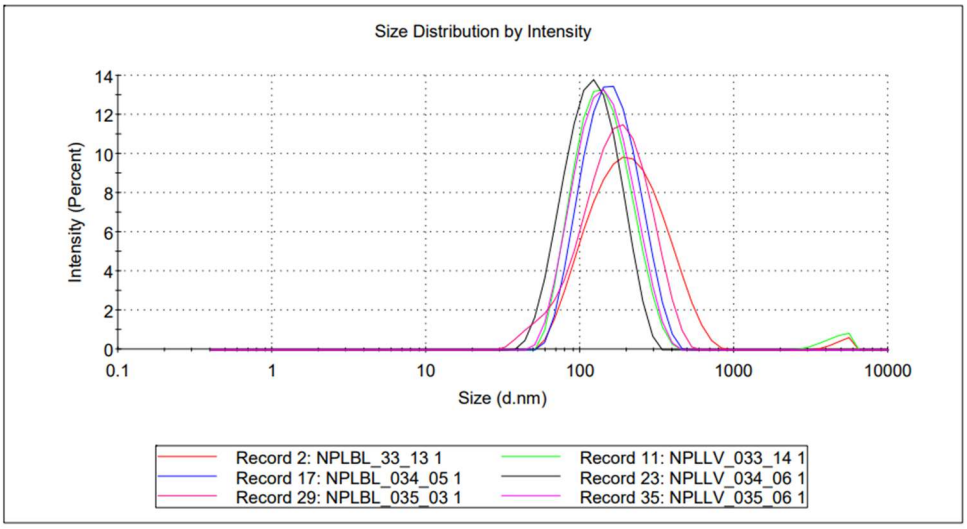

Supplementary Figure 1. Representation of NLCs particle size distribution by intensity measured by Dynamic Light Scattering. NLCs dilution 1:200 in NaCl 10 mM.

4.8.2. Particle size distribution by intensity measured by Nanotracking analysis

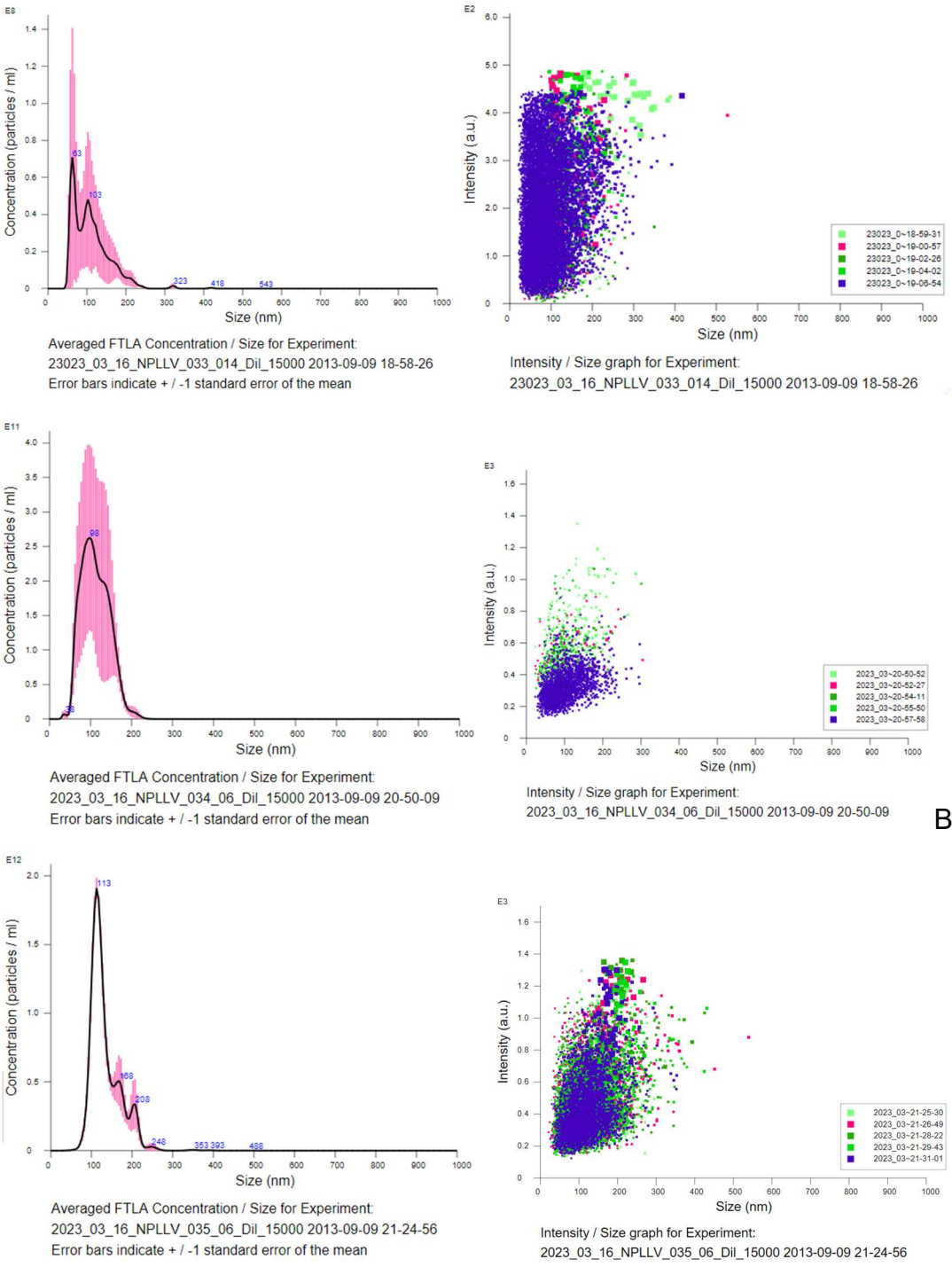

Supplementary Figure 2. Representation of NLCs concentration distribution according to the particle size (left side) and particle size distribution by intensity (right side) of NLCs made with P80 (A), P407 (B) and P188 (C), measured by Nanotracking Analysis. NLCs diluted 15000x in ultrapure water.

Calu-3 differentiation:

4.8.3. Differentiated Calu-3 imaging by Scanning Electron Microscopy (SEM)

Differentiated Calu-3 cells were prepared based on the method described in (Cozens et al. 2018; Kreft et al. 2015) to have their images captured. Calu-3 from transwells were fixed in 1.5% (v/v) glutaraldehyde in 0.1 M sodium cacodylate buffer for 1 h at 4 °C. Then, both apical and basal compartments were rinsed tree times with sodium cacodylate buffer 0.1 M. Samples were then dehydrated with crescent concentrations of ethanol up to 100 % ethanol overnight. In the next day, membranes were cut from transwell inserts and dried at the critical point, then mounted onto aluminium SEM stubs and spattered with gold and examined with a Quanta FEG 250 SEM microscope at 10 kV.

4.8.4. Differential Calu-3 monolayer visualization – Hoechst stain

Hoechst 33342 is a useful fluorescent stain for DNA of fixed or living cells. Hoechst solution was prepared by diluting stock solution in cell culture medium to the concentration 2 μg/mL.100 μL of the diluted stain was added to the apical compartment of the transwell insert and incubated for 5 to 10 min protected from the light. Fluorescence images were obtained with a Leica DM IL LED Inverted Laboratory Microscope equipped with 3 position fluorescence sliders (Leica Microsystems, Brazil) and qualitatively evaluated.

4.8.5. Calu-3 differentiation

Conventional submerged techniques for culturing immortalized cells, while simple and reliable, do not fully replicate the properties of the lung, such as cell polarization, mucus production, and motile cilia. The air-liquid interface (ALI) culture technique, in which cells are grown on semipermeable membranes with exposure to both air and medium, provides a more physiological and accurate *in vitro* model for preclinical studies. ALI allows for cell differentiation and production of mucus and motile

cilia, making the cells highly similar to *in vivo* cells in terms of gene expression (Woodall et al. 2021). For this reason, we performed the following experiments in differentiated Calu-3 cells, and adherent cell line that differentiates when in ALI environment.

Before conducting the experiments, right before and after differentiation, we checked the integrity of a tight cell monolayer, by measuring the transepithelial electrical resistance of cell membrane (TEER) (Morales, Peters, e Williams 2011). It is described in the literature that a TEER value superior to 300 $\Omega.cm^2$ indicates the existence of an integer cell monolayer (Chen et al. 2021; Foster et al. 2000). After 5 days of seeding the transwell inserts with Caly-3 at a density of 1.5×10^5 cells/insert, the measurements of TEER for all the inserts (at least 3 measurements per insert) gave values > 700 $\Omega.cm^2$ (data not shown), confirming that that period was sufficient for Calu-3 to grow and expand into a monolayer. After this period, they were differentiated, removing the medium from apical compartment (ALI condition). Cells were differentiated during 14 ± 2 days until being tested (confirmed by SEM image, Figure 6 (b)).

Another strategy to confirm cell monolayer is to stain nucleus using Hoechst stain (Figure 6 (a)) (Meindl et al. 2021). For confirmation of cell differentiation, we imaged Calu-3 post- differentiation process using scanning electron microscopy (SEM) (Figure 6 (b)). In this image, it is possible to see microvilli on the cell surface, indicating polarization and formation of these structures, similar to alveolar environment, also seen in (van Rensburg, van Zyl, e Smith 2018).

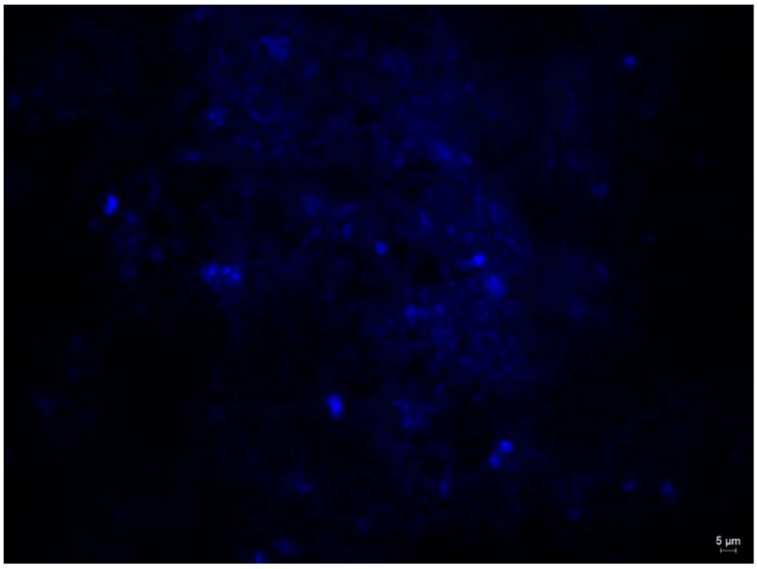

(a)

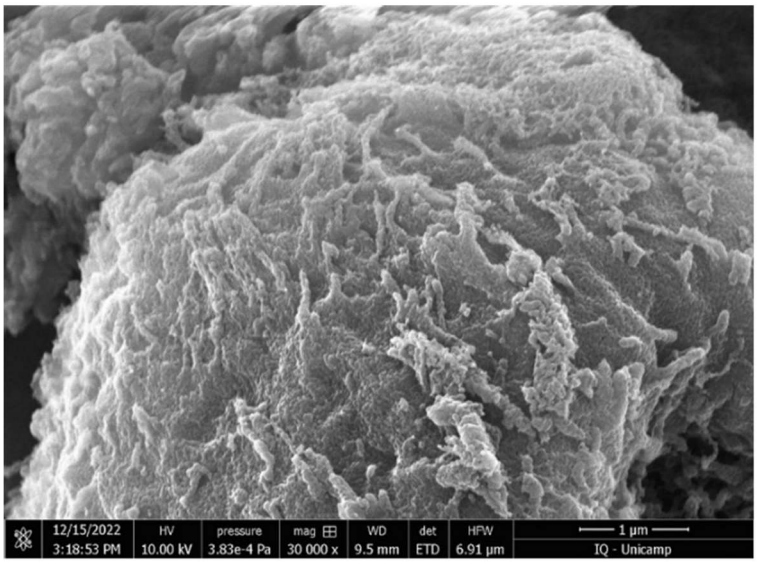

(b)

Supplementary Figure 3. Calu-3 cell monolayer with nuclei stained using Hoechst 33342 fluorescent stain. Fluorescence images were obtained with a Leica DM IL LED Inverted Laboratory Microscope. Scale bar = 5 µm (a); Scanning electron microscopy image of differentiated Calu-3 epithelial layer grown at air-liquid interface. Cilia on the cell surface is visible, indicating cell differentiation. Scale bar = 1 µm. Magnification: 30,000x, WD = 9.5 mm, HV = 10.00 kV.

5. DISCUSSION

This thesis comprised the development of three chapters. Chapter one presented a section of the book chapter written by our lab collaborators, where we highlighted the significance of developing nanomaterials as drug delivery systems. These nanostructures can enhance or modify the performance characteristics of the drug by serving as carriers for the active pharmaceutical ingredient (API). This development can lead to modifications in the physicochemical properties of the APIs, as well as the rate and location of their release. For this reason, we presented the importance of conducting a comprehensive evaluation of the physicochemical properties of the API, the safety of the nanomaterials with regards to impurities, and the quality attributes and reproducibility of the manufacturing process. Specifically, we focused on the presentation of techniques such as thermal, spectroscopic, x-ray and microscopy-based methods to evaluate the composition, surface, dimensional properties, and morphology of nanomedicines, and how these techniques can be applied to meet standards and general applications.

Chapter 2 is an application of these techniques to characterize a lipid-based nanoparticle loading the antibiotic LV, which yielded an experimental paper publication. First, we conducted preformulation studies, selecting biodegradable and non-toxic excipients, optimizing this selection to ensure drug compatibility, solubility and reaching higher LV entrapment efficiency in NLCs than other lipid nanocarriers described in the literature. Solid state analysis revealed that the NLCs had a lipid core in which most of the LV was solubilized, while the outside was more hydrophilic and contained the remaining LV molecules in a lamellar-like structure. From a DoE, we discovered that LV impurities, specifically the degradation product levofloxacin N-oxide (LNO), could be present in different concentrations in the NLCs, depending on the critical process parameters (sonication time, amplitude, and temperature of production). As LNO has no antimicrobial activity, its presence in the formulation could impact the final LV dose, emphasizing the importance of stability-indicating methods when formulating this drug. Then, we created an optimized NLC using the specific process parameters adjusted and confirmed its stability over 30 days under accelerated conditions (40°C/75% RH) with no significant changes in particle size, polydispersity, zeta potential, and EE. Impurities increased slightly after 30 days, but this was mainly due to the degradation of non-entrapped drug, which showed that the

NLCs protected the drug. We also verified that, when diluted in buffer, the LV had a fast release from the NLC, but a sustained release when tested using the Franz cell method, suggesting that it could be used in mucus membranes such as pulmonary or nasal routes of administration. Approximately 10-15% of LV remained entrapped in the NLCs, which could enhance LV internalization and improve intracellular bacterial killing. These promising outcomes of a pulmonary application for the optimised NLC, added to the LV degradation issue led us to restructure our goals and try punctual modifications in the optimized NLC, resulting in the final chapter.

In light of this, we wrote Chapter 3, focusing on the development of two complementary NLC formulations, NPLLV_034 and NPLLV_035, while keeping the same parameters, and compared them to NPLLV_033. These new formulations exhibited favourable physicochemical properties, particle size distribution, morphology, and zeta potential for pulmonary application, and importantly, the accelerated stability tests demonstrated that both NLCs protected LV from degradation after 30 days at 40 °C/ 75% RH. With these promising outcomes, we assayed the LV release studies in Franz cell diffusion and the simulated lung fluid as a biorelevant acceptor medium. After comparing drug release between free LV and the three formulations, we found no difference between LV and NPLLV_033 drug release, while NPLLV_034 and NPLLV_035 had different profiles, and NPLLV_035 having the slower LV. Notably, the antimicrobial activity of LV was not reduced when incorporated into NLCs with any of the three surfactants, and the entrapped drug remained effective against *K. pneumoniae* and *S. aureus*. Additionally, cell viability assays on undifferentiated and differentiated Calu-3 cells with these formulations, both with and without the drug (NPLBL and NPLLV) and compared to free drug (LV) and surfactants indicated that blank or loaded formulations were cytotoxic to Calu-3 at a concentration of 100 µg/mL. However, depending on the surfactant of the NLC, 50 µg/mL is not harmful for cell viability. Overall, NPLLV_035 tended to reduce Calu-3 viability, while NPLLV_034 did not change cell viability. The free LV did not reduce cell viability under all the conditions tested. Lastly, it was observed that Calu-3 secretion of IL-8 was not exacerbated after cell exposure to stimuli and with LPS, comparing to secretion exposed only to LPS. NPLLV_034 showed a discrete, buy significative reduction in IL-8 secretion when compared to free LV in differentiated cells, indicating that this formulation is promising for pulmonary drug delivery. Upon comparing the haemolytic capacity of NLCs, it was found that NPLLV_034 had the lower haemolytic profile, while

NPLLV_035 was the most haemolytic one. Nonetheless, considering the dilution to reach the MIC values, all the NLCs were considered non-haemolytic and safe for pulmonary delivery.

As a whole, this thesis was meaningful, where we comprised a theoretical comprehension of the main tools used to characterize nanomaterials, with a deep experimental application of them. Besides, the optimization of the NLCs considering their process of production and effects on the LV degradation product was an innovative approach in the literature so far. Further investigations are in progress and will boost our knowledge on this formulation, such as drug permeation analysis across Calu-3 monolayer, nanoparticles drying to simulate and evaluate the physicochemical properties and efficacy of dry powder as a new LV drug delivery formulation. These following steps will be conducted by our research group.

6. CONCLUSION

The aim of this thesis was to produce a nanocarrier to deliver LV, in a safe and advantageous way, formulations to treat pulmonary infections, compared to the proposed in the literature. The text comprehended the merge of the three main aspects of this research: the explanation of the theoretical background on nanomaterials, the construction of an optimized NLC from the beginning of preformulation studies up to the formulation, and the amplification of the formulations, by increasing two different surfactants in new NLCs. The outcomes obtained were very promisor, increasing LV protection and stability in NPLLV_034, maintenance of LV antimicrobial activity when incorporated in the NLCs and safe application for the treatment of pulmonary infections, with potential reduction of the body's inflammatory response. Further experiments are in progress by our research group and will boost our knowledge on the selected formulation (NPLLV_034), such as NLC antimicrobial activity against *Streptococcus pneumoniae*, drug permeation analysis across Calu-3 monolayer, and nanoparticles drying studies to simulate and evaluate the physicochemical properties and efficacy of dry powder as a new LV drug delivery formulation for pulmonary delivery.

7. REFERENCES

"15.1: Theory of Fluorescence and Phosphorescence". 2022. Chemistry LibreTexts. 30 de janeiro de 2022. https://chem.libretexts.org/Bookshelves/Analytical_Chemistry/Instrumental_Analysis_(LibreTexts)/15%3A_Molecular_Luminescence/15.01%3A_Theory_of_Fluorescence_and_Phosphorescence.

Abed, Nadia, e Patrick Couvreur. 2014. "Nanocarriers for antibiotics: A promising solution to treat intracellular bacterial infections". *International Journal of Antimicrobial Agents* 43 (6): 485–96. https://doi.org/10.1016/j.ijantimicag.2014.02.009.

Allotey-Babington, Grace Lovia, Henry Nettey, Sucheta D'Sa, Kimberly Braz Gomes, e Martin J. D'Souza. 2018. "Cancer Chemotherapy: Effect of Poloxamer Modified Nanoparticles on Cellular Function". *Journal of Drug Delivery Science and Technology* 47 (outubro): 181–92. https://doi.org/10.1016/j.jddst.2018.06.012.

Amin, Ketan, e Rose-Marie Dannenfelser. 2006. "In Vitro Hemolysis: Guidance for the Pharmaceutical Scientist". *Journal of Pharmaceutical Sciences* 95 (6): 1173–76. https://doi.org/10.1002/jps.20627.

Austin, Jake, Caterina Minelli, Douglas Hamilton, Magdalena Wywijas, e Hanna Jankevics Jones. 2020. "Nanoparticle Number Concentration Measurements by Multi-Angle Dynamic Light Scattering". *Journal of Nanoparticle Research* 22 (5): 108. https://doi.org/10.1007/s11051-020-04840-8.

Bantz, Christoph, Olga Koshkina, Thomas Lang, Hans-Joachim Galla, C James Kirkpatrick, Roland H Stauber, e Michael Maskos. 2014. "The surface properties of nanoparticles determine the agglomeration state and the size of the particles under physiological conditions". *Beilstein Journal of Nanotechnology* 5 (outubro): 1774–86. https://doi.org/10.3762/bjnano.5.188.

Beraldo-Araújo, Viviane Lucia, Ana Flávia Siqueira Vicente, Marcelo van Vliet Lima, Anita Umerska, Eliana B. Souto, Lidia Tajber, e Laura Oliveira-Nascimento. 2022. "Levofloxacin in Nanostructured Lipid Carriers: Preformulation and Critical Process Parameters for a Highly Incorporated Formulation". *International Journal of Pharmaceutics* 626 (outubro): 122193. https://doi.org/10.1016/j.ijpharm.2022.122193.

Beraldo-de-Araújo, Viviane Lucia, Anderson Beraldo-de-Araújo, Juliana Souza Ribeiro Costa, Ana Carolina Martins Pelegrine, Lígia Nunes Moraes Ribeiro, Eneida de Paula, e Laura Oliveira-Nascimento. 2019. "Excipient-Excipient Interactions in the Development of Nanocarriers: An Innovative Statistical Approach for Formulation Decisions". *Scientific Reports* 9 (1): 10738. https://doi.org/10.1038/s41598-019-47270-w.

Bhakay, Anagha, Mahbubur Rahman, Rajesh N. Dave, e Ecevit Bilgili. 2018. "Bioavailability Enhancement of Poorly Water-Soluble Drugs via Nanocomposites: Formulation–Processing Aspects and Challenges". *Pharmaceutics* 10 (3): 86. https://doi.org/10.3390/pharmaceutics10030086.

Bhattacharjee, Sourav. 2016. "DLS and zeta potential – What they are and what they are not?" *Journal of Controlled Release* 235 (agosto): 337–51. https://doi.org/10.1016/j.jconrel.2016.06.017.

Bickel, M. 1993. "The Role of Interleukin-8 in Inflammation and Mechanisms of Regulation". *Journal of Periodontology* 64 (5 Suppl): 456–60.

Bol, Ludivine, Jean-Christophe Galas, Hervé Hillaireau, Isabelle Le Potier, Valérie Nicolas, Anne-Marie Haghiri-Gosnet, Elias Fattal, e Myriam Taverna. 2014. “A Microdevice for Parallelized Pulmonary Permeability Studies”. *Biomedical Microdevices* 16 (2): 277–85. https://doi.org/10.1007/s10544-013-9831-3.

Brunaugh, Ashlee D., Hugh D. C. Smyth, e Robert O. Williams III. 2019. “Pulmonary Drug Delivery”. Em *Essential Pharmaceutics*, editado por Ashlee D. Brunaugh, Hugh D. C. Smyth, e Robert O. Williams III, 163–81. AAPS Introductions in the Pharmaceutical Sciences. Cham: Springer International Publishing. https://doi.org/10.1007/978-3-030-31745-4_11.

Caputo, F., J. Clogston, L. Calzolai, M. Rösslein, e A. Prina-Mello. 2019. “Measuring Particle Size Distribution of Nanoparticle Enabled Medicinal Products, the Joint View of EUNCL and NCI-NCL. A Step by Step Approach Combining Orthogonal Measurements with Increasing Complexity”. *Journal of Controlled Release: Official Journal of the Controlled Release Society* 299 (abril): 31–43. https://doi.org/10.1016/j.jconrel.2019.02.030.

“Causes of Pneumonia | CDC”. 2023. 10 de fevereiro de 2023. https://www.cdc.gov/pneumonia/causes.html.

Chen, Jianting, Maizbha U. Ahmed, Chune Zhu, Shihui Yu, Weisan Pan, Tony Velkov, Jian Li, e Qi (Tony) Zhou. 2021. “In Vitro Evaluation of Drug Delivery Behavior for Inhalable Amorphous Nanoparticle Formulations in a Human Lung Epithelial Cell Model”. *International Journal of Pharmaceutics* 596 (março): 120211. https://doi.org/10.1016/j.ijpharm.2021.120211.

Cilloniz, Catia, Ignacio Martin-Loeches, Carolina Garcia-Vidal, Alicia San Jose, e Antoni Torres. 2016. “Microbial Etiology of Pneumonia: Epidemiology, Diagnosis and Resistance Patterns”. *International Journal of Molecular Sciences* 17 (12): 2120. https://doi.org/10.3390/ijms17122120.

CLSI. 2018. *Methods for Dilution Antimicrobial Susceptibility Tests for Bacteria That Grow Aerobically*. 11th ed. Wayne, PA.

“Community-Acquired Pneumonia in the Era of COVID-19”. s.d. Relias Media | Online Continuing Medical Education | Relias Media - Continuing Medical Education Publishing. Acedido a 27 de abril de 2023. https://www.reliasmedia.com/articles/149264-community-acquired-pneumonia-in-the-era-of-covid-19.

Cortés, Hernán, Héctor Hernández-Parra, Sergio A. Bernal-Chávez, María L. Del Prado-Audelo, Isaac H. Caballero-Florán, Fabiola V. Borbolla-Jiménez, Maykel González-Torres, Jonathan J. Magaña, e Gerardo Leyva-Gómez. 2021. “Non-Ionic Surfactants for Stabilization of Polymeric Nanoparticles for Biomedical Uses”. *Materials* 14 (12): 3197. https://doi.org/10.3390/ma14123197.

“Country Profiles”. 2016. Institute for Health Metrics and Evaluation. 3 de agosto de 2016. https://www.healthdata.org/results/country-profiles.

Cox, Michael J., Nicholas Loman, Debby Bogaert, e Justin O’Grady. 2020. “Co-Infections: Potentially Lethal and Unexplored in COVID-19”. *The Lancet Microbe* 1 (1): e11. https://doi.org/10.1016/S2666-5247(20)30009-4.

Cozens, Daniel, Edward Grahame, Erin Sutherland, Geraldine Taylor, Catherine C. Berry, e Robert L. Davies. 2018. “Development and Optimization of a Differentiated Airway Epithelial Cell Model of the Bovine Respiratory Tract”. *Scientific Reports* 8 (1): 853. https://doi.org/10.1038/s41598-017-19079-y.

Croom, Katherine F., e Karen L. Goa. 2003. “Levofloxacin: A Review of Its Use in the Treatment of Bacterial Infections in the United States”. *Drugs* 63 (24): 2769–2802. https://doi.org/10.2165/00003495-200363240-00008.

Darweesh, Ruba S., e Masahiro Sakagami. 2018. “In Vitro Lung Epithelial Cell Transport and Anti-Interleukin-8 Releasing Activity of Liposomal Ciprofloxacin”. *European Journal of Pharmaceutical Sciences* 115 (março): 68–76. https://doi.org/10.1016/j.ejps.2018.01.018.

Dave, Vivek S. 2019. “Chapter 4 - QbD Considerations for Excipient Manufacturing”. Em *Pharmaceutical Quality by Design*, editado por Sarwar Beg e Md Saquib Hasnain, 65–76. Academic Press. https://doi.org/10.1016/B978-0-12-815799-2.00004-6.

Derayea, Sayed M., e Hytham M. Ahmed. 2019. “Applications of Ion-Exchange Chromatography in Pharmaceutical Analysis”. Em *Applications of Ion Exchange Materials in Biomedical Industries*, editado por Inamuddin, 119–38. Cham: Springer International Publishing. https://doi.org/10.1007/978-3-030-06082-4_5.

Derbali, Rabeb Mouna, Valery Aoun, Ghina Moussa, Giorgia Frei, Soudeh F. Tehrani, Juliana Campos Del’Orto, Patrice Hildgen, V. Gaëlle Roullin, e Jeanne Leblond Chain. 2019. “Tailored Nanocarriers for the Pulmonary Delivery of Levofloxacin against Pseudomonas aeruginosa: A Comparative Study”. *Molecular Pharmaceutics* 16 (5): 1906–16. https://doi.org/10.1021/acs.molpharmaceut.8b01256.

Dongargaonkar, Alpana A., e Jeffrey D. Clogston. 2018. “Quantitation of Surface Coating on Nanoparticles Using Thermogravimetric Analysis”. Em *Characterization of Nanoparticles Intended for Drug Delivery*, editado por Scott E. McNeil, 57–63. Methods in Molecular Biology. New York, NY: Springer. https://doi.org/10.1007/978-1-4939-7352-1_6.

Dumortier, Gilles, Jean Louis Grossiord, Florence Agnely, e Jean Claude Chaumeil. 2006. “A Review of Poloxamer 407 Pharmaceutical and Pharmacological Characteristics”. *Pharmaceutical Research* 23 (12): 2709–28. https://doi.org/10.1007/s11095-006-9104-4.

Elmowafy, Mohammed, Nabil K. Alruwaili, Khaled Shalaby, Khalid S. Alharbi, Waleed M. Altowayan, Naveed Ahmad, Ameeduzzafar Zafar, e Mohammed Elkomy. 2020. “Long-Acting Paliperidone Parenteral Formulations Based on Polycaprolactone Nanoparticles; the Influence of Stabilizer and Chitosan on In Vitro Release, Protein Adsorption, and Cytotoxicity”. *Pharmaceutics* 12 (2): 160. https://doi.org/10.3390/pharmaceutics12020160.

Elmowafy, Mohammed, e Mohammad M. Al-Sanea. 2021. “Nanostructured lipid carriers (NLCs) as drug delivery platform: Advances in formulation and delivery strategies”. *Saudi Pharmaceutical Journal : SPJ* 29 (9): 999–1012. https://doi.org/10.1016/j.jsps.2021.07.015.

Fangueiro, Joana F., Tatiana Andreani, Maria A. Egea, Maria L. Garcia, Selma B. Souto, e Eliana B. Souto. 2012. “Experimental factorial design applied to mucoadhesive lipid nanoparticles via multiple emulsion process”. *Colloids and Surfaces B: Biointerfaces* 100 (dezembro): 84–89. https://doi.org/10.1016/j.colsurfb.2012.04.014.

Faria, Matthew, Mattias Björnmalm, Kristofer J. Thurecht, Stephen J. Kent, Robert G. Parton, Maria Kavallaris, Angus P. R. Johnston, et al. 2018. “Minimum Information Reporting in Bio–Nano Experimental Literature”. *Nature Nanotechnology* 13 (9): 777–85. https://doi.org/10.1038/s41565-018-0246-4.

Fattal, E., J. Rojas, L. Roblot-Treupel, A. Andremont, e P. Couvreur. 1991. “Ampicillin-loaded liposomes and nanoparticles: comparison of drug loading, drug release

and in vitro antimicrobial activity". *Journal of Microencapsulation* 8 (1): 29–36. https://doi.org/10.3109/02652049109021855.

Fattal, E., J. Rojas, M. Youssef, P. Couvreur, e A. Andremont. 1991. "Liposome-Entrapped Ampicillin in the Treatment of Experimental Murine Listeriosis and Salmonellosis." *Antimicrobial Agents and Chemotherapy* 35 (4): 770–72. https://doi.org/10.1128/AAC.35.4.770.

FDA/CDER/"Yeaton, Ayse". 2017. "Drug Products, Including Biological Products, That Contain Nanomaterials - Guidance for Industry", 29.

Filipczak, Nina, Xiang Li, Gaurav Rajan Saawant, Satya Siva Kishan Yalamarty, Ed Luther, e Vladimir P. Torchilin. 2023. "Antibody-Modified DNase I Micelles Specifically Recognize the Neutrophil Extracellular Traps (NETs) and Promote Their Degradation". *Journal of Controlled Release* 354 (fevereiro): 109–19. https://doi.org/10.1016/j.jconrel.2022.12.062.

Flume, Patrick A., Donald R. VanDevanter, Elizabeth E. Morgan, Michael N. Dudley, Jeffery S. Loutit, Scott C. Bell, Eitan Kerem, et al. 2016. "A Phase 3, Multi-Center, Multinational, Randomized, Double-Blind, Placebo-Controlled Study to Evaluate the Efficacy and Safety of Levofloxacin Inhalation Solution (APT-1026) in Stable Cystic Fibrosis Patients". *Journal of Cystic Fibrosis* 15 (4): 495–502. https://doi.org/10.1016/j.jcf.2015.12.004.

Foligno, Silvia, Barbara Loi, Lucilla Pezza, Marco Piastra, Chiara Autilio, e Daniele De Luca. 2020. "Extrapulmonary Surfactant Therapy: Review of Available Data and Research/Development Issues". *The Journal of Clinical Pharmacology* 60 (12): 1561–72. https://doi.org/10.1002/jcph.1675.

Foster, K. A., M. L. Avery, M. Yazdanian, e K. L. Audus. 2000. "Characterization of the Calu-3 Cell Line as a Tool to Screen Pulmonary Drug Delivery". *International Journal of Pharmaceutics* 208 (1–2): 1–11. https://doi.org/10.1016/s0378-5173(00)00452-x.

Gabbott, Paul. 2008a. "A Practical Introduction to Differential Scanning Calorimetry". Em *Principles and Applications of Thermal Analysis*, 1–50. John Wiley & Sons, Ltd. https://doi.org/10.1002/9780470697702.ch1.

———. 2008b. "Fast Scanning DSC". Em *Principles and Applications of Thermal Analysis*, 51–86. John Wiley & Sons, Ltd. https://doi.org/10.1002/9780470697702.ch2.

Garcia, Laetitia G., Sandrine Lemaire, Barbara C. Kahl, Karsten Becker, Richard A. Proctor, Olivier Denis, Paul M. Tulkens, e Françoise Van Bambeke. 2013. "Antibiotic activity against small-colony variants of Staphylococcus aureus: review of in vitro, animal and clinical data". *Journal of Antimicrobial Chemotherapy* 68 (7): 1455–64. https://doi.org/10.1093/jac/dkt072.

Ghosh, Baishakhi, Bongsoo Park, Debarshi Bhowmik, Kristine Nishida, Molly Lauver, Nirupama Putcha, Peisong Gao, et al. 2020. "Strong Correlation between Air-Liquid Interface Cultures and in Vivo Transcriptomics of Nasal Brush Biopsy". *American Journal of Physiology. Lung Cellular and Molecular Physiology* 318 (5): L1056–62. https://doi.org/10.1152/ajplung.00050.2020.

Grillon, Antoine, Frédéric Schramm, Magali Kleinberg, e François Jehl. 2016. "Comparative Activity of Ciprofloxacin, Levofloxacin and Moxifloxacin against Klebsiella pneumoniae, Pseudomonas aeruginosa and Stenotrophomonas maltophilia Assessed by Minimum Inhibitory Concentrations and Time-Kill Studies". *PLoS ONE* 11 (6). https://doi.org/10.1371/journal.pone.0156690.

Guo, Shiqi, Yanan Shi, Yanzi Liang, Lanze Liu, Kaoxiang Sun, e Youxin Li. 2021. "Relationship and improvement strategies between drug nanocarrier

characteristics and hemocompatibility: What can we learn from the literature". *Asian Journal of Pharmaceutical Sciences* 16 (5): 551–76. https://doi.org/10.1016/j.ajps.2020.12.002.

Haghi, Mehra, Paul M. Young, Daniela Traini, Ritu Jaiswal, Joyce Gong, e Mary Bebawy. 2010. "Time- and Passage-Dependent Characteristics of a Calu-3 Respiratory Epithelial Cell Model". *Drug Development and Industrial Pharmacy* 36 (10): 1207–14. https://doi.org/10.3109/03639041003695113.

Halwani, Abdulrahman A. 2022. "Development of Pharmaceutical Nanomedicines: From the Bench to the Market". *Pharmaceutics* 14 (1): 106. https://doi.org/10.3390/pharmaceutics14010106.

Heal, G. R. 2002. "Thermogravimetry and Derivative Thermogravimetry". Em *Principles of Thermal Analysis and Calorimetry*, 10–54. https://doi.org/10.1039/9781847551764-00010.

Holder, Cameron F., e Raymond E. Schaak. 2019. "Tutorial on Powder X-ray Diffraction for Characterizing Nanoscale Materials". *ACS Nano* 13 (7): 7359–65. https://doi.org/10.1021/acsnano.9b05157.

Hoshyar, Nazanin, Samantha Gray, Hongbin Han, e Gang Bao. 2016. "The effect of nanoparticle size on in vivo pharmacokinetics and cellular interaction". *Nanomedicine* 11 (6): 673–92. https://doi.org/10.2217/nnm.16.5.

Huang, Guiting, Shuyuan Shuai, Weicheng Zhou, Yingchong Chen, Baode Shen, e Pengfei Yue. 2022. "To Enhance Mucus Penetration and Lung Absorption of Drug by Inhalable Nanocrystals-In-Microparticles". *Pharmaceutics* 14 (3): 538. https://doi.org/10.3390/pharmaceutics14030538.

Hurst, Miriam, Harriet M. Lamb, Lesley J. Scott, e David P. Figgitt. 2002. "Levofloxacin: An Updated Review of Its Use in the Treatment of Bacterial Infections". *Drugs* 62 (14): 2127–67. https://doi.org/10.2165/00003495-200262140-00013.

ICH. 2005. "Validation of analytical procedures: text and methodology Q2 (R1)".

Islan, Germán A., Pablo Cortez Tornello, Gustavo A. Abraham, Nelson Duran, e Guillermo R. Castro. 2016. "Smart Lipid Nanoparticles Containing Levofloxacin and DNase for Lung Delivery. Design and Characterization". *Colloids and Surfaces. B, Biointerfaces* 143 (julho): 168–76. https://doi.org/10.1016/j.colsurfb.2016.03.040.

ISO 10993-5:2009. 2009. "Biological Evaluation of Medical Devices — Part 5: Tests for in Vitro Cytotoxicity". Geneva, Switzerland. https://www.iso.org/standard/36406.html.

"ISO/TR 27628:2007(en), Workplace atmospheres — Ultrafine, nanoparticle and nano-structured aerosols — Inhalation exposure characterization and assessment". s.d. Acedido a 30 de dezembro de 2022. https://www.iso.org/obp/ui/#iso:std:iso:tr:27628:ed-1:v1:en.

Jackson, J. K., C. M. Springate, W. L. Hunter, e H. M. Burt. 2000. "Neutrophil Activation by Plasma Opsonized Polymeric Microspheres: Inhibitory Effect of Pluronic F127". *Biomaterials* 21 (14): 1483–91. https://doi.org/10.1016/s0142-9612(00)00034-x.

Jaques, P. A., e C. S. Kim. 2000. "Measurement of Total Lung Deposition of Inhaled Ultrafine Particles in Healthy Men and Women". *Inhalation Toxicology* 12 (8): 715–31. https://doi.org/10.1080/08958370050085156.

Jeong, Mi Ho, Ha Ryong Kim, In Jae Bang, So Hee Yoo, Sang Jin Lee, Kyu Hong Lee, e Kyu Hyuck Chung. 2019. "In Vitro Model for Predicting Acute Inhalation Toxicity by Using a Calu-3 Epithelium Cytotoxicity Assay". *Journal of*

Pharmacological and Toxicological Methods 98 (julho): 106576. https://doi.org/10.1016/j.vascn.2019.04.002.

Karp, Philip H., Thomas O. Moninger, S. Pary Weber, Tamara S. Nesselhauf, Janice L. Launspach, Joseph Zabner, e Michael J. Welsh. 2002. "An in Vitro Model of Differentiated Human Airway Epithelia. Methods for Establishing Primary Cultures". *Methods in Molecular Biology (Clifton, N.J.)* 188: 115–37. https://doi.org/10.1385/1-59259-185-X:115.

Kéri, Albert, András Sápi, Ditta Ungor, Dániel Sebők, Edit Csapó, Zoltán Kónya, e Gábor Galbács. 2020. "Porosity Determination of Nano- and Sub-Micron Particles by Single Particle Inductively Coupled Plasma Mass Spectrometry". *Journal of Analytical Atomic Spectrometry* 35 (6): 1139–47. https://doi.org/10.1039/D0JA00020E.

Kondor, Anett, Alba Santmarti, Andreas Mautner, Daryl Williams, Alexander Bismarck, e Koon-Yang Lee. 2021. "On the BET Surface Area of Nanocellulose Determined Using Volumetric, Gravimetric and Chromatographic Adsorption Methods". *Frontiers in Chemical Engineering* 3. https://www.frontiersin.org/articles/10.3389/fceng.2021.738995.

Kradin, Richard L., e Subbha Digumarthy. 2017. "The Pathology of Pulmonary Bacterial Infection". *Seminars in Diagnostic Pathology* 34 (6): 498–509. https://doi.org/10.1053/j.semdp.2017.06.001.

Kreft, Mateja Erdani, Urška Dragin Jerman, Eva Lasič, Neli Hevir-Kene, Tea Lanišnik Rižner, Luka Peternel, e Katja Kristan. 2015. "The Characterization of the Human Cell Line Calu-3 under Different Culture Conditions and Its Use as an Optimized in Vitro Model to Investigate Bronchial Epithelial Function". *European Journal of Pharmaceutical Sciences* 69 (março): 1–9. https://doi.org/10.1016/j.ejps.2014.12.017.

Kuti, Joseph L., e David P. Nicolau. 2015. "Presence of Infection Influences the Epithelial Lining Fluid Penetration of Oral Levofloxacin in Adult Patients". *International Journal of Antimicrobial Agents* 45 (5): 512–18. https://doi.org/10.1016/j.ijantimicag.2014.12.028.

Lauweryns, J. M., e J. H. Baert. 1977. "Alveolar Clearance and the Role of the Pulmonary Lymphatics". *The American Review of Respiratory Disease* 115 (4): 625–83. https://doi.org/10.1164/arrd.1977.115.4.625.

Lawless, Harry T., Frank Rapacki, John Horne, e April Hayes. 2003. "The Taste of Calcium and Magnesium Salts and Anionic Modifications". *Food Quality and Preference* 14 (4): 319–25. https://doi.org/10.1016/S0950-3293(02)00128-3.

Lee, Diane F., Michael I. Lethem, e Alison B. Lansley. 2021. "A Comparison of Three Mucus-Secreting Airway Cell Lines (Calu-3, SPOC1 and UNCN3T) for Use as Biopharmaceutical Models of the Nose and Lung". *European Journal of Pharmaceutics and Biopharmaceutics* 167 (outubro): 159–74. https://doi.org/10.1016/j.ejpb.2021.07.016.

"Levofloxacin monograph." 2017. Em *UNITED States Pharmacopeia*, 40º ed, 4831–33.

Li, Jiaqi, Huangliang Zheng, e Sharon Shui Yee Leung. 2022. "Pulmonary Delivery of Emerging Antibacterials for Bacterial Lung Infections Treatment". *Pharmaceutical Research*, setembro, 1–16. https://doi.org/10.1007/s11095-022-03379-8.

Lister, Philip D. 2001. "Pharmacodynamics of Moxifloxacin and Levofloxacin against Staphylococcus Aureus and Staphylococcus Epidermidis in an In Vitro

Pharmacodynamic Model". *Clinical Infectious Diseases* 32 (Supplement_1): S33–38. https://doi.org/10.1086/319374.

Liu, Rui, Zhidong Liu, Chengui Zhang, e Boli Zhang. 2012. "Nanostructured Lipid Carriers as Novel Ophthalmic Delivery System for Mangiferin: Improving in Vivo Ocular Bioavailability". *Journal of Pharmaceutical Sciences* 101 (10): 3833–44. https://doi.org/10.1002/jps.23251.

López-García, Jorge, Marián Lehocký, Petr Humpolíček, e Petr Sáha. 2014. "HaCaT Keratinocytes Response on Antimicrobial Atelocollagen Substrates: Extent of Cytotoxicity, Cell Viability and Proliferation". *Journal of Functional Biomaterials* 5 (2): 43–57. https://doi.org/10.3390/jfb5020043.

Maguire, Ciarán Manus, Matthias Rösslein, Peter Wick, e Adriele Prina-Mello. 2018. "Characterisation of particles in solution – a perspective on light scattering and comparative technologies". *Science and Technology of Advanced Materials* 19 (1): 732–45. https://doi.org/10.1080/14686996.2018.1517587.

Mansfield, Elisabeth, e Mark Banash. 2021. "Thermal Analysis of Nanoparticles: Methods, Kinetics, and Recent Advances". *NIST*, outubro. https://www.nist.gov/publications/thermal-analysis-nanoparticles-methods-kinetics-and-recent-advances-0.

Martin, Paul D., Graeme R. Jones, Frances Stringer, e Ian D. Wilson. 2003. "Comparison of Normal and Reversed-Phase Solid Phase Extraction Methods for Extraction of β-Blockers from Plasma Using Molecularly Imprinted Polymers". *Analyst* 128 (4): 345–50. https://doi.org/10.1039/B211787H.

Meindl, Claudia, Kristin Öhlinger, Verena Zrim, Thomas Steinkogler, e Eleonore Fröhlich. 2021. "Screening for Effects of Inhaled Nanoparticles in Cell Culture Models for Prolonged Exposure". *Nanomaterials* 11 (3): 606. https://doi.org/10.3390/nano11030606.

Mesallati, Hanah, Anita Umerska, e Lidia Tajber. 2019. "Fluoroquinolone Amorphous Polymeric Salts and Dispersions for Veterinary Uses". *Pharmaceutics* 11 (6). https://doi.org/10.3390/pharmaceutics11060268.

Metlay, Joshua P., e Grant W. Waterer. 2020. "Treatment of Community-Acquired Pneumonia During the Coronavirus Disease 2019 (COVID-19) Pandemic". *Annals of Internal Medicine*, maio, M20-2189. https://doi.org/10.7326/M20-2189.

Mir, Maria, Naveed Ahmed, e Asim ur Rehman. 2017. "Recent Applications of PLGA Based Nanostructures in Drug Delivery". *Colloids and Surfaces B: Biointerfaces* 159 (novembro): 217–31. https://doi.org/10.1016/j.colsurfb.2017.07.038.

Miyazawa, Taiki, Mayuko Itaya, Gregor C Burdeos, Kiyotaka Nakagawa, e Teruo Miyazawa. 2021. "A Critical Review of the Use of Surfactant-Coated Nanoparticles in Nanomedicine and Food Nanotechnology". *International Journal of Nanomedicine* 16 (junho): 3937–99. https://doi.org/10.2147/IJN.S298606.

Modena, Mario M., Bastian Rühle, Thomas P. Burg, e Stefan Wuttke. 2019. "Nanoparticle Characterization: What to Measure?" *Advanced Materials* 31 (32): 1901556. https://doi.org/10.1002/adma.201901556.

Morales, Javier O., Jay I. Peters, e Robert O. Williams. 2011. "Surfactants: Their Critical Role in Enhancing Drug Delivery to the Lungs". *Therapeutic Delivery* 2 (5): 623–41. https://doi.org/10.4155/tde.11.15.

Mourdikoudis, Stefanos, Roger M. Pallares, e Nguyen T. K. Thanh. 2018. "Characterization Techniques for Nanoparticles: Comparison and

Complementarity upon Studying Nanoparticle Properties". *Nanoscale* 10 (27): 12871–934. https://doi.org/10.1039/C8NR02278J.

Müller, R. H., M. Radtke, e S. A. Wissing. 2002. "Solid lipid nanoparticles (SLN) and nanostructured lipid carriers (NLC) in cosmetic and dermatological preparations". *Advanced Drug Delivery Reviews*, Human skin: the Medium of Touch, 54, Supplement (novembro): S131–55. https://doi.org/10.1016/S0169-409X(02)00118-7.

Nafee, N., K. Forier, K. Braeckmans, e M. Schneider. 2018. "Mucus-Penetrating Solid Lipid Nanoparticles for the Treatment of Cystic Fibrosis: Proof of Concept, Challenges and Pitfalls". *European Journal of Pharmaceutics and Biopharmaceutics: Official Journal of Arbeitsgemeinschaft Fur Pharmazeutische Verfahrenstechnik e.V* 124 (março): 125–37. https://doi.org/10.1016/j.ejpb.2017.12.017.

Nasrollahzadeh, Mahmoud, Monireh Atarod, Mohaddeseh Sajjadi, S. Mohammad Sajadi, e Zahra Issaabadi. 2019. "Chapter 6 - Plant-Mediated Green Synthesis of Nanostructures: Mechanisms, Characterization, and Applications". Em *Interface Science and Technology*, editado por Mahmoud Nasrollahzadeh, S. Mohammad Sajadi, Mohaddeseh Sajjadi, Zahra Issaabadi, e Monireh Atarod, 28:199–322. An Introduction to Green Nanotechnology. Elsevier. https://doi.org/10.1016/B978-0-12-813586-0.00006-7.

Nightingale, Charles H., Edward M. Grant, e Richard Quintiliani. 2000. "Pharmacodynamics and Pharmacokinetics of Levofloxacin". *Chemotherapy* 46 (Suppl. 1): 6–14. https://doi.org/10.1159/000048487.

Page-Clisson, Marie-Estelle, Huguette Pinto-Alphandary, Elisabeth Chachaty, Patrick Couvreur, e Antoine Andremont. 1998. "Drug Targeting by Polyalkylcyanoacrylate Nanoparticles Is Not Efficient Against Persistent Salmonella". *Pharmaceutical Research* 15 (4): 544–49. https://doi.org/10.1023/A:1011921608964.

Papadimitriou, Sofia, e Dimitrios Bikiaris. 2009. "Novel self-assembled core-shell nanoparticles based on crystalline amorphous moieties of aliphatic copolyesters for efficient controlled drug release". *Journal of Controlled Release* 138 (2): 177–84. https://doi.org/10.1016/j.jconrel.2009.05.013.

Pardeike, Jana, Sabrina Weber, Hans Peter Zarfl, Maximilian Pagitz, e Andreas Zimmer. 2016. "Itraconazole-Loaded Nanostructured Lipid Carriers (NLC) for Pulmonary Treatment of Aspergillosis in Falcons". *European Journal of Pharmaceutics and Biopharmaceutics: Official Journal of Arbeitsgemeinschaft Fur Pharmazeutische Verfahrenstechnik e.V* 108 (novembro): 269–76. https://doi.org/10.1016/j.ejpb.2016.07.018.

Patlolla, Ram R., Mahavir Chougule, Apurva R. Patel, Tanise Jackson, Prasad NV Tata, e Mandip Singh. 2010. "Formulation, Characterization and Pulmonary Deposition of Nebulized Celecoxib Encapsulated Nanostructured Lipid Carriers". *Journal of controlled release : official journal of the Controlled Release Society* 144 (2): 233–41. https://doi.org/10.1016/j.jconrel.2010.02.006.

Pettitt, Michala E., e Jamie R. Lead. 2013. "Minimum Physicochemical Characterisation Requirements for Nanomaterial Regulation". *Environment International* 52: 41–50. https://doi.org/10.1016/j.envint.2012.11.009.

Raghavan, R., e Jose C. Joseph. 2015. "Chromatographic Methods of Analysis: High-Performance Liquid Chromatography". Em *Encyclopedia of Pharmaceutical Science and Technology, Fourth Edition*, 4º ed. CRC Press.

Rahman, Habibur, e Sk Manirul Haque. 2021. “Development and Validation of Chromatographic and Spectrophotometric Methods for the Quantitation of Rufinamide in Pharmaceutical Preparations”. *Turkish Journal of Pharmaceutical Sciences* 0 (0): 0–0. https://doi.org/10.4274/tjps.galenos.2021.37043.

Ravichandran, Vasanthan, Minjong Lee, Thuy Giang Nguyen Cao, e Min Suk Shim. 2021. “Polysorbate-Based Drug Formulations for Brain-Targeted Drug Delivery and Anticancer Therapy”. *Applied Sciences* 11 (19): 9336. https://doi.org/10.3390/app11199336.

Rensburg, Lyné van, Johann M. van Zyl, e Johan Smith. 2018. “Deposition and Transport of Linezolid Mediated by a Synthetic Surfactant Synsurf® within a Pressurized Metered Dose Inhaler: A Calu-3 Model”. *Drug Design, Development and Therapy* 12: 1107–18. https://doi.org/10.2147/DDDT.S147035.

Repetto, Guillermo, Ana del Peso, e Jorge L. Zurita. 2008. “Neutral Red Uptake Assay for the Estimation of Cell Viability/Cytotoxicity”. *Nature Protocols* 3 (7): 1125–31. https://doi.org/10.1038/nprot.2008.75.

Richter, Sara, Cristina Parolin, Manlio Palumbo, e Giorgio Palù. 2004. “Antiviral Properties of Quinolone-Based Drugs”. *Current Drug Targets. Infectious Disorders* 4 (2): 111–16. https://doi.org/10.2174/1568005043340920.

Riss, Terry L., Richard A. Moravec, Andrew L. Niles, Sarah Duellman, Hélène A. Benink, Tracy J. Worzella, e Lisa Minor. 2004. “Cell Viability Assays”. Em *Assay Guidance Manual*, editado por Sarine Markossian, Abigail Grossman, Kyle Brimacombe, Michelle Arkin, Douglas Auld, Chris Austin, Jonathan Baell, et al. Bethesda (MD): Eli Lilly & Company and the National Center for Advancing Translational Sciences. http://www.ncbi.nlm.nih.gov/books/NBK144065/.

Saupe, Anne, Sylvia A. Wissing, Andreas Lenk, Corinna Schmidt, e Rainer H. Müller. 2005. “Solid Lipid Nanoparticles (SLN) and Nanostructured Lipid Carriers (NLC) -- Structural Investigations on Two Different Carrier Systems”. *Bio-Medical Materials and Engineering* 15 (5): 393–402.

Schöler, N., H. Hahn, R. H. Müller, e O. Liesenfeld. 2002. “Effect of Lipid Matrix and Size of Solid Lipid Nanoparticles (SLN) on the Viability and Cytokine Production of Macrophages”. *International Journal of Pharmaceutics* 231 (2): 167–76. https://doi.org/10.1016/s0378-5173(01)00882-1.

Schwarz, C., W. Mehnert, J. S. Lucks, e R. H. Müller. 1994. “Solid lipid nanoparticles (SLN) for controlled drug delivery. I. Production, characterization and sterilization”. *Journal of Controlled Release* 30 (1): 83–96. https://doi.org/10.1016/0168-3659(94)90047-7.

Sharma, Amarnath, e Uma S. Sharma. 1997. “Liposomes in Drug Delivery: Progress and Limitations”. *International Journal of Pharmaceutics* 154 (2): 123–40. https://doi.org/10.1016/S0378-5173(97)00135-X.

Shubhra, Quazi T. H., Judit Tóth, János Gyenis, e Tivadar Feczkó. 2014. “Surface Modification of HSA Containing Magnetic PLGA Nanoparticles by Poloxamer to Decrease Plasma Protein Adsorption”. *Colloids and Surfaces. B, Biointerfaces* 122 (outubro): 529–36. https://doi.org/10.1016/j.colsurfb.2014.07.025.

Siddiqui, Masoom Raza, Zeid A. AlOthman, e Nafisur Rahman. 2017. “Analytical Techniques in Pharmaceutical Analysis: A Review”. *Arabian Journal of Chemistry* 10: S1409–21. https://doi.org/10.1016/j.arabjc.2013.04.016.

Singh, Ranjit. 2012. “Current trends in forced degradation study for pharmaceutical product development”. Em . https://www.semanticscholar.org/paper/Current-

trends-in-forced-degradation-study-for-Singh/b08c5fb7f6501cd9423567f1a0b7bc00422cf475.

Sonia, Thundiparambil Azeez, e Chandra P. Sharma. 2014. “5 - Lipids and Inorganic Nanoparticles in Oral Insulin Delivery”. Em *Oral Delivery of Insulin*, editado por Thundiparambil Azeez Sonia e Chandra P. Sharma, 219–56. Woodhead Publishing Series in Biomedicine. Woodhead Publishing. https://doi.org/10.1533/9781908818683.219.

“Standard Practice for Performing Cryo-Transmission Electron Microscopy of Liposomes”. s.d. Acedido a 13 de dezembro de 2022. https://www.astm.org/e3143-18b.html.

Steiner, Verena, Kristin Öhlinger, Carolina Corzo, Sharareh Salar-Behzadi, e Eleonore Fröhlich. 2019. “Cytotoxicity Screening of Emulsifiers for Pulmonary Application of Lipid Nanoparticles”. *European Journal of Pharmaceutical Sciences* 136 (agosto): 104968. https://doi.org/10.1016/j.ejps.2019.104968.

Tang, Xiaozhi, e Sajid Alavi. 2011. “Recent Advances in Starch, Polyvinyl Alcohol Based Polymer Blends, Nanocomposites and Their Biodegradability”. *Carbohydrate Polymers* 85 (1): 7–16. https://doi.org/10.1016/j.carbpol.2011.01.030.

Torrego, Alfons, Virginia Pajares, Carmen Fernández-Arias, Paula Vera, e Jordi Mancebo. 2020. “Bronchoscopy in Patients with COVID-19 with Invasive Mechanical Ventilation: A Single-Center Experience”. *American Journal of Respiratory and Critical Care Medicine* 202 (2): 284–87. https://doi.org/10.1164/rccm.202004-0945LE.

Tsivkovskii, Ruslan, Mojgan Sabet, Ziad Tarazi, David C. Griffith, Olga Lomovskaya, e Michael N. Dudley. 2011. “Levofloxacin reduces inflammatory cytokine levels in human bronchial epithelia cells: implications for aerosol MP-376 (levofloxacin solutionfor inhalation) treatment of chronic pulmonary infections”. *FEMS Immunology & Medical Microbiology* 61 (2): 141–46. https://doi.org/10.1111/j.1574-695X.2010.00755.x.

Tulkens, P. M. 1991. “Intracellular Distribution and Activity of Antibiotics”. *European Journal of Clinical Microbiology and Infectious Diseases* 10 (2): 100–106. https://doi.org/10.1007/BF01964420.

“United States Pharmacopeia. General Chapter, 〈1603〉 Good Cascade Impactor Practices. USP-NF. Rockville, MD: United States Pharmacopeia.” 2022. https://doi.org/10.31003/USPNF_M13055_03_01.

“United States Pharmacopeia Vol 31, National Formulary 26, General Chapter: <621> Chromatography”. s.d. Acedido a 29 de dezembro de 2022. http://www.uspbpep.com/usp31/v31261/usp31nf26s1_c621.asp.

USP. 2022. “〈1153〉 Drug Products Containing Nanomaterials”. https://doi.org/10.31003/USPNF_M13775_02_01.

Vervoort, R. J. M, A. J. J Debets, H. A Claessens, C. A Cramers, e G. J de Jong. 2000. “Optimisation and Characterisation of Silica-Based Reversed-Phase Liquid Chromatographic Systems for the Analysis of Basic Pharmaceuticals”. *Journal of Chromatography A* 897 (1): 1–22. https://doi.org/10.1016/S0021-9673(00)00811-6.

Villiers, André de, François Lestremau, Roman Szucs, Sylvie Gélébart, Frank David, e Pat Sandra. 2006. “Evaluation of Ultra Performance Liquid Chromatography: Part I. Possibilities and Limitations”. *Journal of Chromatography A* 1127 (1): 60–69. https://doi.org/10.1016/j.chroma.2006.05.071.

Weich, Anelise, Daniele Carvalho de OLIVEIRA, Janine de MELO, Karin Goebel, e Clarice Madalena Bueno Rolim. 2007. “Validation of UV Spectrophotometric and HPLC Methods for Quantitative Determination of Atenolol in Pharmaceutical Preparations”. *Latin American Journal of Pharmacy*, 6.

“What Causes Molecules to Absorb UV and Visible Light”. 2013. Chemistry LibreTexts. 3 de outubro de 2013. https://chem.libretexts.org/Bookshelves/Physical_and_Theoretical_Chemistry_Textbook_Maps/Supplemental_Modules_(Physical_and_Theoretical_Chemistry)/Spectroscopy/Electronic_Spectroscopy/Electronic_Spectroscopy_Basics/What_Causes_Molecules_to_Absorb_UV_and_Visible_Light.

Woodall, Maximillian N. J., Tereza Masonou, Katie-Marie Case, e Claire M. Smith. 2021. “Human Models for COVID-19 Research”. *The Journal of Physiology* 599 (18): 4255–67. https://doi.org/10.1113/JP281499.

Yacouba, Abdourahamane, Ahmed Olowo-okere, e Ismaeel Yunusa. 2021. “Repurposing of antibiotics for clinical management of COVID-19: a narrative review”. *Annals of Clinical Microbiology and Antimicrobials* 20 (1): 37. https://doi.org/10.1186/s12941-021-00444-9.

Zhang, Lin, Shou-Ying Du, Yang Lu, Chang Liu, Zhi-Hao Tian, Chang Yang, Hui-Chao Wu, e Zhen Wang. 2016. “Puerarin transport across a Calu-3 cell monolayer – an in vitro model of nasal mucosa permeability and the influence of paeoniflorin and menthol”. *Drug Design, Development and Therapy* 10 (julho): 2227–37. https://doi.org/10.2147/DDDT.S110247.

8. ANEXOS

8.1. Carta de aceite

Carta de aceite para publicação do Capítulo de livro intitulado: “Physicochemical Characterization of Drug Delivery Systems based on nanomaterials” para compor o livro: Molecular Pharmaceutics and Nano Drug Delivery: Fundamentals and Challenges, editado por Umesh Gupta e Amit K. Goyal (Academic Press, 2023, ISBN 9780323919241).

ELSEVIER

April 4, 2023

To whom it may concern:

I am writing to confirm that, following peer review by the editorial team, the chapter “Physicochemical Characterization of Drug Delivery Systems based on nanomaterials” by Viviane Lucia Beraldo de Araújo, Victória Soares Soeiro, Marcelo Van Vliet Lima, Juliana Souza Ribeiro Costa, and Laura de Oliveira-Nascimento has been accepted for publication in *Molecular Pharmaceutics and Nano Drug Delivery: Fundamentals and Challenges*, edited by Umesh Gupta and Amit K. Goyal (Academic Press, 2023, ISBN 9780323919241). The book is scheduled to publish later this year.

Sincerely,

Pat Gonzalez
Senior Editorial Project Manager
Academic Press/Elsevier

8.2. Comprovante de permissão para uso de artigo publicado

Comprovante de permissão para uso do artigo que compõe o Capítulo 2 da tese.

17/02/2023, 15:20 Rightslink® by Copyright Clearance Center

CCC RightsLink

Help Live Chat

Levofloxacin in nanostructured lipid carriers: Preformulation and critical process parameters for a highly incorporated formulation

Author:
Viviane Lucia Beraldo-Araújo,Ana Flávia Siqueira Vicente,Marcelo van Vliet Lima,Anita Umerska,Eliana B. Souto,Lidia Tajber,Laura Oliveira-Nascimento

Publication: International Journal of Pharmaceutics

Publisher: Elsevier

Date: 15 October 2022

© 2022 The Author(s). Published by Elsevier B.V.

Creative Commons

This is an open access article distributed under the terms of the Creative Commons CC-BY license, which permits unrestricted use, distribution, and reproduction in any medium, provided the original work is properly cited.

You are not required to obtain permission to reuse this article.

To request permission for a type of use not listed, please contact Elsevier Global Rights Department.

Are you the author of this Elsevier journal article?

© 2023 Copyright - All Rights Reserved | Copyright Clearance Center, Inc. | Privacy statement | Data Security and Privacy | For California Residents | Terms and ConditionsComments? We would like to hear from you. E-mail us at customercare@copyright.com